Investigation of differentially methylated microRNA genes in Type 2 diabetes

By

Philbè-Jeanne Alley

Thesis presented in partial fulfilment of the requirements for the degree of Master of Science in Molecular Biology in the Faculty of Medicine and Health Sciences at Stellenbosch University

Superisor: Dr Carmen Pheiffer

Co-Supervisor: Dr Sian Hemmings

March 2017

Declaration

By submitting this thesis/dissertation electronically, I declare that the entirety of the work contained therein is my own, original work, that I am the sole author thereof (save to the extent explicitly otherwise stated), that reproduction and publication thereof by Stellenbosch University will not infringe any third-party rights and that I have not previously in its entirety or in part submitted it for obtaining any qualification.

Philbè-Jeanne Alley

March 2017

Summary

Type 2 diabetes is a major source of morbidity and mortality worldwide, accounting for approximately 90% of the 415 million individuals who have Diabetes mellitus globally. The prevalence of T2D in South Africa is currently estimated at 9% and is expected to increase significantly due to the concomitant high prevalence of obesity, a major risk factor for the development of T2D. These metabolic disorders pose a major health burden to an already under-resourced and over-burdened health care system, and create an urgent need to identify therapeutics capable of preventing or treating T2D.

Epigenetic mechanisms, such as microRNAs (miRNAs), reflect the interaction between genetic and environmental factors and are attracting considerable interest as strategies to elucidate the pathophysiology of disease. Investigation of miRNAs could lead to the development of high risk biomarkers for disease prevention, or to therapeutic targets. MiRNAs are dysregulated during T2D, however, the mechanisms regulating miRNAs are largely unknown. The aim of this study was to explore the role of DNA methylation, another important epigenetic mechanism, in the regulation of miRNA genes. Furthermore, we aimed to investigate the relationship between miRNA gene methylation and miRNA expression in an *in vitro* model relevant to T2D.

To identify miRNA genes potentially regulated by DNA methylation, miRNAs that were differentially expressed in the whole blood of n=9 South African women of mixed ethnic ancestry during T2D were integrated with miRNA genes that were differentially methylated in the whole blood of a different subset of n=9 South African women of mixed ethnic ancestry during T2D. The methylation status of the identified miRNA genes were verified using the MassARRAY® EpiTYPER® system. To investigate the relationship between DNA methylation and miRNA gene expression under defined conditions, 3T3-L1 pre-adipocytes were differentiated in glucose conditions that mimic normoglycaemia and hyperglycaemia.

Data integration showed that 43 miRNAs were differentially expressed during T2D compared to normoglycaemia, 21 miRNAs that were differentially expressed during impaired glucose tolerance compared to normoglycaemia, and 32 miRNAs that were differentially expressed during T2D compared to impaired glucose tolerance, were under the potential regulation of DNA methylation. Primers were designed for 26 randomly selected miRNA genes, of which 21 miRNA genes were successfully analysed by MassARRAY® EpiTYPER®. The methylation of two of these, mir-98 and

mir-150, correlated with DNA methylation data conducted using methylated DNA immunoprecipitation sequencing. Differentiation of 3T3-L1 pre-adipocytes in glucose concentrations that mimic normoglycaemia and hyperglycaemia resulted in mature adipocytes that differed in metabolic activity and oxidative stress.

In conclusion, this study provides support for DNA methylation as a mechanism regulating miRNA expression during T2D and demonstrates that 3T3-L1 pre-adipocytes differentiated in different glucose concentrations offer a viable model for investigating the relationship between miRNA expression and DNA methylation during hyperglycaemia, altered metabolic activity and oxidative stress. These findings pave the way for future studies to delineate the effect of DNA methylation on miRNA expression during conditions characteristic of T2D.

Opsomming

Tipe 2 diabetes (T2D) is van die grootste oorsake van morbiditeit and mortaliteit wereldwyd, met ‘n voorkoms van meer as 90% van die 415 miljoen individue wat wereldwyd diagnoseer was met Diabetes mellitus in 2015. Huidiglik word die voorkoms van T2D in Suid Afrika beraam op 9% en dit word geskat dat hierdie voorkoms aansienlik gaan verhoog as gevolg van die gepaardgaande hoë voorkoms van vetsug en die verhoogde kans wat dit n individu bied vir die ontwikkeling van T2D. Ons gesondheidsstelsel is onder geweldige druk en die hoë voorkoms van hierdie metaboliese afwykings dra verder daartoe by. Dit beklemtoon dus die behoefte om terapeutiese middels te identifiseer wat die vermoë het om T2D te verhoed of effektief te behandel.

Epigenetiese meganismes, byvoorbeeld mikroRNAs (miRNAs), weerspieel die interaksie tussen omgewings- en genetiese faktore wat groot belangstelling begin werf het as ‘n strategie om die onderliggende patofisiologie van T2D toe te lig, om ten einde biomerkers te identifiseer wat gebruik kan word om T2D te voorkom en as terapeutiese middels. MikroRNAs word disreguleer gedurende T2D, maar die meganismes waarby hierdie disregulasie plaasvind, is steeds grootendeels onbekkend. Die doel van hierdie studie was om te sien of DNA metilasie, nog ‘n belangrike epigenetiese meganisme, een van die maniere is waarop miRNA gene reguleer word. Verder, het ons gemik daarop om die verhouding tussen miRNA geen metilasie en miRNA geen uitdrukking in ‘n *in vitro* model te ondersoek.

Ons het miRNAs wat differensieel uitgedruk was in die bloed van n=9 Suid Afrikaanse kleurling vroue met T2D van gemengde etniese afkoms, wat identifiseer was deur geenvolgordebepaling (miRNA-Seq), met miRNA gene wat identifiseer was om differensieel metileer te wees, deur DNA metilasie immunopresipitasie geenvolgordebepaling (DMIGB), in die bloed van n afsonderlike n=9 Suid Afrikaanse kleurling vroue met T2D van gemengde etniese afkoms, vergelyk om miRNA gene te identifiseer wat moontlik deur metilasie reguleer word. Die metilasie van die ge-identifiseerde miRNAs was bevestig deur die MassARRAY® EpiTYPER® analise. Om die verhouding tussen DNA metilasie en miRNA geen uitdrukking te bepaal onder spesifieke sellulere kondisies, was 3T3-L1 adiposiete differensieer in kondisies wat die patologie van T2D naboots.

Gedurende die vergelykingsproses, was 43 miRNA gene (T2D vs. normoglisemies), 21 miRNA gene (prediabetes vs. normoglisemies) en 32 miRNA gene (T2D vs. prediabetes), respektiewelik, identifiseer wat moontlik deur DNA metilasie reguleer word. Inleiers was was ontwerp vir 26 lukraak gekiesde miRNA gene, waarvan 21 suksesvol geanaliseer was deur MassARRAY® EpiTYPER®. Die metilasie vlak van twee van die 21 miRNA gene, miR-98 en miR-150, het ooreengestem met die metilasie data gegenereer deur DMIGB. Differensiasie van 3T3-L1 pre-adiposiete in verskillende

glukose konsentrasies, het gelei na volwasse adiposiete wat verskillende metabolise aktiwiteite en oksidatiewe stres vlakke het.

Ten slotte, hierdie studie toon dat DNA metilasie wel n meganisme is van miRNA geen uitdrukking regulasie tydens T2D en dit demonstreer dat 3T3-L1 pre-adiposiete gedifferensieerd in verskillende glucose konsentrasies, ‘n praktiese en gepasde model is vir die ondersoek van die verhouding tussen miRNA uitdrukking en DNA metilasie gedurende hiperglisemie en die verandering in metabolise aktiwiteit en oksidatiewe stres is. Hierdie bevindings le grond vir toekomstige studies om die effek van DNA metilasie op miRNA uitdrukking in T2D patologie af te baken.

Acknowledgements

I would like to thank and express my sincere gratitude to my supervisor Dr Carmen Pheiffer that always lent a helping hand when I ran into obstacles in both my research and during writing my thesis. She was a pillar of support, advice, motivation and hope whenever I needed it.

My appreciation for Carmen extends to more than just the professional. She was there for me when personal circumstances hindered my progress in my research.

I would like to give thanks to my co-supervisor Dr Sian Hemmings for keeping me in the loop with campus news and deadlines, and for her contribution to this, my final piece of work.

I would also like to thank my fellow colleagues at the Biomedical Research and Innovation Platform at the South African Medical Research council for the belief they had in me and that I would succeed. A special thanks to Dr Babalwa Jack, Dr Phiwayinkosi Dludla and Miss Charity Masilela for their willingness to help when I needed it.

Some special thanks also goes to the National Research Foundation, South African Medical Research Council, Harry Crossley Foundation and Stellenbosch University Postgraduate Office for the financial support that enabled me to study for the past two years.

I would also like to thank everyone that had a hand in the successful completion of my research and laboratory work, any effort, big or small, was not overlooked and was appreciated.

And lastly, I would like to thank my mother, Jeanetta Mathilda Alley, for the amazing role model she has been all my life. For pushing me to pursue my dreams and supporting those dreams in any and every manner she could. If it was not for her presence in my life, I know, my life would have taken a different turn.

Thank you.

Table of Contents ..... **Page**

Abbreviations

DCFH-DA	2',7'-Dichloro-dihydro-fluorescein diacetate
2-DG	2-Deoxy-[3H]-D-glucose
2DG6P	2-deoxyglucose-6-phosphate
3' UTR	3' Untranslated region
α-cells	Alpha cells
β-cells	Beta cells
JC-1	5,5', 6,6'-Tetrachloro- 1,1', 3,3'-tetraethylbenzimidizolyl-carbocyanine iodide
ADA	American Diabetes Association
ADM	Adipocyte differentiation medium
AMM	Adipocyte maintenance medium
ATCC	American Type Culture Collection
AGO2	Argonaute
AMR	ATP monitoring reagent
BMI	Body mass index
BP	Base pair
C5	Carbon 5
CGM	Complete growth medium
CV	Crystal violet
CVD	Cardiovascular disease
cAMP	Cyclic AMP
dNTPs	Deoxynucleotide triphosphate
DM	Diabetes mellitus
DNMT	DNA methyltranferase
ddH2O	Double distilled water
DPBS	Dulbecco's phosphate buffered saline
EDTA	Ethylenediaminetetraacetic acid
fPG	Fasting plasma glucose
GLUT 1-4	Glucose transporter 1-4
HbA1c	Glycated haemoglobin test
HBSS	Hanks buffered saline solution
HBP	Human Biomarker Project
H_2O_2	Hydrogen peroxide
IDF	International Diabetes Federation

IGT	Impaired glucose tolerance
hMC	MassCLEAVE™ reaction
MeDIP-Seq	Methylated DNA Immunoprecipitation sequencing
mRNA	Messenger RNA
MiRNA	MicroRNA
MiRNA-seq	MicroRNA sequencing
m/z	mass to charge ratio
NGT	Normoglycaemia
ORO	Oil Red O
OGTT	Oral glucose tolerance test
OS	Oxidative stress
PBMCs	Peripheral blood mononuclear cells
PMSF	Phenylmethane sulfonyl fluoride
PCR	Polymerase chain reaction
Pre-miRNA	Precursor microRNA
Pri-miRNA	Primary microRNA
ROS	Reactive oxygen species
RISC	RNA-induced silencing complex
RT	Room temperature
SA	South Africa
SAP	Shrimp alkaline phosphatase
SDS	Sodium Dodecyl Sulfate
O2-	Superoxide radical
T1D	Type 1 diabetes mellitus
T2D	Type 2 diabetes mellitus
WHO	World Health Organization
w/o phenol red	Without phenol red

List of Tables

List of Figures

1. Introduction

1.1 Diabetes mellitus

Diabetes mellitus (DM) is a chronic metabolic disorder characterized by hyperglycaemia due to an inability of cells to respond to insulin, or a deficit in insulin production (International Diabetes Federation, 2015). The exact mechanisms that lead to hyperglycaemia differ between the three most common forms of DM (American Diabetes Association, 2010, 2016; Zimmet, 2000).

1.1.1 Type 1 diabetes

Type 1 diabetes mellitus (T1D) is a hereditary form of diabetes where affected individuals lack the ability to produce insulin due to the autoimmune destruction of pancreatic β-cells (World Health Organization, 2006). This form of diabetes is predominantly diagnosed in children, adolescents and young adults and requires the administration of exogenous insulin daily for survival. It is estimated that T1D accounts for 5-10% of all DM cases worldwide (Melmed et al., 2015; World Health Organization, 2016).

1.1.2 Type 2 diabetes

Type 2 diabetes mellitus (T2D) is characterized by insulin resistance, the condition where peripheral tissues fail to increase glucose uptake in response to physiological concentrations of insulin (Kahn et al., 2006). Insulin resistance is accompanied by high levels of circulating insulin, due to increased insulin secretion by β-cells as a compensatory mechanism, a condition known as hyperinsulinemia. However, β-cells become exhausted and dysfunctional, which ultimately leads to hyperglycaemia (Gauthier and Wollheim, 2006; Weir and Bonner-Weir, 2004). Type 2 diabetes accounts for more than 90 % of DM cases worldwide and is considered the major driving factor of the current DM epidemic (Guariguata et al., 2014; International Diabetes Federation, 2015; Zimmet, 2000). Although Type 2 diabetes is commonly diagnosed in adults, the increased prevalence of T2D in children and adolescents is a major cause for concern (International Diabetes Federation, 2014, 2015).

1.1.3 Gestational diabetes

Gestational diabetes mellitus (GDM) is characterized by hyperglycaemia first detected during pregnancy with return to normal glucose tolerance after delivery (International Diabetes Federation, 2015). In industrialised countries, it is estimated that up to 10% of pregnancies are complicated by GDM (Ratner, 2007). Gestational diabetes confers a greater than 70% risk of developing T2D, while offspring born to GDM mothers also face adverse health consequences (Erem et al., 2015; Ferrara,

2007; Zhu and Zhang, 2016).

1.2 Global prevalence of Diabetes mellitus

The 7th Annual Diabetes Atlas issued by the International Diabetes Federation (IDF) estimated that the global prevalence of DM in individuals between the ages of 20-79 years in 2015 was 415 million, and is projected to increase to 642 million by 2040 (International Diabetes Federation, 2015).

The prevalence of DM in individuals between the ages of 20-79 years in Africa in 2015 was 14.2 million and is projected to increase by 109% over the next 20 years. Furthermore, Africa has the highest number of undiagnosed DM cases, estimated to be up to 75% (Beagley et al., 2014). With a prevalence of 9%, South Africa (SA) is estimated to be in the top seven countries with the highest DM prevalence in Africa (Bertram et al., 2013).

1.3 Risk factors for the development of Type 2 diabetes

Type 2 diabetes is a multifactorial disease with both genetic and environmental factors implicated in the pathophysiology thereof. Genome wide association and twin studies have identified a total of 80 susceptibility loci for T2D (Morris, 2014), a total that has increased to 91 during the past two years (Stettler et al., 2016). However, these susceptibility variants have a modest effect, accounting for only 5-10% of all diagnosed T2D cases (Voight et al., 2010). This modest effect of susceptibility loci underscores the importance of environmental factors in disease onset and progression. Environmental factors, which include the consumption of diets high in fats and sugars, physical inactivity, age, ethnicity, poor socio-economic conditions, smoking, drinking, mental illness and obesity play an integral role in the development of T2D (Ardisson Korat et al., 2014; Chen et al., 2012a; Ley et al., 2016; Piccolo et al., 2016; Zoungas et al., 2014).

1.4 Glucose homeostasis

Glucose homeostasis is required for normal cellular functioning and constitutes one of the most important regulatory pathways within the body (Shrayyef and Gerich, 2010). Glucose homeostasis is achieved by a tightly regulated balance between insulin and glucagon secretion by the pancreas.

1.4.1 Glucose uptake from circulation

Glucose is the main source of fuel for cells (Berg et al., 2002). After ingesting a meal, blood glucose levels rise, signalling pancreatic β-cells to produce and secrete insulin into the circulatory system (Gauthier and Wollheim, 2006). In the pancreas, the secretion of insulin-containing vesicles into the

circulatory system is dependent on the second messengers Ca^{2+}, cyclic AMP (cAMP) and phospholipid derivatives that control vesicle docking, priming and fusion with the plasma membrane (Figure 1).

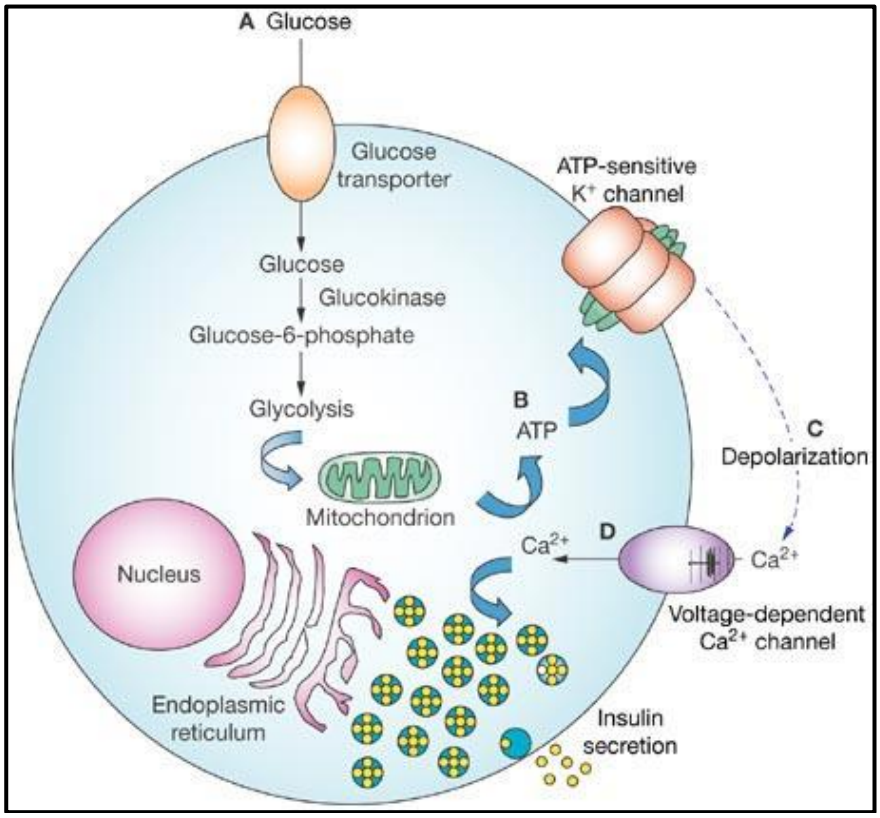

Figure 1. Insulin secretion from pancreatic β-cells.
The uptake of glucose (A) and its metabolism within the cell leads to: ATP production (B), the closing of ATP-sensitive K+ channels, plasma-membrane depolarization (C), the opening of Ca^{2+} channels, the influx of Ca^{2+} molecules (D) from the extracellular environment and, finally, insulin secretion.

Since glucose is too large to diffuse into cells, it is transported across the plasma membrane by glucose transporters, GLUT 1 and GLUT 3 (Maher et al., 1991; Simpson et al., 2008; Vannucci, 1994), responsible for facilitating basal glucose uptake. Insulin-stimulated glucose uptake is facilitated by GLUT 2 and GLUT 4 in the liver and muscle, respectively (Ebeling et al., 1998; Leney and Tavaré, 2009). Insulin binds to the insulin receptor in the plasma membrane leading to the activation of the downstream insulin signalling cascade that stimulate the translocation of intracellular vesicles containing the protein subunits that make GLUTs to the plasma membrane, where they are incorporated and facilitate glucose uptake as illustrated in Figure 2.

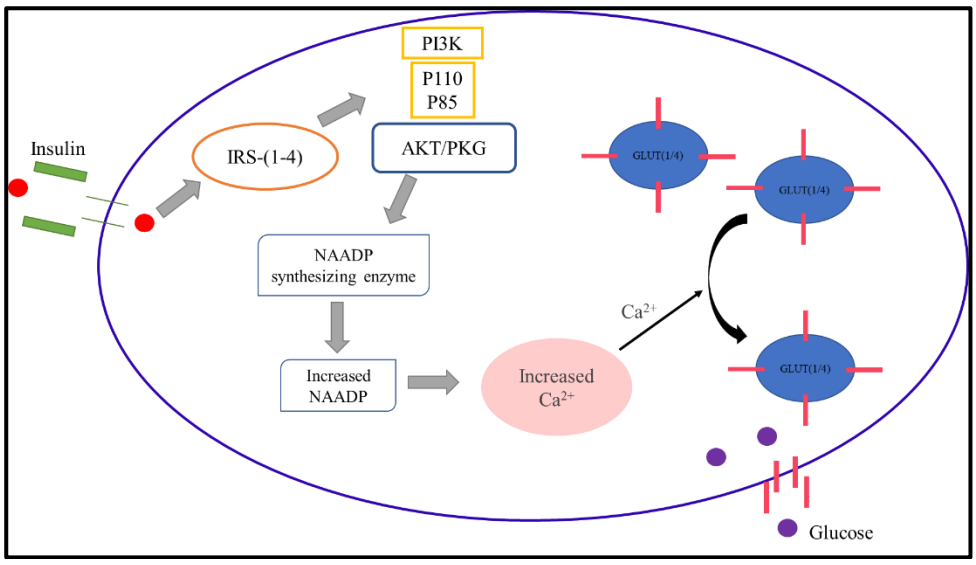

Figure 2. Insulin stimulated glucose uptake.
Insulin binding to the insulin receptors on the plasma membrane leads to the activation of the insulin signalling pathway and the translocation of glucose transporters to the plasma membrane where they facilitate glucose uptake.

1.4.2 Endogenous glucose production

During starvation or glucose deprivation, pancreatic α-cells are stimulated to produce and secrete glucagon. Glucagon and insulin exert antagonistic effects on glucose homeostasis (Giacca et al., 1997; Lewis et al., 1997; Mittelman et al., 1997). In contrast to insulin which stimulates circulatory glucose uptake and breakdown, glucagon stimulates gluconeogenesis (endogenous hepatic glucose production) and glycogenesis (conversion of glycogen stored in the liver to glucose), thereby raising blood glucose concentrations.

1.5 Diagnosis of Type 2 diabetes

Type 2 diabetes is diagnosed by measuring fasting plasma glucose (fPG), glycated haemoglobin (HbA1c) concentrations or conducting the oral glucose tolerance test (OGTT), according to World Health Organization (World Health Organization, 2006) or the American Diabetes Association (American Diabetes Association, 2010, 2016) criteria (Table 1).

The fPG test is the most common test for the diagnosis of T2D and measures blood glucose concentrations after an eight hour fast. The OGTT is considered the gold standard and measures blood glucose concentrations two hours after the ingestion of 75 g of glucose, following an eight hour fast (Salmasi and Dancy, 2005). The HbA1c test is a blood test that reflects blood glucose levels over a period of three months and does not require fasting (The International Expert Committee, 2009). However, all tests have limitations and their use is dependent on the consideration of several factors

(American Diabetes Association, 2012; National Institute of Diabetes and Digestive and Kidney Diseases, 2015).

Impaired glucose tolerance (IGT) is characterized by elevated blood glucose concentrations that are higher than normal, but not high enough to be considered T2D (American Diabetes Association, 2016; National Institute of Diabetes and Digestive and Kidney Diseases, 2015; World Health Organization, 2006). A diagnosis of IGT is associated with an increased risk of developing T2D within the next 10 years if no lifestyle changes are implemented (National Institute of Diabetes and Digestive and Kidney Diseases, 2015). This stage in the pathophysiology of T2D is reversible and is associated with limited micro- and macrovascular damage in tissues and cells, and has therefore attracted considerable interest for the intervention and prevention of T2D progression (National Institute of Diabetes and Digestive and Kidney Diseases, 2015).

Table 1. World Health Organization and American Diabetes Association diagnostic criteria.

	World Health Organization (mmol/L)	**American Diabetes Association (mmol/L)**
Type 2 diabetic		
Fasting plasma glucose	≥ 7	≥ 7
Two-hour glucose (OGTT)	≥ 11.1	≥ 11.1
HbA1c	≥ 6.5	≥ 5.6
Impaired Glucose Tolerant		
Fasting plasma glucose	5.6-6.9	5.6-6.9
Two-hour glucose (OGTT)	7.8-11.0	7.8-11.0
HbA1c	5.7-6.4	5.1-5.5
Normoglycaemic		
Fasting plasma glucose	≤ 5.4	≤ 5.4
Two-hour glucose (OGTT)	≤ 7.7	≤ 7.7
HbA1c	≤ 5	≤ 5

Table adapted from World Health Organization, 2006 and American Diabetes Association, 2012.

1.6 Complications of Type 2 diabetes

Type 2 diabetes is a chronic disorder that progressively worsens over time, with chronic hyperglycaemia leading to microvascular (nephropathy, neuropathy and retinopathy) and macrovascular (angina, myocardial infarction, stroke, peripheral artery disease and congestive heart failure) complications and early death if not managed well (Fowler, 2008; Vinik and Flemmer, 2002). Diabetic retinopathy is the most common diabetic complication. Retinopathy is an eye disease that is characterized by damage to the small blood vessels supplying the eyes and leads to blurred vision, often progressing to blindness. Nephropathy is a kidney disease that arises because of damage to the small blood vessels within the kidney, leading to impaired kidney function or total dysfunction. Diabetes mellitus is the leading cause of chronic nephropathy. Neuropathy or nerve damage, is a

common complication of DM and injuries often go unnoticed, resulting in ulceration and amputation in extreme cases. Macrovascular complications are associated with cardiovascular disease (CVD). The development of DM complications depend on the duration and severity of hyperglycaemia (Fowler, 2008).

1.7 Epigenetics

Epigenetics refers to heritable changes in gene expression that are not due to differences in the DNA sequence and reflect the interplay between genetic and environmental factors (Eccleston et al., 2007; Krupanidhi et al., 2009). Epigenetic mechanisms include chromatin remodelling, histone modification, genomic imprinting, DNA methylation and non-coding RNAs such as long non-coding RNAs and microRNAs (miRNAs) (Pheiffer et al., 2016; Reik, 2007; Yokochi and Robertson, 2002).

MicroRNAs, short and highly conserved non-coding RNA, molecules are important mediators of biological function (Fabian et al., 2010; He et al., 2007; Rottiers and Näär, 2012), with reports suggesting that up to 60% of our genome is regulated by miRNAs (Bajan and Hutvagner, 2014; Yuan et al., 2016). They are dysregulated during many diseases, including T2D (Filios and Shalev, 2015; Rome, 2013; Wang et al., 2014; Zhao et al., 2010) illustrating their fundamental role in disease pathophysiology.

1.7.1 MicroRNAs

MiRNAs are approximately 22 nucleotides long and regulate gene expression post-transcriptionally (He et al., 2007; Rottiers and Näär, 2012). They bind to the 3'-untranslated region (UTR) of messenger RNA (mRNA), leading to mRNA degradation or inhibition of translation. One miRNA can regulate up to 200 different mRNA targets and one mRNA molecule can be regulated by more than one miRNA (Rottiers and Näär, 2012) . Since they are predicted to regulate up to 60% of protein coding genes (Bajan and Hutvagner, 2014; Yuan et al., 2016), their dysregulation has been associated with aberrant gene expression during many diseases including cancer, neurological and metabolic disorders. MiRNAs associated with T2D are indicated in Table 2.

Table 2. MiRNAs associated with Type 2 diabetes.

MicroRNA	Target tissue	Function	Reference
miR-375	Pancreas	Insulin secretion, islet development	(Baroukh and Van Obberghen, 2009)
miR-124a	Pancreas	Islet development	(Gauthier and Wollheim, 2006)
miR-9	Pancreas	Insulin secretion	(Shantikumar et al., 2012)
miR-29a,b,c	Muscle, adipose, liver	Glucose transport	(He et al., 2007)
miR-143	Adipose	Adipocyte differentiation	(Mao et al., 2013)
miR-145	Soft tissue, Colon	Cell proliferation	(Fan et al., 2012; Zhang et al., 2016)
miR-133	Heart	Heart development	(Chavali et al., 2012)
miR-let-7b	Pancreas	Insulin exocytosis	(Tang et al., 2008)
miR-96	Pancreas	Insulin secretion	(Shantikumar et al., 2012)
miR-195	Kidney	Apoptosis	(Chen et al., 2012b)
miR-222	Adipose	Upregulated during hyperglycaemia	(Chen et al., 2014)
miR-126	Heart	Negative correlation between miR-126 expression and development of macrovascular complications	(Babu et al., 2016; Fernandez-Valverde et al., 2011)
miR-296	Pancreatic β-cell line MIN6	Downregulated in hyperglycaemic conditions	(Tang et al., 2009)
miR-34a	Heart	Impaired angiogenesis in diabetes	(Arunachalam et al., 2014)
miR-146b	Retinal vascular endothelial cells, liver, pancreatic β-cells	Inflammation in diabetes, apoptosis of β-cells	(Fred et al., 2010; Fulzele et al., 2015; Prattichizzo et al., 2015; Roggli et al., 2010)
miR-30d	Pancreas, heart	Insulin transcription, Cardiomyoceyte apoptosis	(Li et al., 2014; Tang et al., 2009)
miR-320	Cardiac vascular endothelium	Upregulated in GK rats with impaired angiogenesis	(Wang et al., 2009)
miR-21	Liver, kidney	Upregulated in diabetes and leads to reduced glucose-induced insulin secretion	(Roggli et al., 2010)
miR-192	Kidney	Development of diabetic nephropathy	(Kato et al., 2007; Krupanidhi et al., 2009)
miR-15a, b	Pancreas	Pancreatic endocrine differentiation	(Fernandez-Valverde et al., 2011)
miR-216	Pancreas	Pancreatic endocrine differentiation	(Fernandez-Valverde et al., 2011)
miR-217	Pancreas	Pancreatic endocrine differentiation	(Fernandez-Valverde et al., 2011)

1.7.1.1 MicroRNA base pairing to target mRNA

MiRNAs exert their function by complimentary base pairing of their seed sequence to the 3' UTR of target mRNA molecules (Rottiers and Näär, 2012). The seed sequence is a 2 to 8 nucleotide region at the 5' end of the mature miRNA molecule (Figure 3), which is complementary to the target mRNA sequence. Base pairing of the 3' end of the miRNA to the target mRNA is not strictly required, but helps to stabilize the miRNA-mRNA complex. Bulges in the miRNA-mRNA complex occur due to the mismatching of bases from nucleotide 10-12 in the miRNA molecule. These bulges inhibit the translocation of mRNA translation machinery, resulting in translational repression. MiRNAs increase the efficacy of translational repression by additional base pairing with its target.

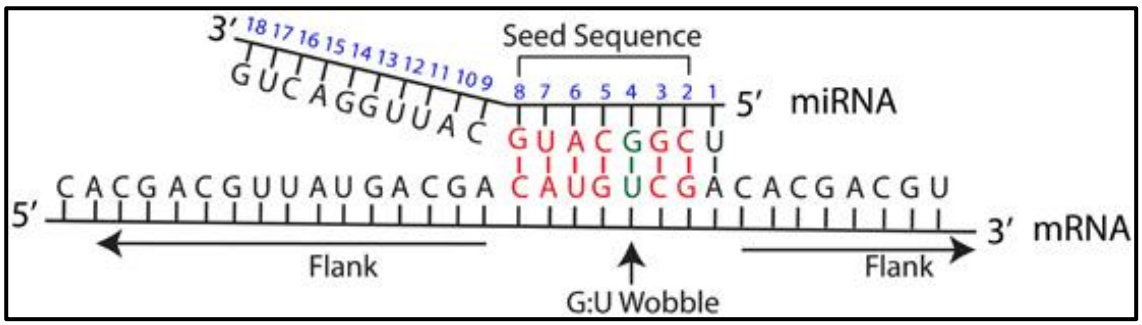

Figure 3. MicroRNA base pairing to the 3'UTR of target mRNA molecules.
The seed sequence, the region of the miRNA molecule that binds mRNA 3' UTR, provides most of the binding specificity. Binding of miRNAs to their target mRNA mediate translational inhibition or mRNA degradation. *A*-Adenine. *C*-Cytosine. *G*-Guanine. *U*-Uracil.

1.7.1.2 Biogenesis

MiRNA genes are transcribed by RNA polymerase II in the nucleus to produce primary miRNA (pri-miRNA) transcripts (Figure 4) (Bajan and Hutvagner, 2014; Fabian et al., 2010; Filios and Shalev, 2015; Ha and Kim, 2014). Pri-miRNAs are 60-70 base pair (bp) molecules with a stem loop structure that is recognized and spliced by the nuclear RNase III enzyme, Drosha, to produce precursor miRNA (pre-miRNA). Pre-miRNAs are double stranded molecules that consists of a guide and passenger strand (Meijer et al., 2014) that are transported into the cytoplasm by RAN-GTP energy dependent Exportin 5 transmembrane proteins. In the cytoplasm, another RNase III enzyme, Dicer, further splices the pre-miRNA molecule by removing the stem loop structure, while Argonaute (AGO2) proteins unwind the miRNA duplex, to produce the mature, active, single stranded miRNA molecule. These AGO2 proteins then facilitate the incorporation of the mature miRNA into the AGO-containing RNA-induced silencing complex (RISC) in a manner that leaves the seed sequence exposed for interaction with target mRNAs. The miRNA- RISC (miRISC) complex is guided to target mRNAs, where the seed sequence of mature miRNAs bind to mRNA targets by Watson-Crick base-pairing (Suzuki et al., 2012).

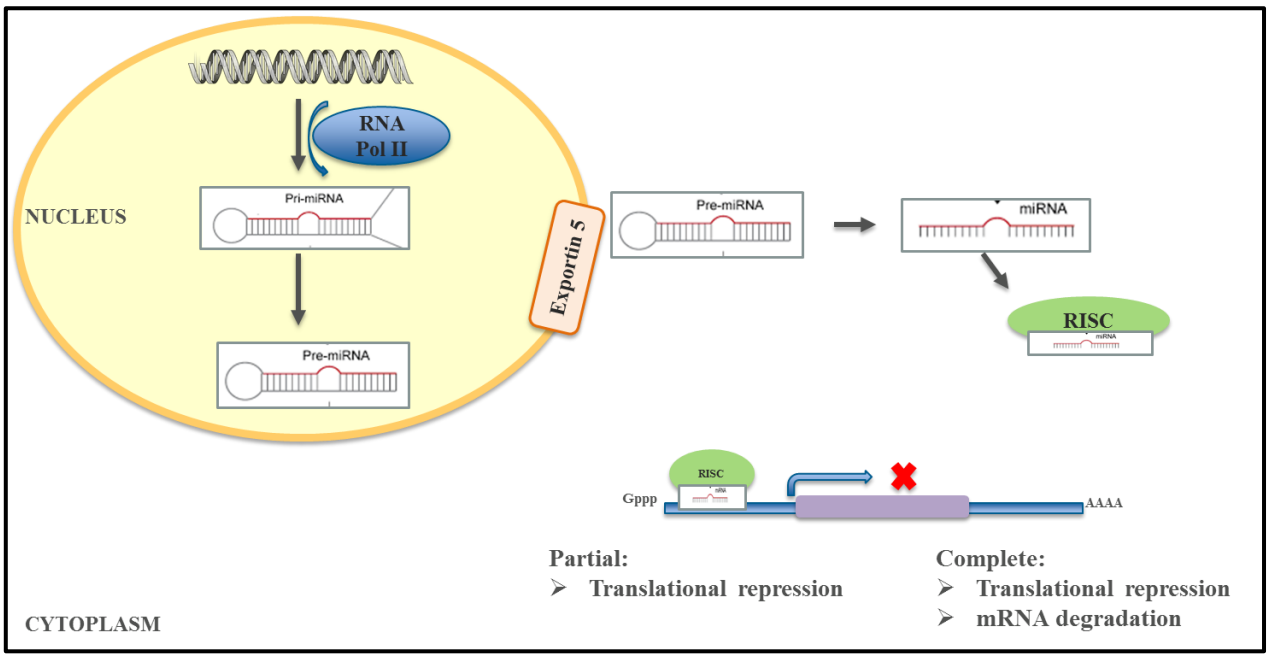

Figure 4. Schematic representation of the biogenesis of the mature miRNA molecules.
MiRNAs are transcribed in the nucleus, where they undergo several processes before being transported to the cytoplasm to mediate their biological function.

1.7.1.3 Nomenclature

The miRBase registry (http://www.mirbase.org/) is a website that provides information on miRNA nomenclature, as well as miRNA gene targets and sequences (Griffiths-Jones et al., 2006). According this registry, there are four characteristics to naming miRNA molecules. The first one describes the species in which the miRNA was discovered, i.e. miRNAs discovered in humans (*Homo sapiens*) has the prefix ***hsa***-miR-99. Secondly, mature miRNA sequences are designated as "mi**R**", and precursor hairpin structures and genes as "mi**r**". MiRNAs are also named to identify orthologous and paralogous sequences. MiRNA orthologues in the mouse and human genomes are named *hsa*-**miR-99** and *mmu*-**miR-99**, respectively. Whilst paralogous sequences within the same species that differ only at one or two positions are designated by a letter suffix, i.e. *mmu*-miR-99**a** and *mmu*-miR-99**b** in the mouse. Precursor miRNA sequences that give rise to identical mature miRNAs have numbered suffixes, i.e. *mmu*-mir-99-**1** and *mmu*-mir-99-**2** in the mouse.

1.7.1.4 Regulation of microRNA expression

The mechanisms underlying miRNA expression are not known, although it has been demonstrated that the promoters of miRNA genes have CpG sites that are susceptible to methylation, suggesting that miRNAs are themselves regulated by epigenetic mechanisms such as DNA methylation (Strmsek and Kunej, 2015).

DNA methylation has been identified as a mechanism regulating miRNA gene expression in 36 cancer types, including lung, hepatocellular carcinoma and breast cancer (He et al., 2015; Li et al., 2015; Shen et al., 2015; Singh and Campbell, 2013; Singh et al., 2016; Strmsek and Kunej, 2015; Suzuki et al., 2012). Several of these miRNAs have been shown to be associated with T2D, suggesting that DNA methylation as a mechanism regulating their dysregulation during T2D. Recently, studies have reported differential methylation of miRNA genes during T2D (Kameswaran et al., 2014). The increased expression of miR-375 which inhibits insulin secretion (Baroukh and Van Obberghen, 2009) during T2D may be due to decreased DNA methylation (Chang et al., 2014a; Cheng et al., 2013; Sun et al., 2014; Wang et al., 2014). Moreover, DNA methylation of let-7a-3 has been associated with diabetic nephropathy (Peng et al., 2015). Recent work in our laboratory has reported differential DNA methylation of miRNA genes during T2D (Pheiffer et al., 2016) and has suggested that DNA methylation represents an important mechanism regulating miRNA expression during T2D.

1.7.2 DNA methylation

DNA methylation is the most studied and best characterized epigenetic mechanism, and refers to the addition of a methyl group to the carbon 5' (C5) position of cytosine residues (C) within CpG dinucleotides (Bird, 2002, 1980). The modification is catalysed by the enzyme DNA methyltransferase (DNMT) (Figure 5). Methylation of CpG islands, unmethylated GC-rich regions with high levels of CpG dinucleotides in the promoter regions of genes, is generally associated with transcriptional repression of genes due to altering protein binding to target sites on DNA, while loss of DNA methylation is associated with gene activation (Bird, 2002) (Figure 6). Recently, CpG islands have been identified in non-promoter regions within (intragenic) or between (intergenic) genes (Illingworth et al., 2010). The function of these orphan CpGs has not been fully elucidated although evidence has suggested that they are transcription start sites for nearby annotated genes or non-coding RNAs (Deaton and Bird, 2011).

DNA methylation plays an important regulatory role in cellular physiology, particularly during gene regulation, growth, embryonic development and differentiation (Pradhan et al., 1999; Yokochi and Robertson, 2002). Aberrant DNA methylation has been associated with many diseases such as cancer (Baylin and Ohm, 2006; Jones and Baylin, 2002; Rhee et al., 2002), T2D (Gilbert and Liu, 2012; Krupanidhi et al., 2009; Ling and Groop, 2009), CVD (Buysschaert et al., 2008; Zhong et al., 2016) and mental illness (Robertson, 2005).

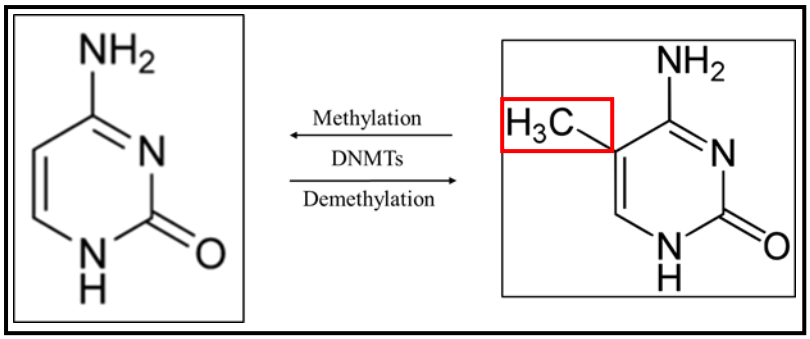

Figure 5. Methylation of C5 of cytosine bases.
DNA methyltransferase (DNMT) catalysis the methylation of Cs within CpG dinucleotides. DNA methylation is reversible (demethylation), whereby methyl groups are removed from methylated cytosine residues.

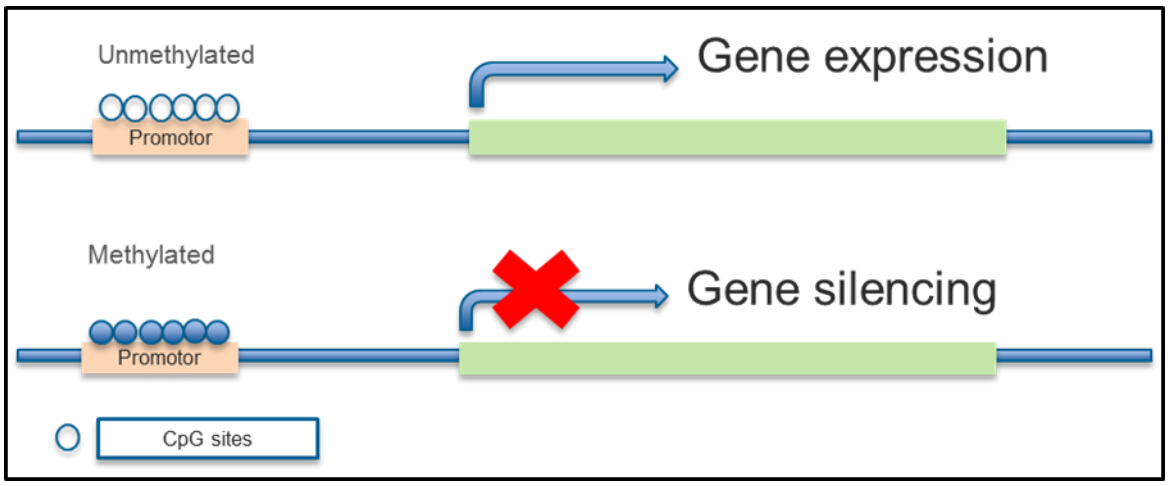

Figure 6. Effect of DNA methylation on transcription.
In unmethylated promoters, the DNA sequence is accessible to the transcription machinery and gene expression is activated, whereas transcription is inhibited in genes wherein the CpG sites in the promotor regions are methylated.

1.7.2.1 DNA methyltransferases

Three main DNMTs are found in mammalian cells; DNMT1, DNMT3a and b (Chédin, 2011; Gowher and Jeltsch, 2001; Kaneda et al., 2004; Suetake et al., 2003). DNMT1 is responsible for the methylation of Cs of hemi-methylated DNA after replication and is referred to as the maintenance DNMT. DNA hemi-methylation is when only one of two (complementary) strands is methylated. DNMT3a and DNMT 3b is referred to as *de novo* DNMTs and methylates unmethylated CpGs (Kato et al., 2007). Although DNMTs show preference to specific DNA sequences, all DNMTs can participate in both maintenance and *de novo* methylation (Yokochi and Robertson, 2002).

1.7.2.2 CpG islands and CpG poor regions

In the context of DNA methylation, both CpG rich and CpG poor regions occur in the genome. As discussed previously, DNA methylation primarily occurs within CpG islands in the promotor regions

of genes (Ehrich et al., 2005; Jones and Baylin, 2002). The distribution of CpG islands is highly variable in the genome and among different cells types, thereby enabling tissue specific control of gene expression (Ehrich et al., 2005; Vinson and Chatterjee, 2012). CpG islands refers to repetitive genomic sequences ranging from 500-5000 bp (Jones and Baylin, 2002) and about 55-90% of all CpG dinucleotides within CpG islands are methylated, constituting approximately 3% of the genome. Exons and introns are referred to as CpG poor regions (Miranda and Jones, 2007). These CpG poor regions are methylated under normal cellular conditions, except during X-chromosome inactivation.

1.8 This study

1.8.1 Problem Statement

Type 2 diabetes is a major source of morbidity and mortality worldwide (International Diabetes Federation, 2015). In SA, recent estimates reported that the prevalence of T2D is 9%, increasing from 5.5% in 2000 (Bertram et al., 2013). Similarly, excess body weight, which contributes to about 90% of T2D cases in SA (Joubert et al., 2007) is rapidly increasing. In 2013 it was estimated that more than 60% of South African women are overweight, 42% of whom are obese (Ng et al., 2014). Since obesity is a major risk factor for T2D, the current trajectory of obesity will increase the prevalence of T2D, placing a major burden on the already over-burdened health system in SA.

1.8.2 Rationale

Type 2 diabetes is a complex metabolic disorder, with both genetic and environmental factors implicated in the development of this disease (Ling and Groop, 2009). Epigenetic modifications, such as miRNAs, reflect the interplay between genetic and environmental factors and provide a plausible mechanism to elucidate the biological processes and pathophysiology of T2D. Furthermore, the identification of the mechanisms that regulate these epigenetic signatures are important to facilitate the development of effective interventions to curb the rising T2D pandemic.

1.8.3 Hypothesis

We hypothesize that miRNAs that are dysregulated during T2D, are regulated by DNA methylation, and that these differentially methylated miRNA genes can regulate miRNA expression in mouse adipocytes cultured in different glucose concentrations.

1.8.4 Aim

The aim of this study was to investigate whether differential miRNA expression in women with T2D is regulated by DNA methylation, and to investigate whether these differentially methylated miRNA genes regulate miRNA expression in mouse adipocytes cultured in different glucose concentrations.

1.8.5 Objectives

- Identify differentially expressed miRNAs in women with T2D that are under the potential regulation of DNA methylation;
- Verify methylation status of miRNA genes using MassARRAY® EpiTYPER®; and
- Evaluate the methylation status of these miRNA genes in 3T3-L1 mouse adipocytes
    - Establish cell culture model and
    - Evaluate both DNA methylation and expression of candidate miRNAs.

2. Materials and Methods

The media and buffers used in the study are listed in the Appendix.

2.1 Participants

Participants in this study were women of self-reported "Coloured" ethnicity. This ethnic group refers to individuals of mixed ethnic ancestry with European, African and Asian origins dating back to about 350 years ago (de Wit et al., 2010). Different subsets of women were used for the different analyses. MiRNA for miRNA sequencing (miRNA-Seq) (Group A) and DNA for MassARRAY® EpiTYPER™ quantitative methylation analysis (Group C), were isolated from women who participated in the Human Biomarker Project (HBP) as described previously (Dias, 2016). Group A consisted of 12 age-, gender-, ethnicity- and body mass index (BMI)-matched normoglycaemic (NGT, n=4), impaired glucose tolerant (IGT, n=4) and type 2 diabetic (T2D, n=4) women, while Group C consisted of a different subset of NGT (n=3), IGT (n=2) and T2D (n=4) women from the HBP. DNA for methylated DNA immunoprecipitation sequencing (MeDIP-Seq) was extracted from NGT (n=3), IGT (n=3) and T2D (n=3) age-, gender-, ethnicity- and BMI-matched women (Group B) as previously described (Pheiffer et al., 2016). Participant characteristics are given in Table 7. This study was approved by the Health Research and Ethics Committee of Stellenbosch University (S15/04/096) and the Ethic Committee of the Medical Research Council (EC010-5/2013) (Appendix).

2.2 Selection of miRNA genes for verification with MassARRAY® EpiTYPER®

2.2.1 Experimental outline for selection of miRNAs

The experimental outline describing the selection process of differentially methylated miRNA genes for verification with the MassARRAY® EpiTYPER® is illustrated in Figure 7. Briefly, miRNAs isolated from peripheral blood mononuclear cells (PBMCs) of NGT, IGT and T2D women (Group A) underwent miRNA-Seq to identify differentially expressed miRNAs (Dias, 2016). DNA isolated from the whole blood of a different subset of NGT, IGT and T2D women (Group B), were subjected to MeDIP-Seq to identify differentially methylated miRNA genes (Pheiffer et al., 2016). Data obtained from the two analyses were integrated to identify miRNAs that were differentially expressed and whose genes were differentially methylated between NGT, IGT and T2D groups. Thereafter, DNA extracted from a different subset of women (Group C) was subjected to MassARRAY® EpiTYPER® quantitative methylation analysis to verify the differential methylation of miRNA genes identified by data integration.

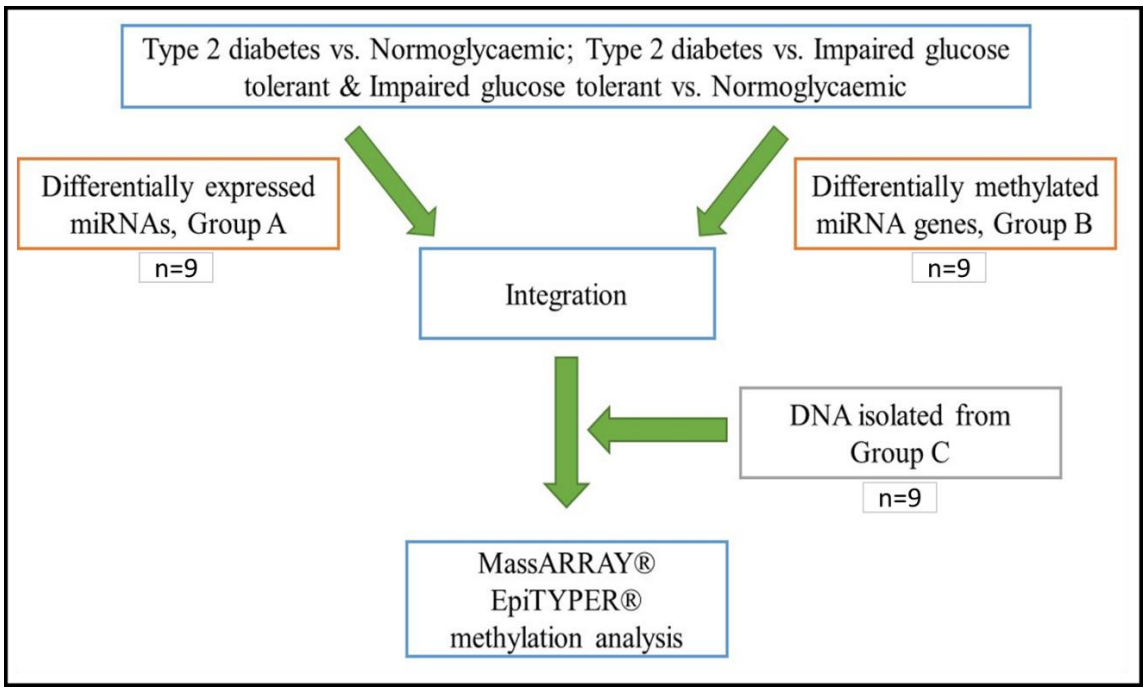

Figure 7. Identifying dysregulated miRNAs potentially regulated by DNA methylation.

2.2.2 Standardization of miRNA nomenclature

As discussed in section 1.7.1.3, miRNAs are named according to specific criteria (http://www.mirbase.org/). To facilitate data integration, the nomenclature of mature miRNAs, which were identified with miRNA-Seq, was changed to the same format as MeDIP-Seq data. The different formats in which miRNA genes were reported by these two techniques are illustrated in Figure 8. For example, the mature miRNA format hsa-miR-99a (miRNA-Seq) was changed to mir99a (MeDIP-Seq) to facilitate data integration with the Venny 2.1 tool.

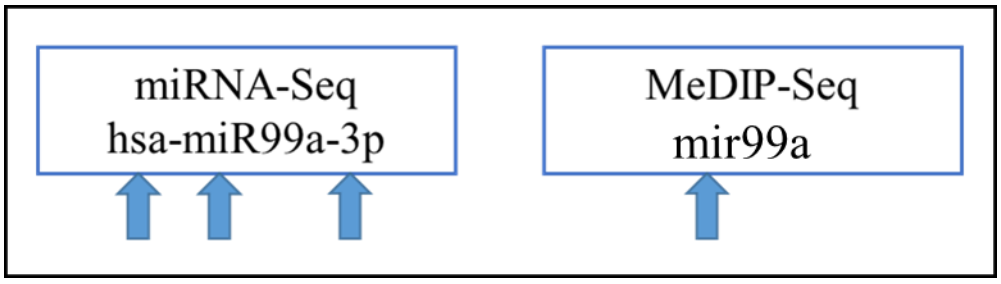

Figure 8. MiRNA annotation using miRNA-Seq and MeDIP-Seq.
Differences in miRNA nomenclature are indicated by the blue arrows. The 3p delineates on which strand the miRNA gene was located, in this example, the miRNA gene is located on the reverse strand (Michael Agostino, 2012).

2.2.3 Integration of miRNA sequencing and methylated DNA sequencing

To identify miRNAs under the potential regulation of DNA methylation during T2D pathogenesis, differentially expressed miRNAs identified by miRNA-Seq and miRNA genes that were

differentially methylated according to MeDIP-Seq were integrated using the web-based Venny 2.1 tool. MeDIP-Seq further grouped miRNA genes according their gene regions (promoter, intergenic and intragenic) as previously described (Pheiffer et al., 2016).

2.2.4 Selection of miRNA genes for MassARRAY® EpiTYPER® analysis

During the integration of the data obtained from both miRNA-Seq and MeDIP-Seq, several miRNA genes were identified that were both differentially expressed and differentially methylated. Due to the expensive nature of the MassARRAY® EpiTYPER® analysis, not all of these miRNA genes could be analysed. A selection of miRNA genes for further analysis were made based on miRNAs literature has suggested to be involved in T2D pathophysiology and miRNA genes that showed interesting expression profiles with the miRNA-Seq.

2.3 DNA extraction

Genomic DNA was extracted from whole blood using the Wizard® Genomic DNA purification kit (Promega, Madison, USA), according to the manufacturer's recommendations. Briefly, 900 µL of Cell Lysis Buffer, supplied with the kit, was added to 300 µL of whole blood in a 1.5 mL microfuge tube (Eppendorf, Hamburg, Germany), thoroughly mixed by vortexing, and incubated at room temperature (RT) for 20 minutes. Tubes were mixed by inversion every five minutes to lyse erythrocytes and then centrifuged (5415R, Eppendorf) at 13,000 × g for 30 seconds. The supernatant was carefully removed ensuring no disruption of the cell pellet. The cell lysis step was repeated thrice or until the pellet formed after centrifugation was white in colour. Thereafter, the pellet was resuspended by vortexing briefly, 300 µL of Nucleic Lysis Solution was added and mixed by pipetting up and down seven times to lyse white blood cells. Another 100 µL of Nucleic Lysis Solution was added to tubes where clumps of cells were still visible, followed by incubation at 37ºC for 60 minutes. Thereafter, 130 µL of Protein Precipitation Solution was added to the nuclear lysates and the tubes were vortexed for 30 seconds. Tubes were centrifuged at 13,000 × g for three minutes, where after proteins were visible as a dark brown pellet at the bottom of the tube. The supernatant of each tube was transferred to clean 1.5 mL microfuge tube containing 200 µL of RT isopropanol, gently mixed by inversion and incubated at -20ºC overnight. After the overnight incubation, tubes were centrifuged at 13,000 × g for two minutes, supernatants decanted and the DNA pellets were washed twice with 100 µL of 70% (v/v) ethanol. After the final wash step, most of the ethanol was removed and the DNA pellet was air-dried for 30 minutes. The DNA pellet was resuspended in 100 µL of DNA Rehydration Solution and the concentration and purity was assessed by measuring its wavelength at 260 nm (A_{260}), 280 nm (A_{280}) and 230 nm (A_{230}), respectively, using the Nanodrop-1000

spectrophotometer according the manufacturer's recommendations (Nanodrop Technologies, Wilmington, USA). DNA of good quality had an $A_{260/280}$ ratio (protein or phenol contamination) of 1.7-1.9 and an $A_{230/260}$ ratio (EDTA, salt and other contaminants) of 1.8-2.0. DNA was then aliquoted and stored at -20ºC.

2.4 MassARRAY® EpiTYPER® quantitative methylation analysis

The MassARRAY® EpiTYPER® allows high-throughput, highly accurate and sensitive quantitative CpG specific methylation analysis (Liu et al., 2016; Thompson et al., 2009). An illustration of the MassARRAY® EpiTYPER® workflow is illustrated in Figure 9. Firstly, DNA is bisulfite treated to enable the conversion of unmethylated cytosine (C) to uracil (U). Thereafter, methylation specific primers are used to amplify the bisulfite converted DNA, which then undergoes several processes. These processes include Shrimp Alkaline Phosphatase (SAP) treatment to deactivate unincorporated dNTPs left in the PCR reactions, *in vitro* transcription to convert the single-strand DNA to RNA; followed by base specific cleavage of the reverse strand at the base U forming fragments of different sizes. MALDI-TOF mass spectrometry separates the cleavage products, enabling differentiation of non-methylated DNA from methylated DNA based on the mass to charge ratio (m/z) of fragments that were formed. The larger the m/z, the larger the fragment. DNA with larger m/z contains methylated Cs. The MassARRAY® EpiTYPER® analysis was conducted by Inqaba Biotec (Pretoria, SA).

2.4.1 Primer design

Forward and reverse primers for the genomic coordinates obtained by MeDIP-Seq were designed using EpiDesigner, a web-based primer design tool recommended by the manufacturers of the MassARRAY® EpiTYERP® assay (http://www.epidesigner.com/; Agena Bioscience, San Diego, USA). EpiDesigner designs primers for bisulfite converted DNA where all unmethylated Cs are considered to be deaminated to form Us and are thus considered as thymine (T) (as during PCR Us in the target sequence become Ts in the PCR amplicons generated). For bisulfite conversion, double stranded DNA with the forward and the reverse strand delineated as A and B, respectively, in Figure 10, is used. During bisulfite conversion, DNA is denatured due to the lack of complementarity because of the C to U (and thus T) conversion. Only the forward strand i.e. strand A (Figure 10) is amplified during the PCR amplification reaction.

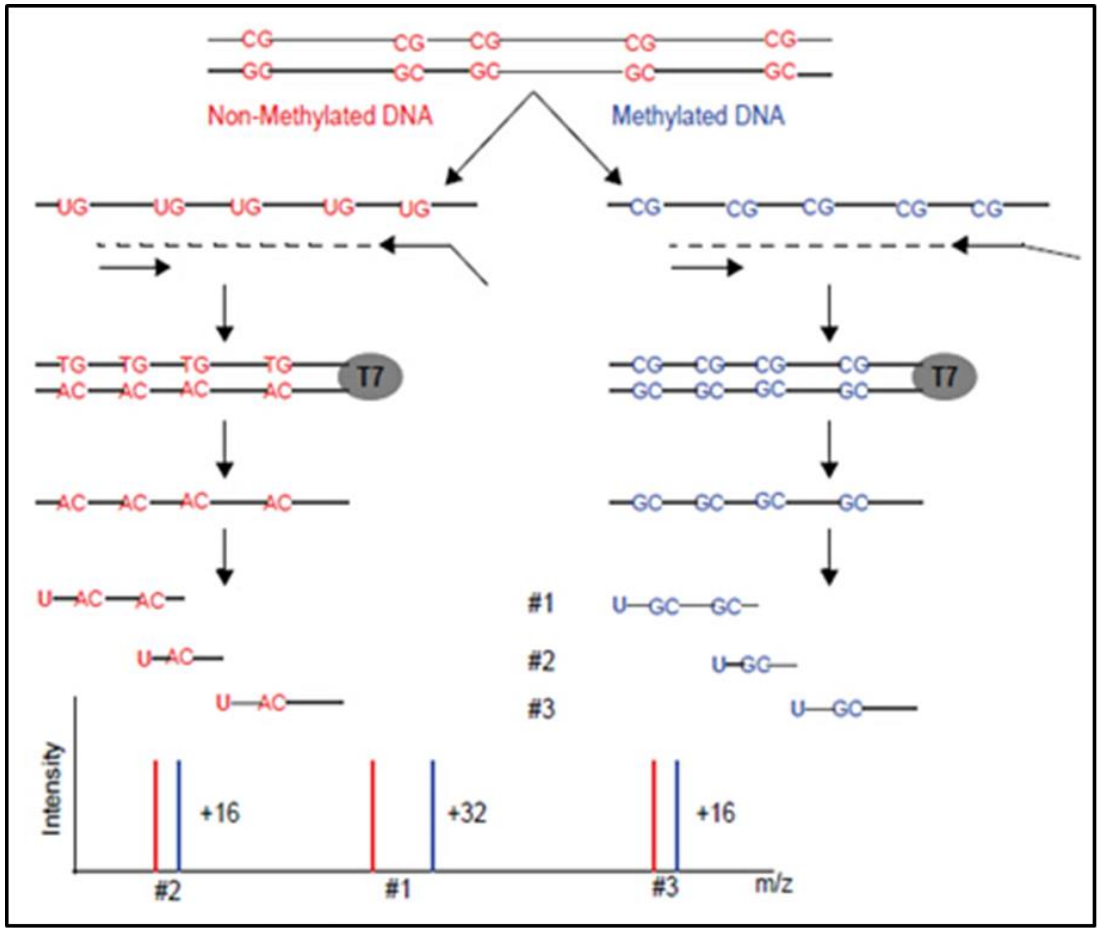

Figure 9. Overview of the MassARRAY® EpiTYPER® assay.
The red and blue sequences represent unmethylated and methylated DNA respectively. After bisulfite conversion and PCR amplification, all Cs were replaced with Us in the red sequence, while no changes were made in the blue sequence. The amplicons produced by the PCR reaction was then treated with SAP, underwent *in vitro* transcription and a base specific cleavage reaction. The MassARRAY® EpiTYPER® culminated in the differentiation of unmethylated and methylated DNA by using MALDI-TOF mass spectrometry.
m/z: mass to charge ratio.

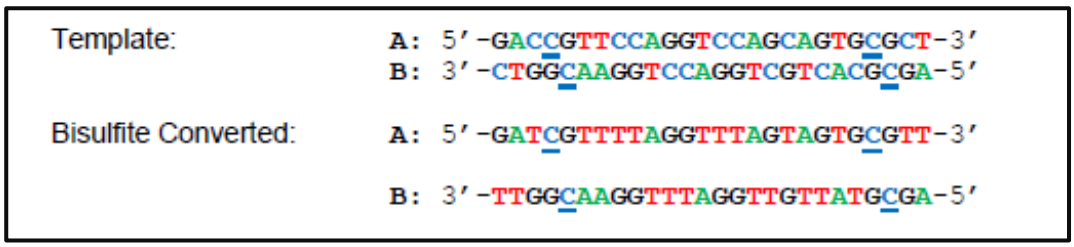

Figure 10. Template DNA and single-stranded DNA obtained after bisulfite conversion.
Different colours indicate the four DNA bases A, C, G, T, and underlined Cs are methylated. During bisulfite treatment, DNA is denatured, resulting in single-stranded DNA with strands that are no longer complementary due to the deamination of unmethylated Cs.

The EpiDesigner program designs the forward and reverse primers on the forward strand, as illustrated in Figure 11.

Figure 11. Forward and reverse primers for amplification of bisulfite converted DNA.
The reverse and forward primers are designed on the bisulfite converted sequence of the forward strand. A primer containing a CpG dinucleotide with uncertain methylation status (Y), is designed containing either a C- or T-residue.

To facilitate *in vitro* transcription, a T_7 promoter tag and an 8-mer bp insert was added to the 5' end of the reverse primer and a 10-mer tag sequence to the forward primer, as illustrated in Figure 12. The purpose of the T_7 promotor tag is to enable the generation of RNA from converted DNA, which can be cleaved by specific RNAse enzymes. The 10-mer tag is added to the forward strand to balance the forward and reverse primers.

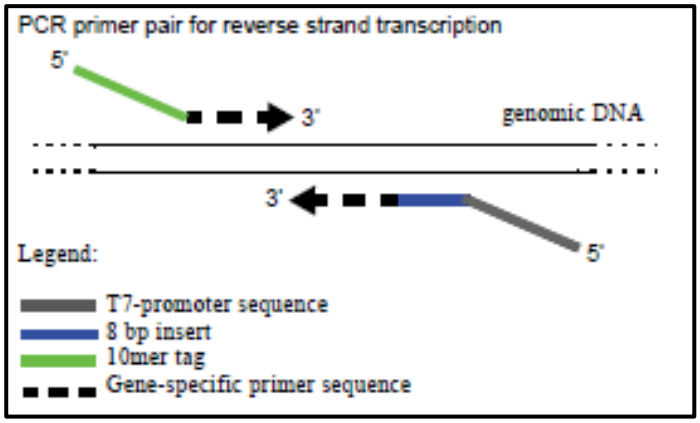

Figure 12. Primer design for in vitro RNA transcription.
The miRNA gene sequence is indicated as a solid black line. The reverse primer (bold, black dotted line with arrow) containing the T_7 tag and 8-mer bp insert, is indicated below the miRNA gene sequence. The forward primer (bold, black dotted line with arrow) containing the 10-mer bp insert is indicated above the sequence.

A screenshot of the EpiDesigner assay design is illustrated in Figure 13. The default primer melting temperature (Tm) and primer size (outlined in green) were used since these parameters were already optimised by the program. For DNA of good quality, the product size minimum (outlined in blue) was increased to 150 bp, while the rest of the parameters in that row were kept the same. Product CpGs refers to the number of CpGs contained within a target sequence, whereas the primer non-CpGs represent Cs that are not in a CpG dinucleotide context (outlined in yellow). No changes were made to the primer non-CpG Cs, the poly X and T settings. However, when no primers could be designed on the forward strand, the stringency of these settings were lowered, or the program was instructed to design primers on the reverse strand as well. The default settings for the Mass Window section (outlined in orange) was used. The Mass Window parameter specifies the mass range within which primers can be designed. Only CpGs in the T-reaction was analysed (outlined in purple). The T reaction refers to the change in nucleotide sequence after bisulfite treatment and the generation of T-rich PCR amplicons.

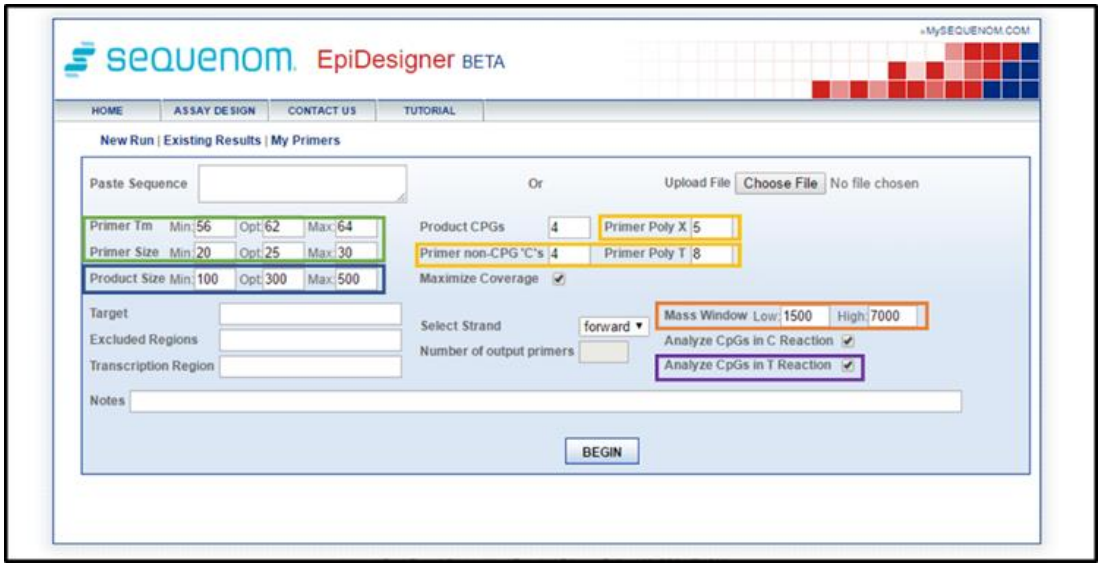

Figure 13. Screenshot of the primer design program.
The primer design software used to design the primers for amplification of methylated DNA, EpiDesigner, recommends primer pairs for individual assays. The primer Tm was set at a range of 56-64ºC and the primer size at a range of 20-30 nt. The primer Poly X was set at 5bp, the primer Poly T at 8bp and the primer non-CpG Cs at 4. The range for the product size after PCR amplification was set to 100-500 bp. The Mass Window was set to 1500-7000 and primers for only the T-reaction was designed. *Primer Tm:* Primer melting temperature. *Primer Poly X:* The maximum number of a mono-nucleotide repeat allowed in the primer sequence. *Primer Poly T:* The maximum number of T repeats allowed in the primer sequence.

2.4.2 Bisulfite conversion

Bisulfite conversion is considered the gold standard for DNA methylation analysis, allowing for the discrimination between methylated and unmethylated Cs at single base resolution (Patterson et al.,

2011). The first step of bisulfite conversion involves the sulphonation of unmethylated Cs to cytosine-sulphonate. Thereafter cytosine-sulphonate is deaminated to uracil-sulphonate, which is desulphonated to Us (Figure 14). Methylated Cs are resistant to bisulfite conversion and will therefore not be converted to Us (Figure 15).

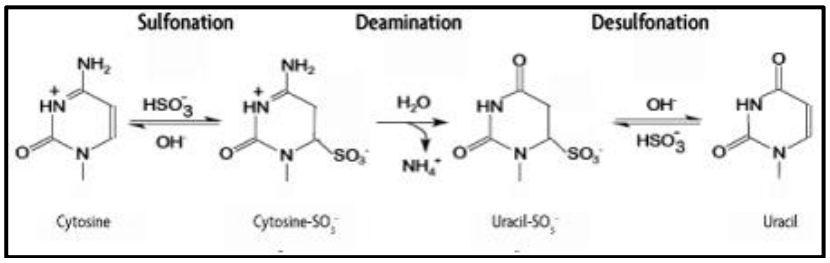

Figure 14. The bisulfite conversion of unmethylated Cs.
Bisulfite conversion is a three-step chemical process that culminates in the conversion of unmethylated Cs to Us.

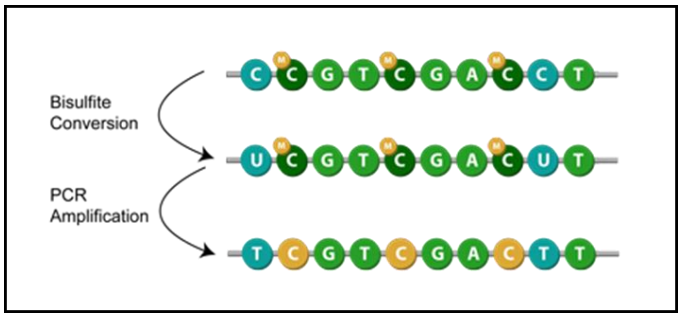

Figure 15. The effect of bisulfite conversion on DNA.
Unmethylated Cs (indicated in blue) are converted to Us, and then Ts after PCR amplification. While methylated Cs (indicated in dark green with gold M attached) are resistant to bisulfite conversion.

Bisulfite conversion was conducted using the EZ DNA Methylation kit™ (Zymo Research, Irvine, USA) according to the manufacturer's instructions using 1.5 mL microfuge tubes. Briefly, 5 µL of M-Dilution buffer (supplied with the kit) was added to 1 µg of DNA, and adjusted to a total volume of 50 µL with water. Thereafter, samples were incubated at 37°C for 15 minutes, followed by the addition of 100 µL of CT Conversion Reagent (supplemented with water and M-Dilution Buffer according to the protocol), lightly vortexed, and incubated in the dark at 50 °C for 16 hours. Thereafter samples were incubated on ice for 10 minutes, 400 µL of M-Binding buffer was added, and the samples were mixed by pipetting up and down six times. Samples were loaded into a Zymo-Spin™ IC Column in a 2 ml collection tube (Zymo Research). Thereafter 100 µL of M-Wash buffer was added and the spin columns were centrifuged with the Microfuge 20 centrifuge (Beckman Coulter Life Sciences, Brea, California, USA) at 13, 000 × *g* for 30 seconds. Thereafter 200 µL of M-Desulphonation buffer was added to the column, after which spin columns were incubated at RT for

20 minutes and centrifuged at 13, 000 × *g* for 30 seconds. Columns were washed by adding 200 µL of M-Wash buffer and centrifuging at 13, 000 × *g* for 30 seconds. The column was placed into a clean 1.5 mL microfuge tube, and DNA eluted by pipetting 40 µL of M-Elution buffer directly to the column membrane, incubating spin columns at RT for one minute, and then centrifuged at13,000 × *g* for 30 seconds at RT. This step was repeated to ensure that all DNA was eluted from the spin column.

DNA was quantified and its purity assessed using the Nanodrop 3300 spectrophotometer (Thermo Fisher Scientific, Massachusetts, USA) and the RiboGreen® RNA reagent kit (Thermo Fisher Scientific). RiboGreen® is a sensitive fluorescent nucleic acid stain that binds RNA and single stranded DNA. DNA was quantified by adding 2 µL of RiboGreen® dye to 2 µL of bisulfite-converted DNA, where after, samples were loaded on the pedestal of the Nanodrop 3300.

2.4.3 Polymerase chain reaction

Polymerase chain reaction (PCR) amplification was conducted using the Agena Biosciences PCR accessory kit (Sequenom, San Diego, USA) with a Hotstart Taq polymerase (Qiagen, Hilden, Germany), according to the manufacturer's instructions. Briefly, 1 µL (5 ng/ µL) of bisulfite converted DNA was added to the wells of a 96-well plate (Corning Inc., Corning, USA) containing 9 µL of the PCR reaction mix as shown in Table 3. The plate was sealed with sealing film and centrifuged for one minute at 560 × g (Allegra X-12, Beckman Coulter Life Sciences, Brea, USA) and placed in a thermocycler (Thermo 1, Thermo Fisher Scientific). PCR conditions were 94°C for 4 minutes to denature double stranded DNA, 45 cycles of 94°C for 20 seconds, 56°C for 30 seconds to anneal primers to substrate DNA strands and 72°C for one minute to extend the produced amplicons, followed by a final cycle of 72°C for three minutes.

Table 3. EpiTYPER PCR proctocol for a 10 µL reaction.

Reagent	**Volume (µL)**
10 x PCR Buffer	1.00
dNTP 25 mM each	0.08
PCR enzyme (5 u/µl)	0.08
Forward primer (1 µM)	2.00
Reverse primer (1 µM)	2.00
Distilled H_2O	3.84
DNA	1.00
Total Reaction volume	10.00

2.4.4 Processing EpiTYPER® reactions in 96-well plates

2.4.4.1 Shrimp Alkaline Phosphatase treatment of PCR products

Shrimp Alkaline Phospatase (SAP) neutralizes unincorporated dNTPs after PCR amplification of bisulfite converted DNA by dephosphorylating these dNTPs, thereby ensuring that they cannot be used in further reactions. The SAP (included in the EpiTYPER® kit, Sequenom) solution was prepared according to the manufacturer's instructions in a clean 1.5 mL microfuge tube as shown in Table 4 and 4 µL dispensed into each well of a 96-well plate (Corning Inc.). Thereafter, 6 µL of the PCR product (section 2.4.3) was added to each well. A plastic seal was placed over the plate and the SAP/PCR mixture was centrifuged at 3, 000 × g (Allegra X-12, Beckman Coulter Life Sciences) for one minute. The plate was then incubated in a thermocycler (Thermo 1, Thermo Scientific) at 37°C for 20 minutes, 85°C for five minutes and 4°C overnight, after which it was processed further.

Table 4.Preparation of the SAP solution.

Reagent	**Volume (µL)**	**Mastermix (µL)**
RNase free ddH_20	3.4	374.0
Shrimp Alkaline Phospatase	0.6	66.0
Total	4.0	440.0

2.4.4.2 The MassCLEAVE™ reaction

The MassCLEAVE™ (hMC) reaction was prepared using the EpiTYPER® Complete Reagent Set and SpectroCHIP Set (Sequenom), according to the manufacturer's instructions. Briefly, the SAP/ PCR mixture underwent *in vitro* RNA transcription and base-specific cleavage by RNase A (included in the kit) at converted Us to enable differentiation of methylated and unmethylated DNA according to size and mass, depending on the sequence changes generated by bisulfite treatment. Differences are detected using the MassARRAY® EpiTYPER® system (Sequenom), which combines MALDI-TOF mass spectrometry with the EpiTYPER® analytic software to generate quantitative data for each analysed fragment.

2.4.4.3 *In vitro* transcription reaction

The *in vitro* transcription reaction was prepared by adding the reagents (included in the EpiTYPER® Complete Reagent Set) in order of appearance in Table 5 below. Thereafter, 50 µL of the mixture was dispensed into each well of row H of a clean 96-well assay plate (Corning Inc.) as shown in Figure 16. The sample plate was sealed with film making sure that all the edges were sealed off properly. The 96-well plate that contained the SAP treated PCR amplicons was removed from the thermocycler. This SAP/PCR plate as well as the T Cleavage/RNase A cocktail plate was centrifuged

(Allegra X-12, Beckman Coulter Life Sciences) at 540 × *g* for one minute. The plate seals were removed from both plates in order of their usage. Two microliters per well from the SAP/PCR plate was transferred to the wells of a clean 96-well plate, changing tips between dispensing. The new plate was centrifuged at 540 × g for one minute and using a multichannel pipette (Gilson Inc., Middleton, USA), 5 µL of the T Cleavage/RNase A cocktail was added to each well of the new plate. Here, too, pipette tips were changed after each dispensing. Both the new plate and the SAP/PCR plates were sealed and the SAP/PCR plate was stored at -20ºC for future use. The new plate was centrifuged at 540 × g for one minute again. The new plate was incubated at 37ºC for three hours and processed immediately after.

Table 5.Preparation of the T Cleavage Transcription/RNase A cocktail for 5 µL reactions.

T Cleavage Transcription/RNase A cocktail	Volume (µL)	Mastermix for 96-well assay plate (µL)
RNase free ddH_2O	3.21	409.80
5× T7 polymerase Buffer	0.89	113.50
T Cleavage mix	0.22	28.00
CTT mix, 100 mM	0.22	28.00
T7 RNA & DNA Polymerase	0.40	51.00
RNase A	0.06	7.70
Total	5.00	638.00

*Mastermix volumes include approximately 33% overhang to account for possible pipetting errors.

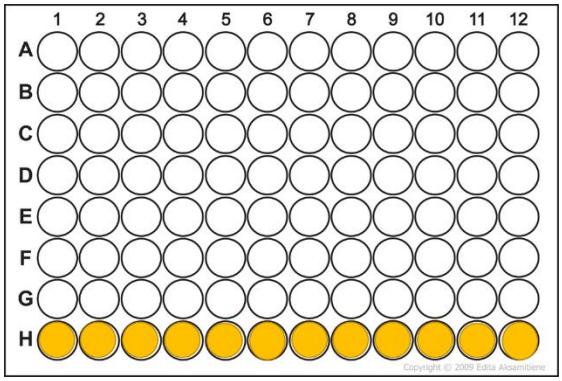

Figure 16. The T Cleavage/RNase A cocktail dispensed into each well of row H.

2.4.4.4 Conditioning the hMC reaction products

The new plate containing the hMC reaction was conditioned, as it is important for optimal mass spectrometry analysis. This was conducted by using clean resin (included in the EpiTYPER® Complete Reagent Set) as described in Figure 17.

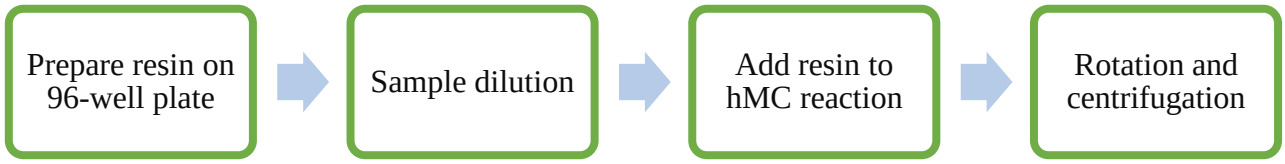

Figure 17. Steps for conditioning the hMC reaction.

2.4.4.5 Preparation of clean resin on a 96-well plate

Approximately 3 g of clean resin was transferred from its container onto a clean 96-well resin plate (Sigma-Aldrich, St Louis, USA) using a clean resin spoon and carefully spread into each well. The excess resin was removed from the plate using a clean resin scraper and deposited back into the resin container as illustrated in Figure 18. The clean resin plate was incubated at RT for 20 minutes.

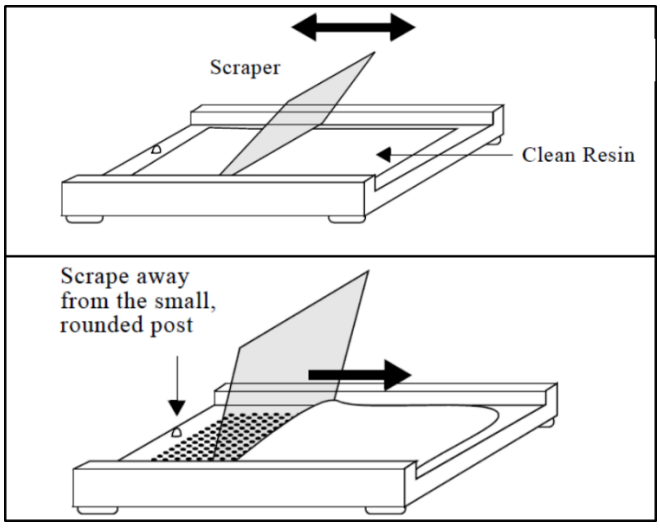

Figure 18. Adding and removing excess resin.

2.4.4.6 Sample dilution

During incubation of the 96-well resin plate, the new reaction plate containing the hMC (section 2.4.4.3) was removed from the thermocycler and centrifuged at 540 × g for one minute. Thereafter, 41 µL of water was pipetted into each well using a twelve-channel multichannel pipette (Gilson Inc.). The hMC plate was sealed and centrifuged at 540 × g for one minute.

2.4.4.7 Addition of clean resin to the hMC reaction products

The clean resin was added to the hMC plate by placing the hMC plate upside down onto the resin plate. Then, by holding the hMC and resin plates together, the plates were inverted so that the resin fell into the each well of the hMC plate. The resin plate was gently tapped to dislodge all the residual resin into the wells of the hMC plate.

2.4.4.8 Rotation and centrifugation of hMC Reaction Products

The hMC plates containing the resin were rotated using a rotator for 10 minutes at RT. The rotator rotated the hMC plate 360º perpendicular to its long axis. Thereafter, the hMC plate was centrifuged for five minutes at 3,200 × g.

2.4.4.9 Nanodispensing

Reaction products were transferred to the SpectroCHIP™ array using the MassARRAY® Nanodispenser RS100 (Sequenom) as shown in Figure 19. The Nanodispenser RS1000 is a self-contained, enclosed instrument that uses computer-controlled robotics to dispense nanoliter volumes of fluid from 96-well assay plates onto chips. The system has a video to monitor dispensing onto chips and has an auto-tuning system to correct for over- or under-dispensing. The Nanodispenser RS100's pins were washed before spotting samples onto the SpectroCHIP™ by sonication in 70% ethanol, rinsing in water, vacuum drying and rinsing with 0.1 M NaOH and 100% ethanol. Spotting refers to the transfer of nanoliters of samples onto the SpectroCHIP™ by the pins.

Figure 19. The MassARRAY Nanodispenser RS1000 with the SpectroCHIP.
The Nanodispenser RS1000 is shown in the left, upper corner inside the MassARRAY®. The enlarged pictures on the right side of the MassARRAY®, illustrates the SpectroCHIP upon which nano volumes of the samples are loaded.

2.4.5 MassARRAY® EpiTYPER® data analysis

Methylation values of individual CpG sites within miRNA genes were determined by the EpiTYPER® software. For each miRNA gene, the methylation at each of the CpG sites that were analysed, was added to obtain the methylation status of the entire miRNA gene sequence analysed. The additive methylation status of miRNA genes was averaged for individuals with T2D, IGT and NGT, and thereafter the different groups were compared.

2.5 Cell Culture

In vitro studies was conducted on 3T3-L1 mouse embryonic fibroblasts to establish a cell culture model for T2D pathophysiology to investigate the relationship between DNA methylation and miRNA expression. Cell culture was conducted by using aseptic techniques adhering to the standard operating procedures prescribed by the Tissue Culture laboratory, Biomedical Research and Innovation Platform, South African Medical Research Council. The experimental outline of the cell culture experiments is illustrated in Figure 20.

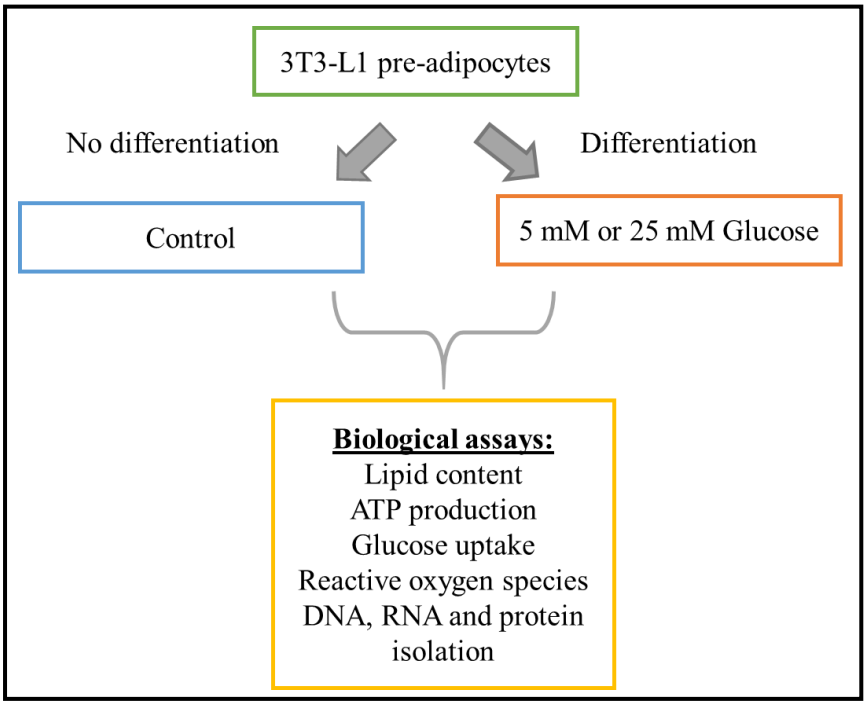

Figure 20. Experimental outline for cell culture of 3T3-L1 pre-adipocytes.

2.5.1 Cell line

Pre-adipocytes were obtained from the American Type Culture Collection (ATCC, Manassas, USA) and cells between passage seven (T7) and passage nine (T9) were used for experiments. The cells were grown in a controlled and consistent environment of 37ºC, 5% CO_2 in 96% humidified air.

2.5.2 Thawing of cryopreserved cells

Cryopreserved pre-adipocytes were removed from long-term storage in liquid nitrogen and placed on ice prior to use. Frozen vials were then placed in a water bath at 37ºC until at least 75% of the contents had thawed. Thereafter, vials were transferred to the biological safety cabinet and the cells pipetted into a 15 mL tube (Nest Scientific, Rahway, USA). The cells were then centrifuged at 800 x g for five minutes, after which the supernatant was aspirated and the cells were resuspended in 1 mL of pre-warmed complete growth medium (CGM) (Appendix). The cell suspension was transferred to a 75

cm^2 flask (Corning Inc., Corning, USA) containing 17 mL of pre-warmed CGM and mixed properly by pipetting up and down thrice. To ensure that all cells were removed from the vial, vials were washed with one millilitre of pre-warmed CGM, where after the mixture was transferred to the 75 cm^2 flask. The flask containing the cells was incubated at 37ºC with 96% humidity and 5% CO_2 and after 24 hours, the CGM was aspirated and replaced with 18 mL of fresh medium. The cells were subcultured when they were 70-80% confluent.

2.5.3 Subculture of 3T3-L1 pre-adipocytes

When cells reached 70-80% confluency, as visualised with an inverted light microscope (Olympus CKX31, Olympus Life Science, Waltham, USA), the CGM was aspirated and cells were rinsed with 8 mL of pre-warmed Dulbecco's phosphate buffered saline (DPBS; Lonza, Basel, Switzerland) to remove traces of serum. The flask was gently swirled, where after DPBS was aspirated, taking care to remove all DPBS. Thereafter, 2 mL of RT trypsin-versene (Lonza) was added directly to the cell monolayer and incubated at 37ºC for five minutes. The rounding of cells and their detachment from the flask surface was visualised under the microscope. Trypsinization was stopped by adding 8 mL of pre-warmed CGM to the flask and the contents of the flask was pipetted up and down at least five times to disaggregate cell clumps and ensure consistency of the cell density. The 10 mL cell suspension was transferred to a clean, sterile 50 mL tube (Nest Scientific) and centrifuged at 800 x g (SL 16R, Thermo Scientific) for five minutes. Thereafter, the supernatant was aspirated and the pellet was resuspended in 10 mL of CGM. Five hundred microliter of the freshly resuspended cell solution was pipetted into a clean 1.5 mL microfuge tube for cell counting, while the remaining cell suspension was incubated at 37ºC during cell counting.

2.5.4 Cell counting

Cells were counted using the Countess® Automated Cell Counter (Invitrogen, Carlsbad, USA), according to the manufacturer's instructions. A 10 µL aliquot of the cell suspension in the microfuge tube was transferred to a clean tube and mixed with 10 µL of Trypan Blue (Life Technologies, Carlsbad, USA), where after, 10 µL of this mixture was pipetted into a Countess® cell counting chamber slide. The counting chamber slide was inserted into the automated counter where both live (clear) and dead (blue) cells were counted.

2.5.5 Cryopreservation of cells

A suspension of 2 x 10^6 cells per mL was needed for the cryopreservation of cells to serve as stocks. After determining the concentration of cells/mL (section 2.5.4) and the concentration of cells in 10

mL media, the amount of freezing medium to add to cells to obtain the desired 2 x 10^6 cells per 1 mL concentration, was calculated. An example of this calculation is shown in Figure 21. The 50 mL tube containing the cell solution was centrifuged at 800 x g, the supernatant aspirated and the cell pellet was resuspended in sterile filtered freezing medium (Appendix). After the pellet was dissolved, 1 mL of the cell suspension was transferred to labelled, cold cryotubes (Corning Inc.) and temporarily placed on ice before being incubating at -80 °C overnight. The following day, tubes were transferred to liquid nitrogen for long-term storage.

Need: $2{,}0 \times 10^6$ cells/mL in each cryotube containing 1 mL cell suspension

Cell Count:

Total	$3{,}3 \times 10^6$ cells/mL
Live	$3{,}2 \times 10^6$ cells/mL
Dead	$1{,}0 \times 10^5$ cells/mL

Viability 97%

Cells in 10 mL:

$(3{,}2 \times 10^6 \text{cells/mL}) \times 10 = 3{,}2 \times 10^7 \text{cells}$

Thus, $\frac{3{,}2 \times 10^7 \text{cells}}{2{,}0 \times 10^6 \text{ cells/mL}}$ = 16 mL cell suspension can be prepared, i.e. add 16 mL Freezing media to cell pellet.

Figure 21. The calculation used to obtain cell concentrations for freezing.

2.5.6 Seeding cells into plates

Before seeding cells into plates, the procedure to thaw, maintain and subculture and split pre-adipocytes was followed as explained previously. For *in vitro* assays, cells were seeded into CellBIND® plates (Corning Inc.) at different seeding densities according to the assay plates used (Table 6). For the determination of intracellular lipid content, cell viability and glucose uptake, cells were seeded into 24-well plates, while cells for DNA, RNA and protein extractions were seeded into 6-well plates. Cells used to analyse oxidative stress were seeded into 96-well plates, of which only 54 wells were seeded as the perimeter wells were filled with 200 µL of DPBS (Lonza). No cells were seeded in the perimeter wells as media in these outside wells, evaporate quickly.

Table 6.Seeding densities

Plate	Volume cell suspension/well	Volume cell suspension/plate	Number of plates used/ experiment	Cell density/well
6-well	3 mL	20 mL	5	6 x 10^4
24-well	1 mL	25 mL	2	2 x 10^4
96-well	200 µL	15 mL	2	5 x 10^3

2.5.8 Adipocyte differentiation

Adipocyte differentiation is an eleven-day procedure and requires four different types of media (Appendix), a) CGM, b) adipocyte differentiation media (ADM), c) adipocyte maintenance media (AMM) with insulin and d) AMM only. Cells were differentiated using DMEM, with either 5 mM or 25 mM glucose, supplemented with 10% FBS or left undifferentiated in CGM for controls. The procedures for the preparation of media are described in the Appendix. After the plates were seeded, cells were cultured in CGM for three days at 37°, 5% CO_2 and 96% humidity until they reached 100% confluency. Upon confluency, CGM was aspirated and replaced with either CGM (undifferentiated control), 5 mM ADM or 25 mM ADM at the recommended volumes (Table 6) as shown in Figures 22 to 25, and incubated at 37ºC. This day was referred to as Day 0. The adipocyte differentiation timeline is shown in Figure 26. On day 3, the ADM was aspirated and replaced with 5.5 mM or 25 mM AMM with insulin, while the CGM was refreshed with new CGM. On Day 5, the AMM with insulin and CGM was refreshed with 5.5 mM or 25 mM AMM and fresh CGM, respectively. The respective media was refreshed again on Day 7. Day 8 was the day all assays were completed.

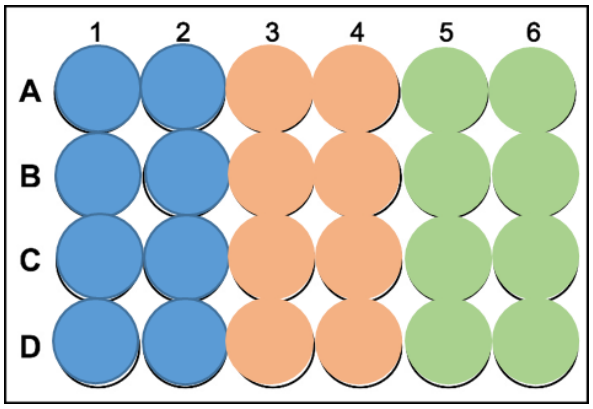

Figure 22. Plate layout for Oil Red O, Cell viability and Glucose Uptake assay.
Blue: Undifferentiated pre-adipocytes. *Orange*: Pre-adipocytes differentiated at 5.5 mM Glucose. *Green*: Pre-adipocytes differentiated at 25 mM Glucose.

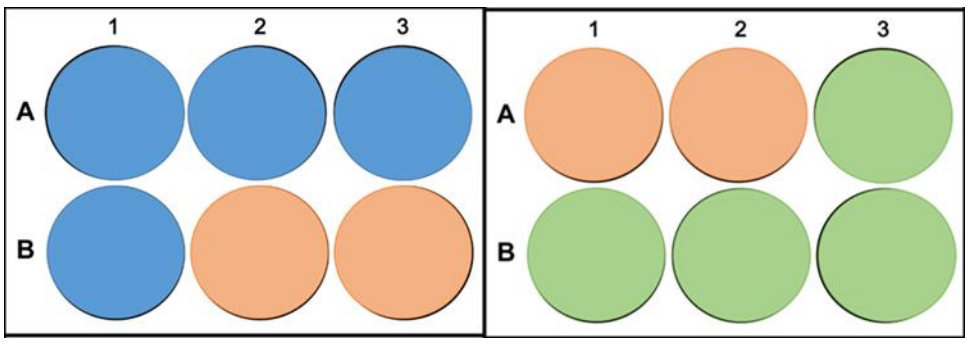

Figure 23. Plate layout for harvesting of cells for DNA and RNA isolation.
Blue: Undifferentiated pre-adipocytes. *Orange:* Pre-adipocytes differentiated at 5.5 mM Glucose. *Green:* Pre-adipocytes differentiated at 25 mM Glucose.

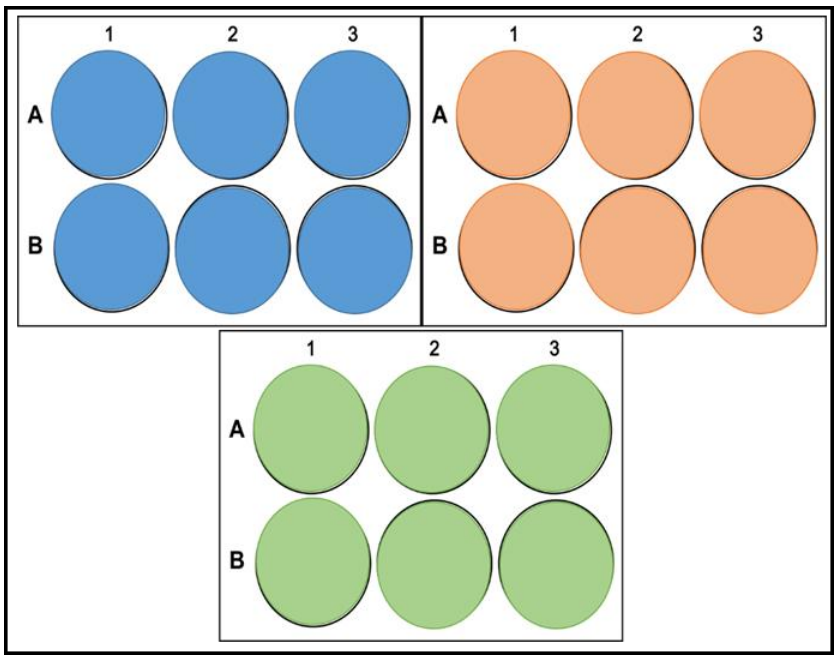

Figure 24. Plate layout for harvesting cells for protein isolation.
Blue: Undifferentiated pre-adipocytes. *Orange:* Pre-adipocytes differentiated at 5.5 mM Glucose. *Green:* Pre-adipocytes differentiated at 25 mM Glucose.

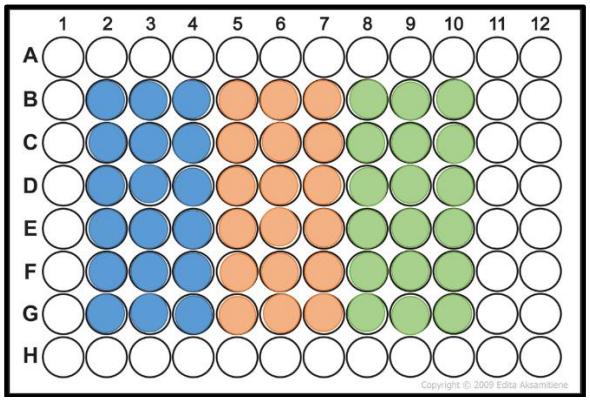

Figure 25. Plate layout for oxidative stress assessment for both DCFH-DA and JC-1 assays.
Blue: Undifferentiated pre-adipocytes. *Orange:* Pre-adipocytes differentiated at 5.5 mM Glucose. *Green:* Pre-adipocytes differentiated at 25 mM Glucose.

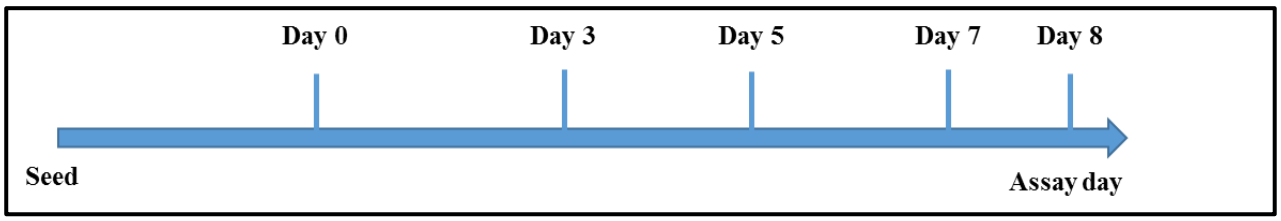

Figure 26. Timeline for adipocyte differentiation.
Cells were seeded in CGM that was refreshed on Day 0 for controls or replaced with ADM (5.5 mM or 25 mM) to differentiate pre-adipocytes. On days, Day 3, 5 and 7, the CGM media was refreshed for controls. Whereas on Day 3 for the differentiating pre-adipocytes, the ADM was removed and replaced with AMM (5.5 mM or 25 mM) with insulin. On Day 5, the AMM with insulin was replaced with just AMM (5.5 mM or 25 mM). The AMM was then refreshed on Day 7.

2.5.9 Oil Red O

Oil Red O (ORO) is a hydrophobic/lipid, diazo dye used in staining and quantifying lipids in cell culture (Wang et al., 2011). It is based on the principle that this stain is more soluble in neutral fats than in any other solutes. Therefore, upon adding the dye to formalin fixed cells, it dissolves into the lipids contained within mature adipocytes. The crystal violet stain (CV) is used to determine the cell density or cell viability as it binds to DNA and proteins of live cells that are bound to the culture plate surface. It discriminates between dead and alive cells in that it does not bind dead cells as these cells lift from the surface of the plate (Chiba et al., 1998).

After 9 days of differentiation (Day 8), cells were washed twice with pre-warmed DPBS and incubated for at least 30 minutes with DMEM (Sigma-Aldrich, St. Louis, USA) without phenol red media containing either 5.5 mM or 25 mM glucose, to completely remove phenol red traces. Thereafter, the cells were washed once with RT DPBS and fixed with 10% buffered formalin for 15 minutes and then washed again with DPBS. The DPBS was aspirated to near dryness and the culture plate was left to dry for five minutes at RT. When the plate was dry, 200 µL of the ORO working solution (Appendix) was added to each well of the plate and incubated at RT for 30 minutes. The ORO stain was then removed and the cells were washed thrice with 500 µL of distilled H_2O. The H_2O was removed to near dryness after the last wash and 200 µL of RT isopropanol was added to the wells. The culture plate was gently rocked back and forth to completely dissolve the bound ORO stain. To detect the level of lipid content, 100 µL of the isopropanol in each of the wells was transferred to a labelled 96-well non-binding assay plate (CELLSTAR®, Greiner Bio-One, Kremsmünster, Austria) as shown in Figure 27. Lipid content was determined by measuring the absorbance of the ORO stain at 510 nm using the Gen 5 software (BioTek, Winooski, United States) and the ELx800 absorbance reader (BioTek, Winooski, United States). The remainder of the isopropanol was aspirated and the cells were washed with 200 µL of RT 70% (v/v) ethanol. The ethanol was removed to near dryness and the plate was incubated at RT for five minutes to evaporate the ethanol.

When the wells were dry, 400 µL of the CV working solution (Appendix) was added to each well and the plates were incubated for five minutes at RT. The CV was removed completely and the cells were washed twice with 500 µL of RT DPBS. The DPBS was then removed and 200 µL of RT 70% ethanol was added to each well to extracted the CV stain from the cells. The culture plate was rocked back and forth to aid in the stain extraction. Thereafter, 100 µL of the ethanol was transferred to the remaining wells of the 96-well non-binding assay plate that was used previously (Figure 27). The CV absorbance was measured at 570 nm also using the Gen 5 software (BioTek) and the ELx800

absorbance reader (BioTek).

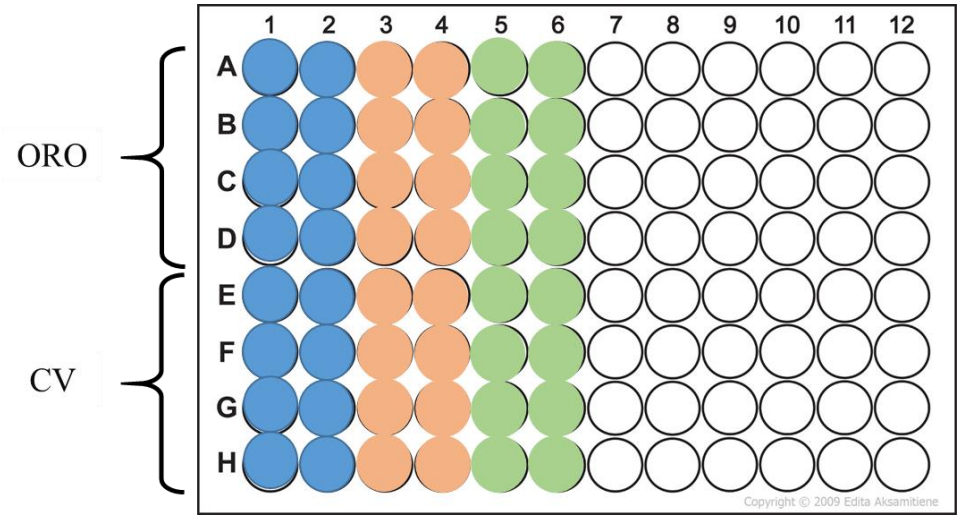

Figure 27. 96-well plate layout for determination of lipids and cell number using ORO and CV. *Blue:* Undifferentiated pre-adipocytes. *Orange:* Pre-adipocytes differentiated at 5.5 mM Glucose. *Green:* Pre-adipocytes differentiated at 25 mM Glucose.

2.5.10 2-Deoxy-[^{3}H]-*D*-glucose uptake assay

Glucose is rapidly metabolized within cells for energy production and is thus hard to measure under cellular conditions. Thus, non-metabolizable analogues of glucose, such as 2-deoxy-[^{3}H]-D-glucose (2DG) (Perret et al., 2004), are used to measure glucose transport across the cellular membrane by GLUTs. A few of the characteristics of 2DG are that it has good tissue specificity, a good interaction with the downstream glucose phosphorylating enzyme hexokinase, good affinity for GLUTs and is retained at high enough concentrations intracellularly for effective radioactivity analysis (Henry et al., 1995; Sols and Crane, 1954). After the transport of 2DG into the cytoplasm, it is then phosphorylated by the hexokinase enzymes to form the impermeable 2-deoxyglucose-6-phosphate (2DG6P) derivative that can accumulate within the cell. Measurements of 2DG radioactivity was conducted in mature adipocytes in the absence (basal glucose uptake) and the presence (insulin-stimulated glucose uptake) of insulin to determine whether the presence of insulin does, indeed, increase glucose uptake by activating GLUT 4 as previously suggested (Leney and Tavaré, 2009).

After 9 days of differentiation (Day 8), cells were washed twice with pre-warmed DPBS and incubated for at least 30 minutes in DMEM (Sigma-Aldrich) without glucose and phenol red media, to glucose and serum starve cells and to completely remove phenol red traces. During the incubation, the basal and insulin media containing either 5.5 mM or 25 mM glucose, without phenol red, was prepared (Appendix). Thereafter, the cells were washed once with 500 µL of pre-warmed DPBS,

whereafter it was aspirated and 500 µL of the basal and insulin media was added to the wells as indicated in Figure 28. The culture plate was incubated for another 15 minutes at 37ºC, after which it was removed and transferred to the radioactivity laboratory. In the radioactivity laboratory, the 2DG basal and insulin media was prepared (Appendix) during the 15-minute incubation step mentioned above. The basal and insulin media was then aspirated and replaced by 500 µL of the 2DG basal and insulin media as indicated in Figure 28. The plate was incubated at 37ºC for 15 minutes, after which the media was aspirated and cells were washed with RT DPBS to stop the glucose uptake reaction. Thereafter, 500 µL of 0.1 M NaOH and 0.1% SDS lysis buffer (Appendix) was added to each well and the plate was incubated for 60 minutes at 37ºC on an orbital shaker (VXR basicVibrax®, IKA, Staufen, Germany). During this time, scintillation vials (Perkin Elmer, Waltham, USA) were prepared with 2.5 mL of scintillation fluid (Perkin Elmer) and 500 µL of distilled H_2O. After the incubation, 500 µL of the cell suspension was added to the scintillation vials. The lid of each vial was labelled according to the sample number as indicated in Figure 28. These vials were incubated in the dark for 60 minutes to equilibrate the samples and then placed into the scintillation counter racks to read the ^3H radioactivity on the 2810 Tri-carb Series liquid scintillation counter (Perkin Elmer, Waltham, USA).

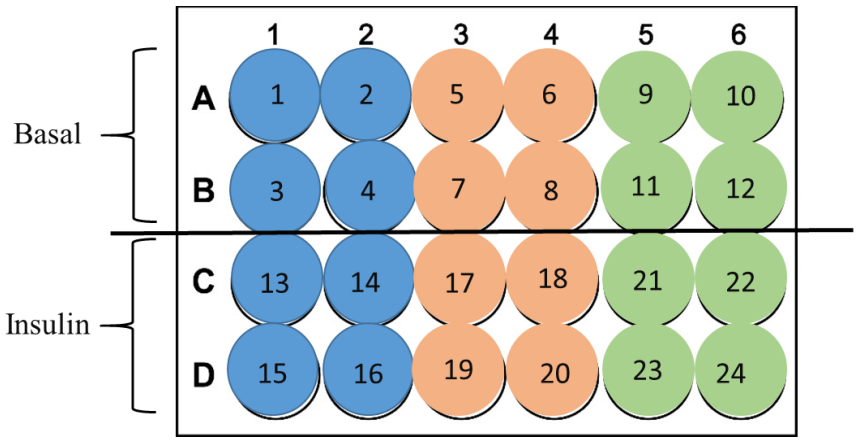

Figure 28. Plate layout for the glucose uptake assay.
The plate was divided into two section for analysis of both basal and insulin-stimulated glucose uptake. Each sample was numbered for ease of analysis. *Blue:* Undifferentiated pre-adipocytes. *Orange:* Pre-adipocytes differentiated at 5.5 mM Glucose. *Green:* Pre-adipocytes differentiated at 25 mM Glucose.

2.5.12 Cell viability assay

The Vialight® plus Cell Proliferation and Cytotoxicity BioAssay Kit (Lonza, Basel, Switzerland) detects ATP by the measurement of bioluminescence in a reaction catalysed by the enzyme luciferase as shown in Figure 29. The intensity of the bioluminescence generated by this reaction is linearly related to the ATP concentration within cells.

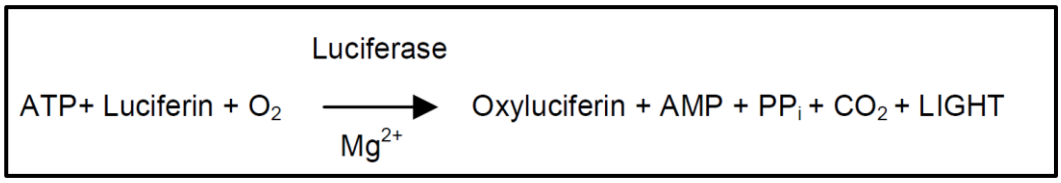

Figure 29. The production of light from ATP and luciferin by the action of the enzyme luciferase.

After 9 days of differentiation (Day 8), cells were washed twice with RT DPBS, while the reagents in the kit were brought to RT before use. Thereafter the ATP monitoring reagent (AMR) plus was reconstituted in the assay buffer and incubated at RT for 15 minutes. During the last five minutes of this incubation step, the 24-well plate allocated for the cell viability assay, was taken out of the incubator and allowed to reach RT on a benchtop. After these incubation steps, 100 µL of the cell lysis buffer (provided in the kit) was added to each well of the 24-well plate and incubated for 10 minutes. Thereafter, 200 µL of the AMR plus was added to each of the wells and the plate was incubated in the dark at RT for two minutes. The samples from each well of the 24-well plate was transferred to a 96-well non-binding assay plate (Corning Inc.) as illustrated in Figure 30. The bioluminescence was measured using the Gen 5 software (BioTek) with the FLx 800 luminometer (BioTek).

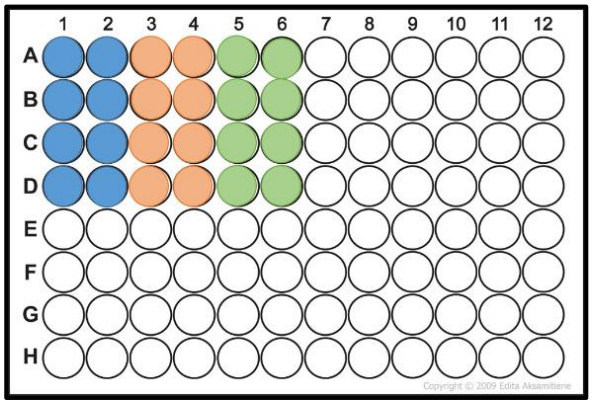

Figure 30. Plate layout for the cell viability assay.
Blue: Undifferentiated pre-adipocytes. *Orange:* Pre-adipocytes differentiated at 5.5 mM Glucose. *Green:* Pre-adipocytes differentiated at 25 mM Glucose.

2.5.13 Harvesting of cells for DNA and RNA isolation

Cells for DNA and RNA extraction were harvested using the QIAzol (Qiagen, Hilden, Germany) lysis reagent. At day 9 of differentiation (Day 8), the two 6-well plates allocated to DNA and RNA harvesting were removed from the incubator and the media was aspirated. The cells were washed twice with 500 µL RT DPBS and the DPBS was aspirated to near dryness after the second wash. Thereafter, 250 µL of QIAzol lysis reagent was added to each well and the plate was incubated for five minutes at RT. The cells were removed from the plates using a cell scraper (Celltreat®, Pepperell, USA) and transferred to labelled (one for each of the three treatment conditions) 2 mL microfuge tubes. The harvested cells were stored at -80ºC.

2.5.14 Harvesting of cells for protein isolation

Cells for protein extractions were harvested using RIPA buffer (Cell Signalling Technologies, Danvers, USA). Firstly, the three 6-well plates allocated to protein harvesting were removed from the incubator and the media was aspirated. The cells were equilibrated by adding 500 µL of DMEM, with 5.5 mM or 25 mM glucose, without phenol red to each well. The plates were then incubated at 37ºC for 15 minutes. Thereafter, the phenylmethane sulfonyl fluoride (PMSF; Sigma-Aldrich) was vortexed until all the crystals in the solution were dissolved. The purpose of adding the PMSF, was to inhibit serine protease enzymes that degrade proteins. Thereafter 10 µL of the PMSF was added to 1 mL of the RIPA buffer and this solution was mixed by vortexing for 30 seconds. The plates were removed from the incubator and the DMEM without phenol red media was aspirated and the cells were washed twice with 500 µL of RT DPBS. The DPBS was aspirated to near dryness after the last wash. One hundred and twenty microliters of the PMSF, RIPA buffer solution was added to the top three wells of each 6-well plate. The plates were incubated on ice for five minutes. Then, for each plate, the cells from the top three wells were scraped off the plate by using a cell scraper and the cell suspensions from these wells were transferred to the bottom three wells as shown in Figure 31. The plates were incubated on ice for another five minutes before the cells of the bottom three wells were also scraped off the surface of the plate. The resultant cell suspensions were transferred to clean, labelled (one for each differentiation condition) 2 mL microfuge tubes. The harvested cells were stored at -20ºC.

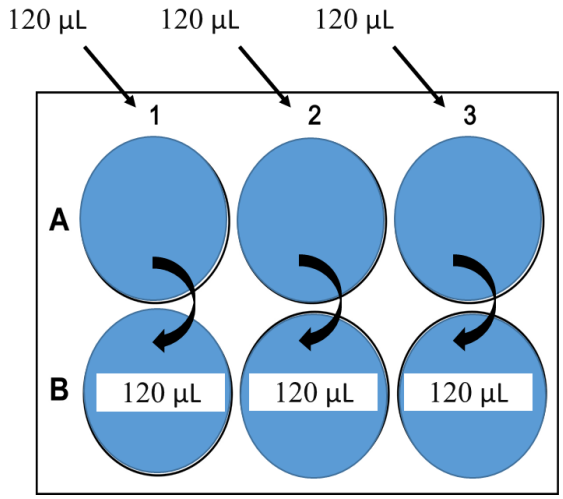

Figure 31. The cell harvesting process for protein isolation from adipocytes.
One hundred and twenty microliter of RIPA buffer was added to the top three wells of the plate. After an incubation of five minutes, the cells were scraped from these wells and the cell suspension transferred to the lower three wells. After another five minute incubation step, the cells were also scraped from the wells and the final cell suspension transferred to a clean, labelled 1.5mL microfuge tube.

2.5.15 Oxidative stress assay

The level of reactive oxygen species (ROS) and changes in mitochondrial membrane potential (ΔΨm) as a measurement of oxidative stress (OS) generation in mature adipocytes, were detected using 2',7'-dichlorfluorescein-diacetate (DCFH-DA; Biolabs, Inc., San Diego, USA) and 5,5',6,6'-Tetrachloro-1,1',3,3'-tetraethylbenzimidazolyl-carbocyanine iodide (JC-1; Sigma-Aldrich) dyes by following previously described protocols (Dludla et al., 2016).

Briefly, for the detection of ROS, a 1 µM final concentration was prepared by removing 10 µL of 1 mM DCFH-DA stock solution and adding it into a 10 mL Hank's buffered saline solution (HBSS; Lonza). Thereafter, after the treatment was removed from each well of a black 96-well tissue culture plate and cells washed once with warm HBSS, the mixed 1 µM DCFH-DA working solution was added to each well and the cells then incubated at 37°C in humidified air and 5% CO_2 for 30 minutes the dark. After 30 minutes, the dye was removed and cells washed once with warm HBSS and fluorescent intensity (Ex 485 ± 20 nm; Em 528 ± 20 nm) was measured using a BioTek FLx800 plate reader and Gen 5 software (Bio-Tek). For JC-1 assay, a 2 µM working solution was prepared by transferring 10 µL of the 200 µM JC-1 stock solution into 1 mL Dulbecco's phosphate-buffered saline (DPBS; Lonza) and then mixed by vortexing for 30 seconds. The cells were then incubated at 37°C in humidified air and 5% CO_2 for 30 minutes the dark before fluorescence (Ex 485 ± 20 nm; Em 530 ± 25 nm and 590 ± 35 nm) was measured using a BioTek FLx800 plate reader and Gen 5 software. In addition, for both DCFH-DA and JC-1 assays, fluorescent photomicrographs were taken at 10x

magnification using a Nikon Eclipse Ti inverted microscope and NIS-Elements imaging software (Tokyo, Japan).

2.6 Statistical analysis

MassARRAY® data was analyzed using the MassARRAY® EpiTYPER® software and Microsoft Excel® 2016 (Microsoft Office). For *in vitro* experiments, data was analysed in Microsoft Excel® 2016 and represent the average of three independent experiments done in triplicate ± the standard error of the mean (SEM), and is represented as a percentage relative to undifferentiated pre-adipocytes (control) which was set as 100%. Statistical analysis was conducted using GraphPad Prism® version 5.04 (GraphPad Software Inc., La Jolla, USA). Differences between groups were analysed by one-way analysis of variance (ANOVA) and the Tukey post hoc test. When variances between groups were significantly different, as measured with the Bartlett's test for equal variances, the non-parametric Kruskal Wallis test that does not assume Gaussian distribution was used, together with the Dunn's post hoc test. A p value < 0.05 was considered statistically significant.

3. Results

3.1 Population characteristics

Participant characteristics are indicated in Table 7. Subjects were classified as T2D, IGT or NGT based on fasting and two-hour blood glucose concentrations according to the World Health Organization criteria. Subjects were women of mixed ethnic ancestry of similar age.

Table 7. Participant characteristics.

	Type 2 diabetic	**Impaired glucose tolerant**	**Normoglycaemic**
N	3	2	4
Gender	Female	Female	Female
Race	Mixed ethnic ancestry	Mixed ethnic ancestry	Mixed ethnic ancestry
Age	50.67 ± 6.74	49.50 ± 13.50	49.75 ± 5.76
BMI (kg/m^2)	38.65 ± 3.43	29.40 ± 5.97	32.21 ± 0.29
Fasting glucose (mmol/L)	**6.7 ± 0.5***	5.4 ± 0.3	**5.1 ± 0.1***
2-hour glucose (mmol/L)*	**13.4 ± 0.7***	**8.9 ± 0.3***	**5.6 ± 0.3***

N= number of participants; BMI= body mass index
Bold face values indicate significant statistical differences with *p<0.05

3.2 Common differentially expressed and differentially methylated miRNA genes

To identify miRNA genes potentially regulated by DNA methylation, differentially expressed miRNAs (miRNA-Seq) and differentially methylated miRNA genes (MeDIP-Seq) between T2D, IGT and NGT individuals were integrated using the Venny 2.1 tool. An example of an analysis conducted using the Venny 2.1 tool is illustrated in Figure 32.

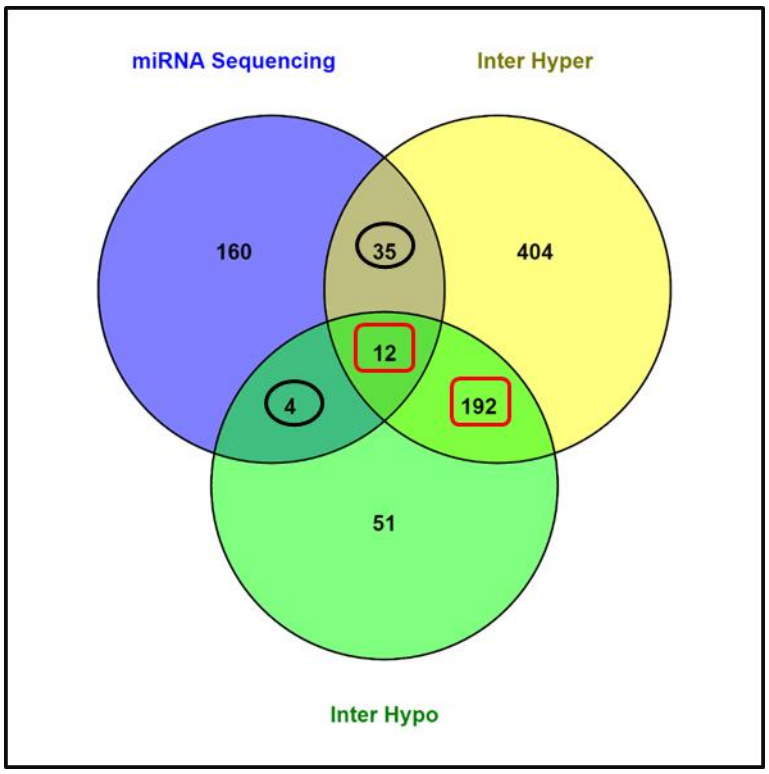

Figure 32. An example of a venn diagram for the comparison of T2D and NGT individuals.
The diagram shows differentially expressed miRNAs, integrated with differentially hypo- and hypermethylated miRNA genes within the intergenic region when individuals with T2D were compared to individuals with NGT. The miRNA genes of interest were those that were both differentially expressed and differentially methylated, i.e. those encircled in black. MiRNAs that were differentially expressed, but whose genes were both differentially hypo- and hypermethylated were excluded (boxed in red). *Inter Hypo*: Hypomethylation within the intergenic region. *Inter Hyper*: Hypermethylation within the intergenic region.

After analyzing all MiRNA-Seq and MeDIP-Seq data for T2D, IGT and NGT individuals, several miRNAs potentially regulated by DNA methylation were identified (Table 8). When individuals with T2D were compared to individuals with NGT, 4 and 39 miRNA genes in the promotor and intergenic regions, respectively, were both differentially expressed and differentially methylated. In the comparison between individuals with IGT and NGT, one and 20 miRNA genes were differentially expressed and differentially methylated in the promotor and intergenic regions, respectively. When comparing individuals with T2D to individuals with IGT, one and 31 miRNA genes were differentially expressed and differentially methylated in the promotor and intergenic regions, respectively. Mir-99a was both differentially expressed and mir-99a was differentially methylated in the promotor region of individuals with T2D compared to individuals with NGT and IGT. Mir-let-7A was differentially expressed and differentially methylated in the promotor region of individuals with T2D and IGT compared to individuals with NGT. No common differentially expressed and differentially methylated miRNA genes were identified in the intragenic regions.

Table 8.Differentially expressed miRNAs and differentially methylated miRNA genes.

Type 2 diabetic vs. Normoglycaemic			**Impaired glucose tolerant vs. Normoglycaemic**			**Type 2diabetic vs. Impaired glucose tolerant**		
Promotor	**Intergenic**		**Promotor**	**Intergenic**		**Promotor**	**Intergenic**	
Hyper	Hypo	Hyper	Hypo	Hypo	Hyper	Hyper	Hypo	Hyper
mir-let-7a, mir-150, mir-92b, **mir-99a**	mir-1180, mir-126, mir-203a, mir-629	mir-let-7a, mir-let-7d, mir-101, mir-122, mir-128, mir-146a, mir-148a, mir-15a, mir-181a, mir-181c, mir-182, mir-193b, mir-194, mir-196a, mir-197, mir-2110, mir-21, mir-223, mir-26a, mir-29a, mir-30d, mir-30e, mir-3158, mir-320b, mir-34a, mir-4446, mir-4511, mir-502, mir-505, mir-574, mir-618, mir-664, mir-98, mir-99a, mir-99b	**mir-let-7a**	mir-122, mir-183, mir-196a, mir-340, mir-4781, mir-574, mir-629, mir-98	mir-let-7f, mir-125b, mir-148a, mir-181b, mir-182, mir-204, mir-223, mir-30b, mir-4511, mir-744, mir-7706, mir-92a	**mir-99a**	mir-146a, mir-148a, mir-181a, mir-29a, mir-30b, mir-345	mir-1180, mir-128, mir-140, mir-182, mir-183, mir-193b, mir-194, mir-197, mir-2110, mir-21, mir-26a, mir-26b, mir-3200, mir-331, mir-340, mir-34a, mir-363, mir-4732, mir-502, mir-505, mir-574, mir-629, mir-6513, mir-6852, mir-98

This table contains miRNA genes identified by the Venny 2.1 tool that could be under the potential regulation of DNA methylation within three comparison groups: T2D vs. NGT, IGT vs. NGT and T2D vs. IGT. The miRNAs in bold were identified to be both differentially expressed and differentially methylated in two comparison groups.

3.3 DNA concentration

DNA was successfully extracted from all 12 samples. DNA concentrations and yields varied between 112.16-224.35 ng/µL and 33.65 µg-67.31 µg, respectively (Table 9). All samples had an $A_{260/280}$ ratio between 1.84-1.92 and an $A_{260/230}$ between 2.29-2.57, which was indicative of DNA of good quality and purity, and suitable for MassARRAY® EpiTYPER™ analysis.

Table 9. DNA concentration and total yield.

Sample ID	Concentration (ng/µL)[β]	$A_{260/280}$ (nm)[π]	$A_{260/230}$ (nm)[Ω]	Yield (µg)[∞]
106	197.98	1.88	2.46	59.39
4	188.55	1.86	2.29	56.57
105	224.35	1.89	2.47	67.31
80	150.62	1.84	2.41	45.19
200	172.95	1.89	2.40	51.89
66	112.16	1.90	2.40	33.65
97	112.755	1.92	2.57	33.83
100	192.60	1.88	2.46	57.78
109	151.415	1.86	2.48	45.42

[β]DNA concentration was measured at A_{260} nm.
[π]Presence of protein contaminants was measured with $A_{260/280}$.
[Ω]Presence of salt/solvent/other contaminants was measured at $A_{260/230}$.
[∞]DNA yield (µg) was calculated by multiplying DNA concentration in ng/µL by sample volume (300 µL) and dividing (total ng in sample) by 1000.

3.4 Primer sequences

Of the miRNA genes selected for analysis with MassARRAY® (Table 8), 27 primer sets were designed for 26 miRNA genes. Two primer sets were designed for mir-99a(1). Primer sequences are illustrated in Table 10.

Table 10.Primer sequences.

miRNA	Primer Sequence (5' to 3' orientation)	
mir-150	Forward: aggaagagagTTGTTTTTAGTATAGGGTGGAGTGG Reverse: cagtaatacgactcactatagggagaaggctCTCACCTCACCCCTTAAAACCTAC	
mir-92b	Forward: aggaagagagGAATTTTAGATTTTTTGGTTTTGGG Reverse: cagtaatacgactcactatagggagaaggctAACATCCTCCCTCAAACACCCTAT	
mir-99a(1)	Forward: aggaagagagTGTATTTTTATGTTGTTTTAGTTAATGG Reverse: cagtaatacgactcactatagggagaaggctCTTAAAAAACTCACAAAACCCCAC	1.1
	Forward: aggaagagagTATATGAGTAGTTTGGGTGGGGTTT Reverse: cagtaatacgactcactatagggagaaggctTCAAACAACTACTATCTAAAAAAAACATC	1.2
mir-LET7a3	Forward: aggaagagagTTGAGAAGTTTGATAGGTTTAGGTG	

	Reverse: cagtaatacgactcactatagggagaaggctAAAAAAAATACCTTAACCTCCCTTC
mir-99a(2)	Forward: aggaagagagTGTTTGTTTTTTGTTATTGAAGTTTG Reverse: cagtaatacgactcactatagggagaaggctTTAACAAACAATCCCCAAAATAACT
mir-99a(3)	Forward: aggaagagagATAGAAATATAATTGAAGGAGATTTGGTT Reverse: cagtaatacgactcactatagggagaaggctCATTCATCCAAATATATACTTAAAAATCA
mir-99a(4)	Forward: aggaagagagAATAGTTTTGTTTTTGGAGAGGTGA Reverse: cagtaatacgactcactatagggagaaggctAACACAAAACACCACAATACACTCT
mir-99a(5)	Forward: aggaagagagTTTAATGTGATAGTATTTGGAGGTGG Reverse: cagtaatacgactcactatagggagaaggctAAATTCACTTAAACAACCCATAAAA
mir-99a(6)	Forward: aggaagagagGATTTAGGGGTAATATGTATAGGTTTG Reverse: cagtaatacgactcactatagggagaaggctCCCAACAACAAAAAACTACATAAAAAA
mir-99a(7)	Forward: aggaagagagGTTGAGTATGGTGATGGGTATTTGT Reverse: cagtaatacgactcactatagggagaaggctTCATTACCTACATTTAAACCTTACTTTT
mir-98c	Forward: aggaagagagGTTTGTTTGTTTGTTTGGTTTTTTT Reverse: cagtaatacgactcactatagggagaaggctATTTCCTTACCCCTCTAATTAACACC
mir-98d	Forward: aggaagagagTGGATTTTTTTAGAGTTGTAAGTTTTT Reverse: cagtaatacgactcactatagggagaaggctTCCAAATACCTATTCCTTCCCAATA
mir-29a(1)	Forward: aggaagagagTGTTTTTTTAGTTTTAGAATGTGTTGTTAG Reverse: cagtaatacgactcactatagggagaaggctTCAAATCCAAATAAATTCAACACAA
mir-30d	Forward: aggaagagagTGAGTTTAAAAATGTATATTATTGGTTAGG Reverse: cagtaatacgactcactatagggagaaggctAACATAATCTCTACTCACTACAACCTCC
mir-30e	Forward: aggaagagagTGATTATGATTTAAGTGAGAGTTAAGGATT Reverse: cagtaatacgactcactatagggagaaggctACAATTTCATCTTTTCATTCCTCAATA
mir-29a(2)	Forward: aggaagagagTTTGAGATTAGGAGTTTGGGATTAG Reverse: cagtaatacgactcactatagggagaaggctAACAACCCAACAACCATAAAAACTA
mir-21a	Forward: aggaagagagTTGTTTAGGTTGGAATGTAGTGGTT Reverse: cagtaatacgactcactatagggagaaggctTTATAAACTCCCAAAAAAACAAAAA
mir-21b	Forward: aggaagagagGATTATTGTTGGTTGGGTATAGTGG Reverse: cagtaatacgactcactatagggagaaggctCAAAATCAAACCATTCTCCTACCT
mir-193b(1)	Forward: aggaagagagTTAGGTTGGTTTTAAATTTTTGGGT Reverse: cagtaatacgactcactatagggagaaggctAACATACCTTTTATATTTTTCTCTTACAA
mir-193b(2)	Forward: aggaagagagAGGAGAATTTTAGGAGTTTTGTGTT Reverse: cagtaatacgactcactatagggagaaggctAAAAAATCTTCCTTTCACTACTACTACTAC
mir-193b(3)	Forward: aggaagagagGGTTTTTGTTAGGAATTTAGTTGGG Reverse: cagtaatacgactcactatagggagaaggctTCAATTACAAAATATAAACCAATAACACA
mir-125b2	Forward: aggaagagagAGGTTTATTGTAAGTTTTGTTTTTTGG Reverse: cagtaatacgactcactatagggagaaggctTAATTCACCCCTATAATCCCAACAC
mir-148(1)	Forward: aggaagagagTGAGTGTGTATTATGGATAAGAAAAATAGT Reverse: cagtaatacgactcactatagggagaaggctTTTAATAATCATTCAACACCACCAT
mir-148(2)	Forward: aggaagagagGGTTTTTAAGTGTTTAAGTGAAAAGAAGT Reverse: cagtaatacgactcactatagggagaaggctAACTAAAACTACAAACACCCACCAC

mir-146a(6)	Forward: aggaagagagGAATTATTTGAGTTGTGGAGGTTGG Reverse: cagtaatacgactcactatagggagaaggctAACTCATTACCATTTCCAAAAAAAA
mir-34a(1)	Forward: aggaagagagAGTTTGGTTAGGATAATAGAAGGTAAA Reverse: cagtaatacgactcactatagggagaaggctAACTATACCCAAACTCCTAACCCAC

*After the identification and selection of common differentially expressed and differentially methylated miRNA genes, their sequence data was obtained from the MeDIP-Seq data. During this process multiple sequences for the same gene was present within and amongst certain groups, designated by the numbers in brackets. For mir-99A, two primer sets were designed to include more CpG sites within this gene, i.e. mir-99a 1.1 and 1.2.

3.5 Bisulfite conversion

Of the 5 µg DNA shipped to Inqaba Inc., 1 µg was used for bisulfite conversion. DNA concentrations (132.57-452.67 ng/µL) and yields (5.30-18.11 µg) after bisulfite treatment are illustrated in Table 11.

Table 11. DNA concentration and yield after bisulfite treatment

Sample ID	ng/µl	Yield (µg)∞
106	203.67	8.15
4	132.57	5.30
105	239.83	9.59
80	170.50	6.82
200	452.67	18.11
66	136.97	5.48
97	310.97	12.44
100	232.10	9.28
109	227.65	9.11

∞DNA yield (µg) was calculated by multiplying DNA concentration in ng/ µL by sample volume, and dividing (total ng in sample) by 1000.

3.6 MassARRAY® EpiTYPER™ quantitative methylation analysis

MassARRAY® EpiTYPER™ analysis was used to verify the methylation status of miRNA genes potentially regulated by DNA methylation. The number of CpG sites covered in both the MeDIP-Seq and MassARRAY® EpiTYPER® analyses are shown in Table 12. Only 21 of the 26 miRNA genes were successfully analysed including both primers for mir-99a (Table 13). The comparison between MassARRAY® EpiTYPER™ results and MeDIP-Seq is illustrated in Tables 14 and 15. When using a cut off value of 1.50, only two miRNA genes (indicated in red text in Tables 14 and 15) showed correlation between MassARRAY® and MeDIP-Seq. Yet, six other miRNA genes showed slight correlations (indicated in blue text in Table 14 and 15) between MassARRAY® and MeDIP-Seq. using a less stringent cut off value.

Table 12 The number of CpG sites included in the MeDIP-Seq and MassARRAY® analyses.

miRNA gene	No. of CpGs analysed by MeDIP-Seq*	No. of CpGs covered by primer set#	No. of CpGs analysed by MassARRAY®†	Correlation between MeDIP-Seq and MassARRAY®✞
mir-125b2	12	6	4	0.33
mir-193b(3)	6	6	6	1.00
mir-34a(1) (3p)	7	6	7	1.00
mir-30d	9	6	6	0.67
mir-LET7a3	15	11	13	0.87
mir-92b(3p)	6	4	3	0.50
mir-146a(6)	6	5	5	0.83
mir-193b(1)	7	4	6	0.86
mir-29a(2)	13	11	12	0.92
mir-98	14	8	4	0.28
mir-99a(4)	7	3	7	1.00
mir-99a(1.2)	10	3	3	0.30
mir-99a(5)	7	5	7	1.00
mir-21b	13	9	8	0.62
mir-29a(1)	12	9	9	0.75
mir-30e (3p)	4	3	4	1.00
mir-99a(1.1)	10	4	7	0.70
mir-99a(3)	5	4	5	1.00
mir-150	19	12	8	0.42
mir-99a(6)	5	3	4	0.8
mir-99a(7) (3p)	7	5	4	0.57
mir-21a (3p)	13	11	10	0.77

*The number of CpG sites found in the entire miRNA gene as indicated by the MeDIP-Seq sequencing data.
#The number of CpG sites that were included in the sequence that was amplified by the primer set.
†The number of CpG sites that were successfully analysed by the MassARRAY® system.
✞The correlation between the number of CpG sites analysed by these two tehniques was calculated by dividing the number of CpG sites that were successfully analysed by the MassARRAY® with the number of CpG sites found in the entire miRNA gene as indicated by the MeDIP-Seq sequencing data.
1.00: 100% Correlation. Values lower than 1.00 indicate a decrease in the correlation between techniques.

Table 13. MassARRAY® EpiTYPER™ results.

miRNA gene	T2D vs. NGT	T2D vs. IGT	IGT vs. NGT
mir-125b2	0.71	0.78	0.91
mir-193b(3)	1.06	1.10	0.97
mir-34a(1)	1.05	0.99	1.06
mir-30d	0.95	1.01	0.94
mir-LET7a3	1.01	1.04	0.98
mir-92b	0.92	1.07	0.86
mir-146a(6)	1.02	1.11	0.92
mir-193b(1)	1.05	2.01	0.52
mir-29a(2)	1.33	1.09	1.22
mir-98c	1.01	2.03	0.50
mir-99a(4)	0.98	1.02	0.97
mir-99a(1.2)	1.00	1.01	0.98
mir-99a(5)	0.97	0.97	1.00
mir-21b	1.01	0.98	1.03
mir-29a(1)	0.99	1.00	1.00
mir-30e	1.00	2.02	0.50
mir-99a(1.1)	0.96	2.10	0.46
mir-99a(3)	0.93	0.95	0.99
mir-150	1.70	1.24	1.36
mir-99a(6)	1.06	1.05	1.02
mir-99a(7)	1.01	1.05	0.96
mir-21a	1.00	1.02	0.98

Values =1.00: no difference in DNA methylation
Values < 1.00: Decreased DNA methylation (Hypomethyltation)
Values > 1.00: Increased DNA methylation (Hypermethylation)
T2D: Type 2 Diabetes; *IGT*: Impaired Glucose Tolerant; *NGT*: Normoglycaemic

Table 14. Comparison between the results of the MassARRAY® and MeDIP-Seq in the promoter region.

	miRNA Gene	T2D vs. NGT		T2D vs. IGT		IGT vs. NGT	
		MassARRAY®	**MeDIP-Seq**	**MassARRAY®**	**MeDIP-Seq**	**MassARRAY®**	**MeDIP-Seq**
PROMOTER	**mir-92b**	0.92	Hyper				
	mir-LET7a3					**0.98**	**Hypo**
	mir-99a(1.1)	0.96					
	mir-99a(1.2)	1.00	Hyper				
	mir-150	**1.70**	**Hyper**				

Blue: Low bidirectional consistency. Red: Increased bidirectional consistency.
Values =1.00: no difference in DNA methylation
Values < 1.00: Decreased DNA methylation (Hypomethyltation)
Values > 1.00: Increased DNA methylation (Hypermethylation)
T2D: Type 2 Diabetes; *IGT*: Impaired Glucose Tolerant; *NGT*: Normoglycaemic

Table 15.Comparison between MassARRAY® and MeDIP-Seq in the intergenic region.

	miRNA Gene	T2D vs. NGT		T2D vs. IGT		IGT vs. NGT	
		MassARRAY	MeDIP-Seq	MassARRAY	MeDIP-Seq	MassARRAY	MeDIP-Seq
INTERGENIC REGION	**mir-99a(3)**	0.93	Hyper	0.95	Hyper		
	mir-99a(4)			**1.02**	**Hyper**		
	mir-99a(4)	0.97	Hyper	0.97	Hyper		
	mir-99a(6)			1.05	Hypo		
	mir-99a(7)			1.05	Hypo		
	mir-98c					**0.50**	**Hypo**
	mir-29a(1)	0.99	Hyper				
	mir-29a(1)			1.09	Hypo		
	mir-30d	0.95	Hyper				
	mir-30e	1.00	Hyper				
	mir-21a	1.00	Hyper				
	mir-21b			0.98	Hyper		
	mir-193b(1)	**1.05**	**Hyper**				
	mir-193b(3)			**1.10**	**Hyper**		
	mir-125b2					0.91	Hyper
	mir-146a(6)	**1.02**	**Hyper**				
	mir-34a	**1.05**	**Hyper**	0.99	Hyper		

Blue: Low bidirectional consistency. Red: Increased bidirectional consistency.
Values =1.00: no difference in DNA methylation
Values < 1.00: Decreased DNA methylation (Hypomethyltation)
Values > 1.00: Increased DNA methylation (Hypermethylation)
T2D: Type 2 Diabetes; *IGT*: Impaired Glucose Tolerant; *NGT*: Normoglycaemic

3.7 *In vitro* results

3.7.1 Increased lipid accumulation after 3T3-L1 pre-adipocyte differentiation

Although 3T3-L1 adipocytes are commonly used as an *in vitro* model for obesity studies, 3T3-L1 pre-adipocytes are generally differentiated in high glucose (25 mM) only. Since we aimed to investigate miRNA gene expression in conditions that mimic normoglycaemia and hyperglycaemia, 3T3-L1 pre-adipocytes were differentiated in 5.5 mM or 25 mM glucose. Differentiated adipocytes demonstrated more lipid accumulation as compared to the undifferentiated control (Figure 33). Quantification of these results showed that lipid content was increased after differentiation in both 5.5 mM and 25 mM glucose, compared to undifferentiated pre-adipocytes (100 ± 5% vs. 153 ± 10% vs. 158 ± 13% for controls, 5.5 mM and 25 mM glucose, respectively).

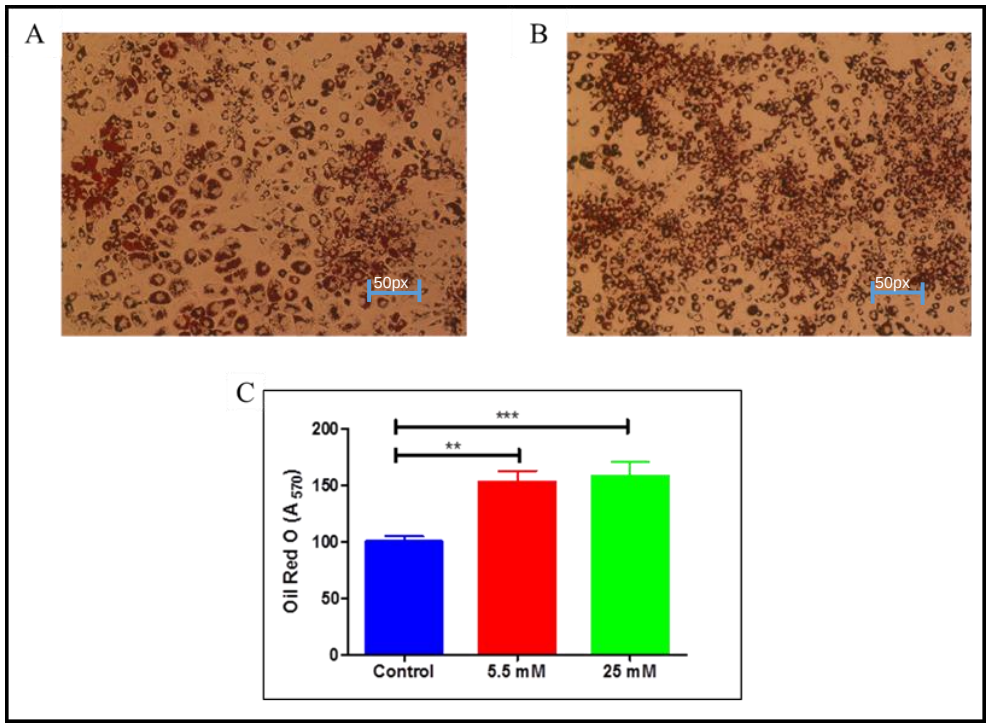

Figure 33. Increased lipid accumulation in differentiated adipocytes.
Oil Red O staining of 3T3-L1 adipocytes differentiated in 5.5 mM (A) and 25 mM glucose (**B**). The quantification of these results are shown in C. No image could be obtained for the undifferentiated controls as the imaging software was not sensitive enough detect up cells that were not stained. Pre-adipocytes were cultured to confluence in CGM and induced to differentiate into matured adipocytes in media containing IBMX, Dex and insulin with 5.5 or 25 mM glucose, or left in CGM for undifferentiated adipocytes. Results are expressed as a percentage relative to the control (set at 100%), and are shown as the mean ± SEM for three independent experiments, each performed in triplicate. Significance is depicted as **P < 0.01, ***P < 0.001.

3.7.2 Increased ATP production in adipocytes differentiated in high glucose

Cell viability, a marker of general cell health and metabolic activity, was assessed by measuring intracellular ATP levels. As illustrated in Figure 34, adipocytes differentiated in 25 mM glucose produced significantly more ATP than undifferentiated pre-adipocytes (100 ± 3% vs. 119 ± 4%, $p < 0.01$). Although ATP content was increased in adipocytes differentiated in 5.5 mM glucose compared to undifferentiated pre-adipocytes (100 ± 3% vs. 114 ± 5%), the difference was not statistically significant.

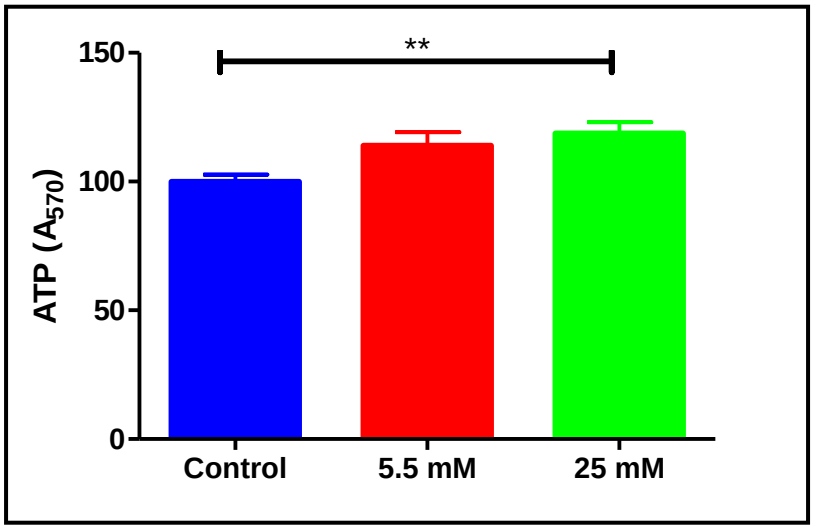

Figure 34. Increased ATP production in adipocytes differentiated in 25 mM glucose.
Pre-adipocytes were cultured to confluence in CGM and induced to differentiate into matured adipocytes in media containing IBMX, Dex and insulin with 5.5 or 25 mM glucose, or left in CGM for undifferentiated adipocytes (control). Results are expressed as a percentage relative to the control (set at 100%), and are shown as the mean ± SEM for three independent experiments, each performed in triplicate. Significance is depicted as **P < 0.01.

3.7.3 Glucose uptake

To assess whether differentiation in 5.5 mM or 25 mM glucose affected glucose uptake, basal and insulin-stimulated glucose uptake was measured in undifferentiated pre-adipocytes and in adipocytes differentiated in different glucose concentrations. No difference in glucose uptake was observed in pre-adipocytes, and between basal and insulin-stimulated glucose uptake (Figure 35).

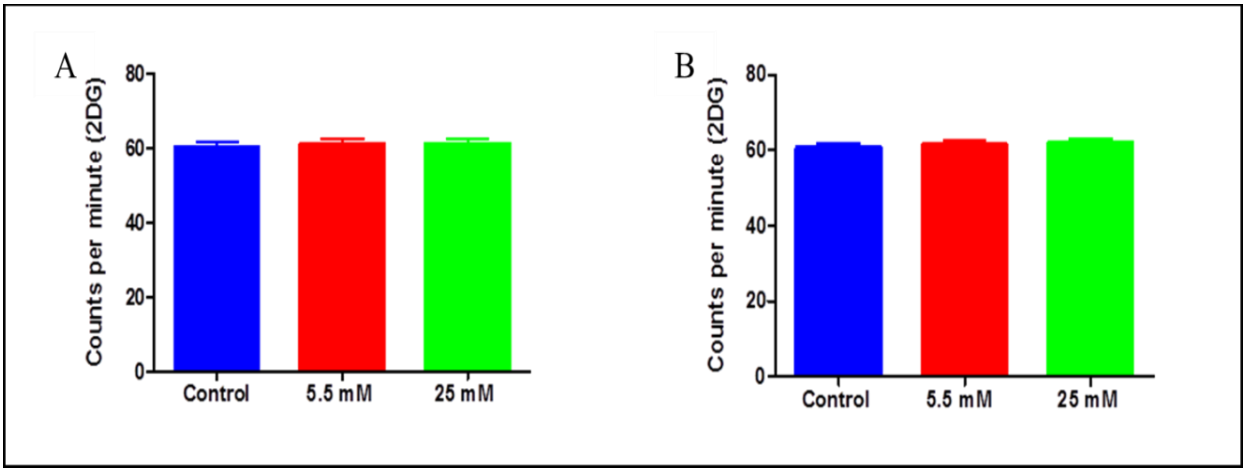

Figure 35. Glucose production.
Basal (A) and insulin-stimulated (B) glucose uptake of pre-adipocytes that were cultured to confluence in CGM and induced to differentiate into matured adipocytes in media containing IBMX, Dex and insulin with 5.5 or 25 mM glucose, or left in CGM for undifferentiated adipocytes (control). Results are expressed relative to the control, and are shown as the mean ± SEM for three independent experiments, each performed in triplicate.

3.7.4 High glucose increases ROS in 3T3-L1 adipocytes

Intracellular ROS was measured using the fluorogenic probe 2', 7'-Dichlorodihydrofluorescin diacetate (DCFH-DA), which diffuses into cells and is deacetylated and oxidized to the highly fluorescent 2', 7'-Dichlorodihydrofluorescein (DCF) by ROS (Dludla et al., 2016). The fluorescence intensity of DCF is proportional to ROS levels within the cell. As illustrated in Figure 36, a difference in morphology of cells was observed in the adipocytes differentiated with high glucose compared to adipocytes differentiated at low glucose (encircled in white). In addition, quantification showed that ROS levels was increased in both 5.5 mM and 25 mM glucose, compared to undifferentiated controls (100 ± 1% vs 110 ± 1% vs. 120 ± 1% vs. $p < 0.001$ for controls, 5.5 mM and 25 mM glucose, respectively) in Figure 37. Moreover, adipocytes

differentiated in 25 mM glucose accumulated significantly more ROS than adipocytes cultured in 5.5 mM glucose (120 ± 1% vs. 110 ± 1%, $p < 0.001$).

Mitochondrial membrane potential was measured using the dye JC-1, which changes fluorescence based on mitochondrial membrane potential, and is used as an indicator of mitochondrial health within cells. As illustrated in Figure 36, differences in JC-1 fluorescence, indicative of membrane potential was significantly higher in differentiated adipocytes compared to undifferentiated pre-adipocytes, irrespective of glucose concentration (100 ± 3% vs 235 ± 10% vs 256 ± 9%, $p < 0.001$ for controls, 5.5 mM and 25 mM glucose).

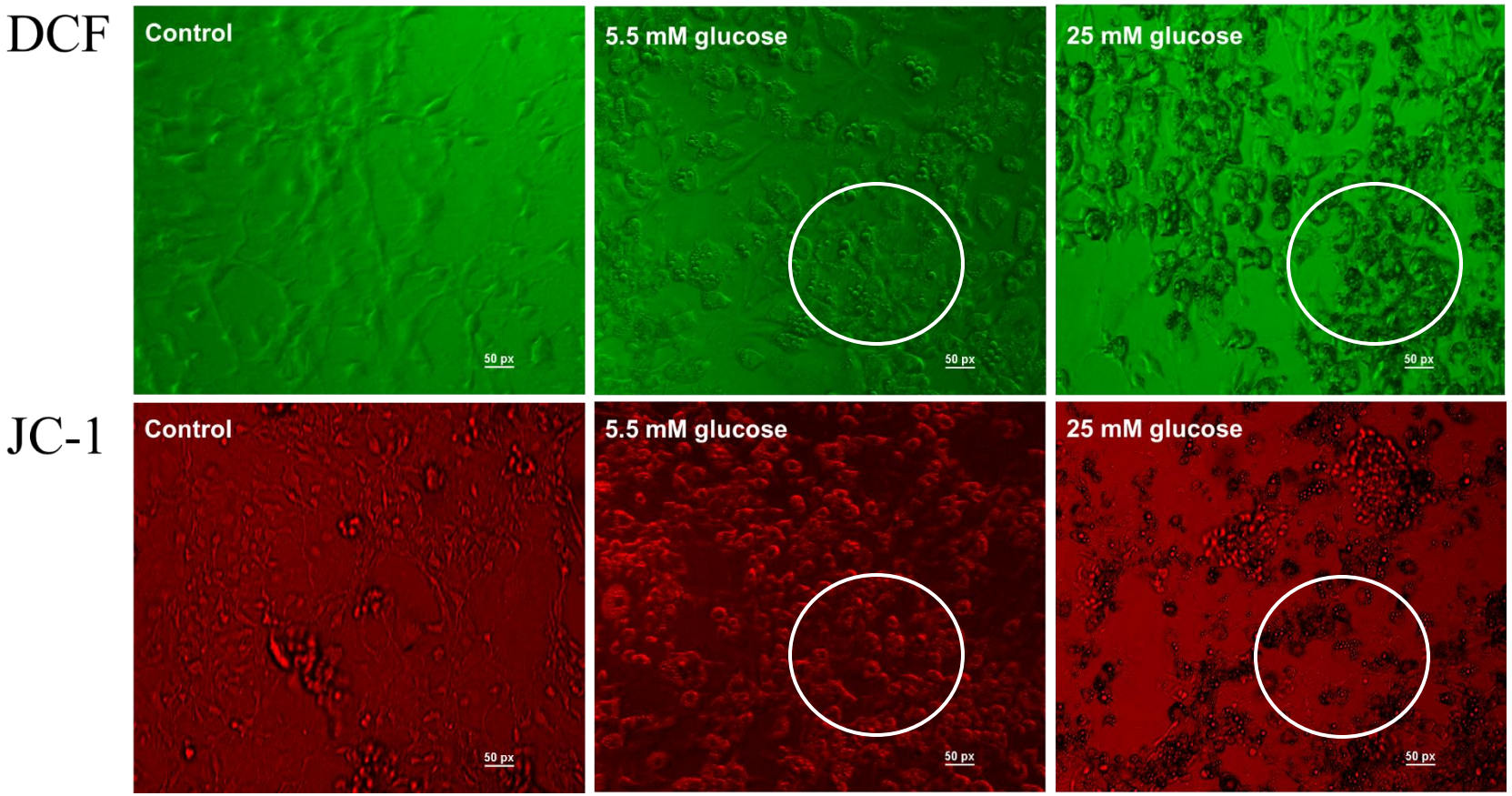

Figure 36. Microscopic images of DCF and JC-1 fluorescence.
Pre-adipocytes were cultured to confluence in CGM and induced to differentiate into matured adipocytes in media containing IBMX, Dex and insulin with 5.5 or 25 mM glucose, or left in CGM for undifferentiated adipocytes (control). Morphological changes in cell shape when comparing adipocytes differentiated in 5.5mM and 25mM glucose are indicated in the white circles. Cells differentiated in lower glucose have a more spherical shape, whereas cells differentiated in high glucose has a more elongated shape.

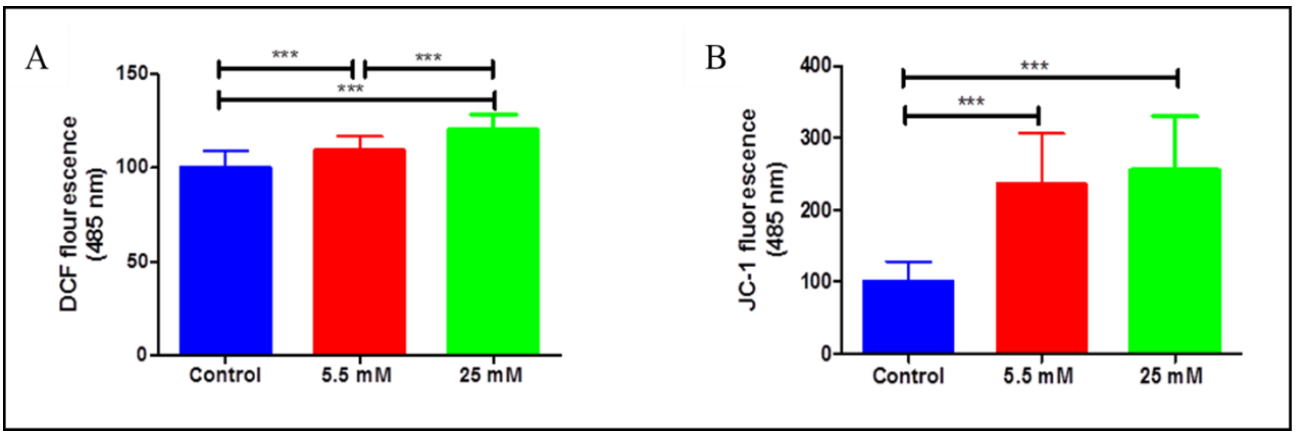

Figure 37. Increased ROS production in adipocytes differentiated in 25mM glucose.
Quantification of DCF (A) and JC-1 (B) fluorescence in undifferentiated pre-adipocytes (control), and adipocytes differentiated in 5.5 or 25 mM glucose. Results are expressed as a percentage relative to the control (set at 100%), and are shown as the mean ± SEM for three independent experiments, each performed in triplicate. Significance is depicted as ***P < 0.001.

4. Discussion

Epigenetics involves the interaction between genetic and environmental factors and has attracted considerable interest globally, particularly in delineating the complex mechanisms underlying metabolic diseases such as T2D (Gilbert and Liu, 2012; Krupanidhi et al., 2009; Ling and Groop, 2009; Prattichizzo et al., 2015). MiRNAs are one of the most widely studied epigenetic mechanisms with potential as a therapeutic target for T2D or as biomarkers to predict disease progression (Fernandez-Valverde et al., 2011; O'Connell and Markunas, 2016; Tang et al., 2008). Despite their important role in regulating biological processes and disease pathogenesis, not much is known about the regulation of miRNA genes themselves. Several researchers, including ourselves, have provided evidence that DNA methylation, another important epigenetic mechanism, regulates miRNA gene expression (Chang et al., 2014b; Pheiffer et al., 2016).

In the present study, we explored the role of DNA methylation in regulating miRNA gene expression during T2D pathogenesis. Firstly, we verified differentially methylated miRNA genes identified by MeDIP-Seq (Pheiffer et al., 2016) in women with T2D, using MassARRAY® EpiTYPER® analysis. Thereafter, we aimed to investigate the relationship between DNA methylation and miRNA gene expression in an *in vitro* model that mimics the pathophysiology of T2D.

4.1 Poor correlation between MeDIP-Seq and MassARRAY®

Previously, we reported differential methylation of miRNA genes during dysglycemia (Pheiffer et al., 2016). We compared genome-wide DNA methylation patterns in the whole blood of South African women of mixed ethnic ancestry using MeDIP-Seq, and found several differences in the methylation status of miRNA genes during T2D pathogenesis. These findings, together with other reports that miRNA genes are regulated by DNA methylation (Cheng et al., 2013; Kameswaran et al., 2014; Suzuki et al., 2012; Wang et al., 2014), sparked further exploration of the miRNA genes that were demonstrated to be differentially methylated during T2D.

Methylated DNA immunoprecipitation sequencing (MeDIP-Seq) involves the enrichment of methylated DNA sequences using immunoprecipitation with a 5-methylcytosine (5mC) antibody, followed by next-generation sequencing (Mohn et al., 2009; Thu et al., 2009). MeDIP-Seq

compares well with array-based methods and bisulfite sequencing, which is currently considered the gold standard for DNA methylation analysis (Clark et al., 2012). However, MeDIP-Seq does not offer single CpG resolution and is prone to false positive results (Liu et al., 2016), therefore, we sought to verify MeDIP-Seq data with MassARRAY® EpiTYPER®, a technique that uses bisulfite conversion and MALDI-TOF mass spectrometry to discriminate between methylated and non-methylated DNA at single base pair resolution (Coolen et al., 2007; Ehrich et al., 2005; Liu et al., 2016; Thompson et al., 2009; Xiang et al., 2014).

Of the 26 miRNA genes (27 sequences, since two sequences were analysed for one of the genes) compared using the two techniques, eight regions were similarly methylated, with only two of these showing significant correlation, mir-98 in the intergenic region when individuals with IGT were compared to individuals with NGT, and mir-150 in the promoter region when individuals with T2D and NGT were compared. For mir-98 and mir-150, only four of the 14 CpG sites, and eight of the 19 CpG sites, respectively, within the miRNA gene was covered using the MassARRAY® analysis. This suggests that the CpG sites analysed by the MassARRAY® system in these two miRNA genes, are those that offer the greatest contribution to the overall methylation status of the entire gene.

The poor correlation between MeDIP-Seq and MassARRAY® could be due to the technical differences between the techniques. Disadvantages of MeDIP-Seq include possible antibody cross-reactivity during immunoprecipitation, reliance on bioinformatic analysis and the challenge of mapping sequencing reads accurately within the highly repetitive and complex regions of the genome and the identification of methylated regions of approximately 150–200 bp, rather than at single nucleotide sites (Clark et al., 2012). With MeDIP-Seq, the entire miRNA gene is analysed, which includes all the CpG sites within the gene. However, MeDIP-Seq is an affinity based method for DNA methylation analysis and has been shown to be more accurate when analysing regions that are highly methylated, with high CpG densities (Li et al., 2010; Xiang et al., 2014). Therefore, a capture bias exists when analysing regions with low methylation status and low CpG densities. Use of the MAssARRAY® system is reliant on primers and due to the inherent limitations of the primer design software used, could not analyse all of the CpG sites identified by MeDIP-Seq. Furthermore, MassARRAY® was not able to analyse all the CpG sites predicted by the primer

design software due to technical limitations of the methodology. MassARRAY® analyses one strand of the DNA sequence only (EpiTYPER® manual), as opposed to MeDIP-Seq that does not differentiate between strands. However, MassARRAY® offers the advantage of quantifying an average of all CpGs per sequence, with base pair accuracy and without the need to map sequences within the complex genome. However, it is dependent on bisulphite conversion, and although bisulfite conversion is considered the gold standard for methylation analysis, incomplete conversion of unmethylated Cs can lead to inaccurate results (Liu et al., 2016). Furthermore, the contradictory results between MeDIP-Seq and MassARRAY® could be due to genetic heterogeneity between the individuals analysed. Due to sample limitations, different subsets of women of mixed ethnic ancestry were analysed with the two techniques. Although women were matched for age, genetic heterogeneity, particularly in individuals of mixed ethnic ancestry (de Wit et al., 2010), could contribute to the poor correlation observed. Furthermore, environmental differences, such as smoking, drinking and socioeconomic conditions could account for the differences observed (Ling and Groop, 2009).

4.2 miR-98 and miR-150

Human mir-98 is a member of the highly conserved let-7 (lethal-7) family, which is composed of nine mature let-7 miRNAs encoded by 12 different genomic loci (Roush and Slack, 2008). Let-7 was first identified as an essential developmental gene in the nematode *Caenorhabditis elegans* and was subsequently identified as the first human miRNA. The precise function of let-7 members in humans is not known, although it is speculated that they promote terminal differentiation in development and may function as tumour suppressors (Roush and Slack, 2008). Kajimoto et al. demonstrated that miR-98 is upregulated during adipogenic differentiation of 3T3-L1 pre-adipocytes (Kajimoto et al., 2006). Overexpression of let-7 in mice resulted in impaired glucose tolerance and reduced glucose-stimulated insulin secretion, implicating miR-98 in the pathogenesis of T2D (Frost and Olson, 2011). More recently, a role for miR-98 in the development of GDM was suggested by Cao et al (Cao et al., 2016). These studies are consistent with quantitative real time PCR findings in our laboratory that miR-98 is upregulated in the whole blood of women with T2D (Dias, 2016), and supports the potential of miR-98 as a therapeutic target against T2D. In contrast, decreased expression of miR-98 was reported in the aorta of T2D rats (Xie et al., 2012). Although these studies suggest tissue-specific regulation of miR-98, they

provide evidence of the importance of this miRNA during T2D. A greater understanding of the mechanisms that regulate miR-98 expression is required to enable the development of therapeutics against T2D. Peng et al. reported that promoter methylation of let-7 is associated with its downregulation during diabetic nephropathy (Peng et al., 2015), thus our findings of decreased methylation of the gene encoding miR-98 by both MeDIP-Seq and MassARRAY® is consistent with its increased expression in women with T2D and IGT compared to NGT.

MiR-150 is highly expressed in lymphocytes, where it regulates B-cell differentiation and activation (Xiao et al., 2007). Ying et al. suggested an important role for miR-150 in regulating obesity-associated insulin resistance by B cell regulation (Ying et al., 2016). They demonstrated that knockdown of miR-150 expression was associated with increased inflammation and insulin resistance. Another study demonstrated that miR-150 was differentially expressed in the plasma of T2D compared to IGT individuals (Chien et al., 2015). MiR-150 has also been associated with CVD, with monocyte-derived miR-150 being associated with promoting angiogenesis (Li et al., 2013) and implicated in the regulation of hyperglycaemia induced cardiomyocyte hypertrophy (Duan et al., 2013). Reduced expression of miR-150 has been associated with the poor survival of individuals with pulmonary hypertension (Rhodes et al., 2013). Increased methylation of mir-150 in individuals with T2D compared to NGT, as observed in this study, would correspond with decreased expression during T2D, as reported by Ying et al.

4.3 Establishment of an *in vitro* adipocyte cell model for normo- and hyperglycaemia

Metabolic diseases such as T2D are complex and involve the interplay between many cell types and tissues within the body (Berg et al., 2002; Chen et al., 2012a; Ley et al., 2016; Zoungas et al., 2014). Although the relevance of *in vitro* models to study metabolic disorders is questioned, they are easy to manipulate, thus enabling mechanistic studies to be conducted in a controlled environment. Obesity, and the dysregulation of biological pathways within adipose tissue, is considered the major driving factor of the T2D epidemic (Ng et al., 2014; Rivera and Bennett, 2010; Shai et al., 2006). Obesity, defined by a BMI above 30 kg/m^2 , is tightly linked to the development of insulin resistance, the most common characteristic of T2D (Hardy et al., 2012; Kahn and Flier, 2000). During obesity, dysregulation of adipose tissue function, leads to

dyslipidemia and dysglycaemia, accompanied by increased oxidative stress. Therefore, the relationship between the methylation of miRNA genes and their expression was investigated in 3T3-L1-pre-adipocytes, the most commonly used adipocyte cell line used in obesity research (Green and Kehinde, 1974). The cell line was developed at New York University, School of Medicine in 1962 and was abbreviated '3T3-L1' because of its 3-day splitting requirement. The 3T3-L1 pre-adipocyte cell line is an immortalized mouse fibroblast cell which can differentiate into adipocyte-like cells under certain conditions (Green and Kehinde, 1975). The differentiated cells have the morphology and properties of adipocytes which make them a good model for studying adipogenesis and adipolysis, the main biological processes which occur within adipocytes (Zezulak and Green, 1985). Although 3T3-L1 cells present an artificial model of obesity, Novakofski reported that many of the factors associated with adipogenesis in these cells are characteristic of obesity in humans (Novakofski, 2004).

3T3-L1 pre-adipocytes are differentiated into mature adipocytes using chemical inducers of adipogenesis (insulin, dexamethasone and 3-isobutyl-1-methylxanthine [IBMX]), that mimic the hormonal, dietary and genetic influences of adipocyte differentiation *in vivo* and this has made a significant impact towards understanding molecular events involved in adipogenesis (Pheiffer et al., 2013). Generally, these cells are differentiated in media containing high glucose concentrations (Pheiffer et al., 2013), which has an adverse effect on the physiology of adipocytes. Studies have shown that differentiating 3T3-L1 pre-adipocytes in high glucose media (25 mM), results in decreased insulin sensitivity and increased ROS (Lin et al., 2005). Since we aimed to compare the relationship between miRNA expression and DNA methylation under conditions that mimic normoglycaemia and chronic hyperglycaemia (Lin et al., 2005), pre-adipocytes were differentiated in 5.5 mM or 25 mM glucose in this study.

4.3.1 Glucose concentration during differentiation does not affect lipid content, but increases metabolic activity and reactive oxygen species

4.4.1.1 Lipid accumulation

Adipocyte maturity, and therefore their level of differentiation, can be measured by the formation of lipid droplets within 3T3-L1 adipocytes (Pheiffer et al., 2013). As expected, differentiated adipocytes accumulated more lipids that undifferentiated pre-adipocytes, although the use of low (5.5 mM) or high (25 mM) glucose differentiation media did not affect lipid content. These findings are consistent with previous studies (Lin et al., 2005) that similarly show that using a physiologically relevant glucose concentration does not influence the extent of 3T3-L1 pre-adipocytes differentiation. However, using electron microscopy, Lin et al demonstrated that 3T3-L1 pre-adipocytes differentiated with 4 mM glucose accumulated smaller lipid droplets compared to 3T3-L1 pre-adipocytes differentiated with 25 mM glucose (Lin et al., 2005). The discrepancy between our studies could be due to the fact that ORO staining may not be as sensitive as electron microscopy to differentiate between lipid droplet sizes.

4.3.1.2 Increased metabolic activity in adipocytes differentiated in high glucose

The level of ATP production within 3T3-L1 adipocytes represents the number of metabolically active cells in culture. Metabolic activity was increased in mature adipocytes differentiated in either low or high glucose, compared to undifferentiated pre-adipocytes. However, the increase in adipocytes differentiated with 5.5 mM glucose was not significant compared undifferentiated controls. During the process of glucose metabolism, glucose is transported into the cell and undergoes processes that culminates in the production of ATP in the mitochondria (Stump et al., 2003; Wibom and Hultman, 1990). It is thus expected that cells that were differentiated in a higher glucose concentration would produce more ATP. Moreover, differentiation of adipocytes in high glucose decreased insulin-stimulated glucose uptake (Gagnon and Sorisky, 1998; Lu et al., 2001; Tang et al., 2001). Unfortunately, due to the absence of data for the glucose uptake assay attempted in this study, this remains speculation. The failure to successfully conduct the glucose uptake assay could be due to operator error, or due to technical error with the instrument used for measuring radioactivity. Since other researchers in the unit experienced a similar problem, it can be deduced that the failure of the assay was due to instrument error. Furthermore, the failure to normalize the

glucose uptake results to protein concentrations due to malfunctioning of equipment, may have contributed to the unsuccessful glucose uptake assays.

4.3.1.3 Increased oxidative stress in adipocytes differentiated in high glucose

Oxidative stress (OS) is a result of an imbalance between the production of reactive oxygen species (ROS),O_2 (superoxide radical), OH (hydroxyl radical) and H_2O_2 (hydrogen peroxide), and the inability of the cell to neutralize these reactive intermediates (Betteridge, 2000). Oxidative stress damages all cellular components including proteins, DNA and RNA, and has been shown to be involved in the pathogenesis of T2D (Lin et al., 2005; Matough et al., 2012; Wright et al., 2006). The level of ROS and OS is indicative of cellular function. To measure the level of OS in mature adipocytes, the OxiSelect™ Intracellular ROS Assay kit (Cell Biolabs, Inc., San Diego, USA) was used for the 2',7'-dichlorfluorescein-diacetate (DCFH-DA) assay and the JC-1 kit (Sigma-Aldrich) was used for the 5,5',6,6'-Tetrachloro-1,1',3,3'-tetraethylbenzimidazolyl-carbocyanine iodide (JC-1) assay.

The significant increase in ROS production, a marker of oxidative stress (Houstis et al., 2006; Inoguchi et al., 2000; Lin et al., 2005), observed in mature adipocytes compared to undifferentiated pre-adipocytes, is corroborated by the findings of other studies (Lin et al., 2005; Lu et al., 2001; Talior et al., 2003; Wu et al., 2005). Interestingly, DCHF fluorescence was increased in adipocytes differentiated in high glucose compared to adipocytes cultured in low glucose, suggesting increased oxidative stress in these adipocytes. Another marked difference between the adipocytes differentiated at low or high glucose, was that cells were malformed in adipocytes differentiated at high glucose concentrations. This could be due to the metabolic changes that result from the increased oxidative stress and the hyperglycaemic conditions the cells were differentiated in. In other studies, the differentiation of adipocytes in high glucose lead to a decrease in insulin-stimulated glucose uptake because of insulin resistance but no down-regulation of basal glucose uptake (Gagnon and Sorisky, 1998; Lu et al., 2001; Tang et al., 2001).

Taken together, these findings demonstrate that using two different glucose concentrations to differentiate 3T3-L1 pre-adipocytes, results in mature adipocytes with different metabolic activity and oxidative stress.

4.5 Limitations of the study

This study has several limitations, which include the small sample size, lack of information about environmental exposures which affect epigenetics (Ling and Groop, 2009; Piccolo et al., 2016), technical challenges and time constraints. In this study women of mixed ethnic ancestry were investigated. Individual heterogeneity, particularly within this ethnic group (de Wit et al., 2010), could have masked differences. However, a strength of the study is the use of different women (with same ethnicity and age) in the different analyses, thus providing strength to the evidence. Although women were matched for age, other environmental factors that affect epigenetics, such as smoking, drinking and socio-economic circumstances were not known. Due to technical challenges and time constraints, the molecular analysis could not be completed. However, cells for DNA, RNA and proteins extractions were harvested, and will be analyzed in future. Furthermore, due to instrument malfunctioning we were not able to normalize glucose uptake assays, which might have contributed to the unsuccessful results obtained. In this study, DNA methylation was investigated in whole blood, which is heterogenous and consists of different cell types that may influence the methylation results obtained but despite this limitation, whole blood is used often for the analysis of methylation because of convenience (Adalsteinsson et al., 2012; Houseman et al., 2015). Houseman et al provided evidence that despite the limitations of whole blood, important biological information may still be obtained from studying DNA methylation in whole blood.

4.6 Future work

In future, DNA, RNA (enriched for miRNAs) and proteins will be isolated, allowing the delineation of the relationship between DNA methylation and miRNA expression, and between miRNA expression and their targets genes and proteins. Due to technical challenges with culturing and maintaining 3T3-L1 pre-adipocytes, which are inherently difficult to culture (Green and Kehinde, 1974), and time constraints, the DNA methylation status of miR-98 and miR-150, and

their expression profile should be investigated in future. Moreover, bioinformatics analysis to identify miRNA gene targets should be conducted, and the expression of target genes and proteins should be correlated with miRNA expression. Glucose uptake assays should be repeated, and the results normalized to protein concentrations, to more accurately define the cell model. It would also be interesting to investigate DNA methylation of miRNA genes in different ethnicities, since Chang et al reported that differential expression of miRNAs in the Han and Kazak Chinese populations is mediated by differential DNA methylation (Chang et al., 2014a).

4.7 Conclusion

In conclusion, this study serves as further evidence that DNA methylation is a mechanism regulating miRNA gene expression during T2D and demonstrates that 3T3-L1 pre-adipocytes differentiated in different glucose concentrations offer a viable model for investigating the relationship between miRNA gene expression and DNA methylation during hyperglycaemia, altered metabolic activity and oxidative stress. This study shows that adipocytes in different glucose concentrations could reflect the different stages in the pathogenesis of T2D and could therefore be an important model for T2D research. These findings pave the way for future studies to delineate the effect of DNA methylation on miRNA expression during conditions characteristic of T2D.

5. References

Adalsteinsson, B.T., Gudnason, H., Aspelund, T., Harris, T.B., Launer, L.J., Eiriksdottir, G., Smith, A.V., and Gudnason, V. (2012). Heterogeneity in white blood cells has potential to confound DNA methylation measurements. PloS One *7*, e46705.

American Diabetes Association (2010). Diagnosis and classification of diabetes Mellitus. Diabetes Care *33*, S62–S69.

American Diabetes Association (2016). 2. Classification and diagnosis of diabetes. Diabetes Care *39*, S13–S22.

American Diabetes Association, A.D. (2012). Standards of medical care in diabetes—2012. Diabetes Care *35*, S11–S63.

Ardisson Korat, A.V., Willett, W.C., and Hu, F.B. (2014). Diet, lifestyle, and genetic risk factors for type 2 diabetes: a review from the Nurses' Health Study, Nurses' Health Study 2, and Health Professionals' Follow-up Study. Curr. Nutr. Rep. *3*, 345–354.

Arunachalam, G., Samuel, S., Ghosh, S., Triggle, C., and Ding, H. (2014). MicroRNA-34a mediates impaired angiogenesis in diabetes: Role of SIRT1 and metformin (1051.2). FASEB J. *28*, 1051.2.

Babu, S.S., Thandavarayan, R.A., Joladarashi, D., Jeyabal, P., Krishnamurthy, S., Bhimaraj, A., Youker, K.A., and Krishnamurthy, P. (2016). MicroRNA-126 overexpression rescues diabetes-induced impairment in efferocytosis of apoptotic cardiomyocytes. Sci. Rep. *6*, 36207.

Bajan, S., and Hutvagner, G. (2014). Regulation of miRNA Processing and miRNA mediated gene repression in cancer. Microrna Shariqah United Arab Emir. *3*, 10–17.

Baroukh, N.N., and Van Obberghen, E. (2009). Function of microRNA-375 and microRNA-124a in pancreas and brain. FEBS J. *276*, 6509–6521.

Baylin, S.B., and Ohm, J.E. (2006). Epigenetic gene silencing in cancer - a mechanism for early oncogenic pathway addiction? Nat. Rev. Cancer *6*, 107–116.

Beagley, J., Guariguata, L., Weil, C., and Motala, A.A. (2014). Global estimates of undiagnosed diabetes in adults. Diabetes Res. Clin. Pract. *103*, 150–160.

Berg, J.M., Tymoczko, J.L., and Stryer, L. (2002). Each organ has a unique metabolic profile.

Bertram, M.Y., Jaswal, A.V.S., Van Wyk, V.P., Levitt, N.S., and Hofman, K.J. (2013). The non-fatal disease burden caused by type 2 diabetes in South Africa, 2009. Glob. Health Action *6*, 19244.

Betteridge, D.J. (2000). What is oxidative stress? Metabolism. *49*, 3–8.

Bird, A. (2002). DNA methylation patterns and epigenetic memory. Genes Dev. *16*, 6–21.

Bird, A.P. (1980). DNA methylation and the frequency of CpG in animal DNA. Nucleic Acids Res. *8*, 1499–1504.

Buysschaert, I., Schmidt, T., Roncal, C., Carmeliet, P., and Lambrechts, D. (2008). Genetics, epigenetics and pharmaco-(epi)genomics in angiogenesis. J. Cell. Mol. Med. *12*, 2533–2551.

Cao, J.-L., Zhang, L., Li, J., Tian, S., Lv, X.-D., Wang, X.-Q., Su, X., Li, Y., Hu, Y., Ma, X., et al. (2016). Up-regulation of miR-98 and unraveling regulatory mechanisms in gestational diabetes mellitus. Sci. Rep. *6*, 32268.

Chang, X., Li, S., Li, J., Yin, L., Zhou, T., Zhang, C., Chen, X., and Sun, K. (2014a). Ethnic differences in microRNA-375 expression level and DNA methylation status in type 2 diabetes of Han and Kazak populations. J. Diabetes Res. *2014*, 761938.

Chang, X., Li, S., Li, J., Yin, L., Zhou, T., Zhang, C., Chen, X., and Sun, K. (2014b). Ethnic Differences in microRNA-375 expression level and DNA methylation status in Type 2 Diabetes of Han and Kazak populations. J. Diabetes Res. *2014*, e761938.

Chavali, V., Tyagi, S.C., and Mishra, P.K. (2012). MicroRNA-133a regulates DNA methylation in diabetic cardiomyocytes. Biochem. Biophys. Res. Commun. *425*, 668–672.

Chédin, F. (2011). The DNMT3 Family of Mammalian De novo DNA methyltransferases. in progress in molecular biology and translational science, (Elsevier), pp. 255–285.

Chen, H., Lan, H.-Y., Roukos, D.H., and Cho, W.C. (2014). Application of microRNAs in diabetes mellitus. J. Endocrinol. *222*, R1–R10.

Chen, L., Magliano, D.J., and Zimmet, P.Z. (2012a). The worldwide epidemiology of type 2 diabetes mellitus—present and future perspectives. Nat. Rev. Endocrinol. *8*, 228–236.

Chen, Y.Q., Wang, X.X., Yao, X.M., Zhang, D.L., Yang, X.F., Tian, S.F., and Wang, N.S. (2012b). Abated microRNA-195 expression protected mesangial cells from apoptosis in early diabetic renal injury in mice. J. Nephrol. *25*, 566–576.

Cheng, J., Wang, L., Xu, L., Wang, H., Liu, P., Bu, S., Ye, M., Zhang, L., Wang, Q., and Duan, S. (2013). Gender-dependent miR-375 promoter methylation and the risk of type 2 diabetes. Exp. Ther. Med. *5*, 1687–1692.

Chiba, K., Kawakami, K., and Tohyama, K. (1998). Simultaneous evaluation of cell viability by neutral red, MTT and crystal violet staining assays of the same cells. Toxicol. In Vitro *12*, 251–258.

Chien, H.-Y., Lee, T.-P., Chen, C.-Y., Chiu, Y.-H., Lin, Y.-C., Lee, L.-S., and Li, W.-C. (2015). Circulating microRNA as a diagnostic marker in populations with type 2 diabetes mellitus and diabetic complications. J. Chin. Med. Assoc. *78*, 204–211.

Clark, C., Palta, P., Joyce, C.J., Scott, C., Grundberg, E., Deloukas, P., Palotie, A., and Coffey, A.J. (2012). A comparison of the whole genome approach of MeDIP-Seq to the targeted approach

of the Infinium HumanMethylation450 BeadChip® for methylome profiling. PLOS ONE *7*, e50233.

Coolen, M.W., Statham, A.L., Gardiner-Garden, M., and Clark, S.J. (2007). Genomic profiling of CpG methylation and allelic specificity using quantitative high-throughput mass spectrometry: critical evaluation and improvements. Nucleic Acids Res. *35*, e119.

Deaton, A.M., and Bird, A. (2011). CpG islands and the regulation of transcription. Genes Dev. *25*, 1010–1022.

Dias, S. (2016). MicroRNA expression profiling in peripheral blood mononuclear cells and serum of type 2 diabetic, pre-diabetic and normo-glycaemic individuals. Thesis. Stellenbosch : Stellenbosch University.

Dludla, P.V., Muller, C.J.F., Joubert, E., Louw, J., Gabuza, K.B., Huisamen, B., Essop, M.F., and Johnson, R. (2016). Phenylpyruvic acid-2-O-β-D-glucoside attenuates high glucose-induced apoptosis in H9c2 cardiomyocytes. Planta Med.

Duan, Y., Zhou, B., Su, H., Liu, Y., and Du, C. (2013). miR-150 regulates high glucose-induced cardiomyocyte hypertrophy by targeting the transcriptional co-activator p300. Exp. Cell Res. *319*, 173–184.

Ebeling, P., Koistinen, H.A., and Koivisto, V.A. (1998). Insulin-independent glucose transport regulates insulin sensitivity. FEBS Lett. *436*, 301–303.

Eccleston, A., DeWitt, N., Gunter, C., Marte, B., and Nath, D. (2007). Epigenetics. Nature *447*, 395–395.

Ehrich, M., Nelson, M.R., Stanssens, P., Zabeau, M., Liloglou, T., Xinarianos, G., Cantor, C.R., Field, J.K., and Boom, D. van den (2005). Quantitative high-throughput analysis of DNA methylation patterns by base-specific cleavage and mass spectrometry. Proc. Natl. Acad. Sci. U. S. A. *102*, 15785–15790.

Erem, C., Kuzu, U.B., Deger, O., and Can, G. (2015). Prevalence of gestational diabetes mellitus and associated risk factors in Turkish women: the Trabzon GDM Study. Arch. Med. Sci. AMS *11*, 724–735.

Fabian, M.R., Sonenberg, N., and Filipowicz, W. (2010). Regulation of mRNA Translation and Stability by microRNAs. Annu. Rev. Biochem. *79*, 351–379.

Fan, L., Wu, Q., Xing, X., Wei, Y., and Shao, Z. (2012). MicroRNA-145 targets vascular endothelial growth factor and inhibits invasion and metastasis of osteosarcoma cells. Acta Biochim. Biophys. Sin. *44*, 407–414.

Fernandez-Valverde, S.L., Taft, R.J., and Mattick, J.S. (2011). MicroRNAs in β-Cell biology, insulin resistance, diabetes and its complications. Diabetes *60*, 1825–1831.

Ferrara, A. (2007). Increasing Prevalence of Gestational Diabetes Mellitus. Diabetes Care *30*, S141–S146.

Filios, S.R., and Shalev, A. (2015). β-Cell microRNAs: small but powerful. Diabetes *64*, 3631–3644.

Fowler, M.J. (2008). Microvascular and macrovascular complications of diabetes. Clin. Diabetes *26*, 77–82.

Fred, R.G., Bang-Berthelsen, C.H., Mandrup-Poulsen, T., Grunnet, L.G., and Welsh, N. (2010). High glucose suppresses human islet insulin biosynthesis by inducing miR-133a leading to decreased polypyrimidine tract binding protein-expression. PLOS ONE *5*, e10843.

Frost, R.J.A., and Olson, E.N. (2011). Control of glucose homeostasis and insulin sensitivity by the Let-7 family of microRNAs. Proc. Natl. Acad. Sci. *108*, 21075–21080.

Fulzele, S., El-Sherbini, A., Ahmad, S., Sangani, R., Matragoon, S., El-Remessy, A., Radhakrishnan, R., and Liou, G.I. (2015). MicroRNA-146b-3p regulates retinal inflammation by suppressing adenosine deaminase-2 in diabetes. BioMed Res. Int. *2015*, e846501.

Gagnon, A.M., and Sorisky, A. (1998). The effect of glucose concentration on insulin-induced 3T3-L1 adipose cell differentiation. Obes. Res. *6*, 157–163.

Gauthier, B.R., and Wollheim, C.B. (2006). MicroRNAs: "ribo-regulators" of glucose homeostasis. Nat. Med. *12*, 36–38.

Giacca, A., Fisher, S.J., McCall, R.H., Shi, Z.Q., and Vranic, M. (1997). Direct and indirect effects of insulin in suppressing glucose production in depancreatized dogs: role of glucagon. Endocrinology *138*, 999–1007.

Gilbert, E.R., and Liu, D. (2012). Epigenetics: the missing link to understanding beta-cell dysfunction in the pathogenesis of type 2 diabetes. Epigenetics *7*, 841–852.

Gowher, H., and Jeltsch, A. (2001). Enzymatic properties of recombinant Dnmt3a DNA methyltransferase from mouse: the enzyme modifies DNA in a non-processive manner and also methylates non-CpA sites1. J. Mol. Biol. *309*, 1201–1208.

Green, H., and Kehinde, O. (1974). Sublines of mouse 3T3 cells that accumulate lipid. Cell *1*, 113–116.

Green, H., and Kehinde, O. (1975). An established preadipose cell line and its differentiation in culture. II. Factors affecting the adipose conversion. Cell *5*, 19–27.

Griffiths-Jones, S., Grocock, R.J., Dongen, S. van, Bateman, A., and Enright, A.J. (2006). miRBase: microRNA sequences, targets and gene nomenclature. Nucleic Acids Res. *34*, D140–D144.

Guariguata, L., Whiting, D.R., Hambleton, I., Beagley, J., Linnenkamp, U., and Shaw, J.E. (2014). Global estimates of diabetes prevalence for 2013 and projections for 2035. Diabetes Res. Clin. Pract. *103*, 137–149.

Ha, M., and Kim, V.N. (2014). Regulation of microRNA biogenesis. Nat. Rev. Mol. Cell Biol. *15*, 509–524.

Hardy, O.T., Czech, M.P., and Corvera, S. (2012). What causes the insulin resistance underlying obesity? Curr. Opin. Endocrinol. Diabetes Obes. *19*, 81–87.

He, A., Zhu, L., Gupta, N., Chang, Y., and Fang, F. (2007). Overexpression of micro ribonucleic acid 29, highly up-regulated in diabetic rats, leads to insulin resistance in 3T3-L1 adipocytes. Mol. Endocrinol. *21*, 2785–2794.

He, X.-X., Kuang, S.-Z., Liao, J.-Z., Xu, C.-R., Chang, Y., Wu, Y.-L., Gong, J., Tian, D.-A., Guo, A.-Y., and Lin, J.-S. (2015). The regulation of microRNA expression by DNA methylation in hepatocellular carcinoma. Mol. Biosyst. *11*, 532–539.

Henry, C., Koumanov, F., Ghezzi, C., Mathieu, J.P., Hamant, S., De Leiris, J., and Comet, M. (1995). Experimental models, protocols, and reference values for evaluation of iodinated analogues of glucose. Nucl. Med. Biol. *22*, 875–885.

Houseman, E.A., Kim, S., Kelsey, K.T., and Wiencke, J.K. (2015). DNA methylation in whole blood: Uses and challenges. Curr. Environ. Health Rep. *2*, 145–154.

Houstis, N., Rosen, E.D., and Lander, E.S. (2006). Reactive oxygen species have a causal role in multiple forms of insulin resistance. Nature *440*, 944–948.

Illingworth, R.S., Gruenewald-Schneider, U., Webb, S., Kerr, A.R.W., James, K.D., Turner, D.J., Smith, C., Harrison, D.J., Andrews, R., and Bird, A.P. (2010). Orphan CpG islands identify numerous conserved promoters in the mammalian genome. PLOS Genet. *6*, e1001134.

Inoguchi, T., Li, P., Umeda, F., Yu, H.Y., Kakimoto, M., Imamura, M., Aoki, T., Etoh, T., Hashimoto, T., Naruse, M., et al. (2000). High glucose level and free fatty acid stimulate reactive oxygen species production through protein kinase C--dependent activation of NAD(P)H oxidase in cultured vascular cells. Diabetes *49*, 1939–1945.

International Diabetes Federation (2014). 6th Annual Diabetes Atlas.

International Diabetes Federation (2015). 7th Annual Diabetes Atlas.

Jones, P.A., and Baylin, S.B. (2002). The fundamental role of epigenetic events in cancer. Nat. Rev. Genet. *3*, 415–428.

Joubert, J., Norman, R., Bradshaw, D., Goedecke, J.H., Steyn, N.P., Puoane, T., and South African Comparative Risk Assessment Collaborating Group (2007). Estimating the burden of disease attributable to excess body weight in South Africa in 2000. South Afr. Med. J. Suid-Afr. Tydskr. Vir Geneeskd. *97*, 683–690.

Kahn, B.B., and Flier, J.S. (2000). Obesity and insulin resistance. J. Clin. Invest. *106*, 473–481.

Kahn, S.E., Hull, R.L., and Utzschneider, K.M. (2006). Mechanisms linking obesity to insulin resistance and type 2 diabetes. Nature *444*, 840–846.

Kajimoto, K., Naraba, H., and Iwai, N. (2006). MicroRNA and 3T3-L1 pre-adipocyte differentiation. RNA N. Y. N *12*, 1626–1632.

Kameswaran, V., Bramswig, N.C., McKenna, L.B., Penn, M., Schug, J., Hand, N.J., Chen, Y., Choi, I., Vourekas, A., Won, K.-J., et al. (2014). Epigenetic Regulation of the DLK1-MEG3 MicroRNA Cluster in Human Type 2 Diabetic Islets. Cell Metab. *19*, 135–145.

Kaneda, M., Okano, M., Hata, K., Sado, T., Tsujimoto, N., Li, E., and Sasaki, H. (2004). Essential role for de novo DNA methyltransferase Dnmt3a in paternal and maternal imprinting. Nature *429*, 900–903.

Kato, Y., Kaneda, M., Hata, K., Kumaki, K., Hisano, M., Kohara, Y., Okano, M., Li, E., Nozaki, M., and Sasaki, H. (2007). Role of the Dnmt3 family in de novo methylation of imprinted and repetitive sequences during male germ cell development in the mouse. Hum. Mol. Genet. *16*, 2272–2280.

Krupanidhi, S., Sedimbi, S.K., Vaishnav, G., Madhukar, S.S., and Sanjeevi, C.B. (2009). Diabetes--role of epigenetics, genetics, and physiological factors. Zhong Nan Da Xue Xue Bao Yi Xue Ban *34*, 837–845.

Leney, S.E., and Tavaré, J.M. (2009). The molecular basis of insulin-stimulated glucose uptake: signalling, trafficking and potential drug targets. J. Endocrinol. *203*, 1–18.

Lewis, G.F., Vranic, M., and Giacca, A. (1997). Glucagon enhances the direct suppressive effect of insulin on hepatic glucose production in humans. Am. J. Physiol. *272*, E371-378.

Ley, S.H., Ardisson Korat, A.V., Sun, Q., Tobias, D.K., Zhang, C., Qi, L., Willett, W.C., Manson, J.E., and Hu, F.B. (2016). Contribution of the nurses' health studies to uncovering risk factors for Type 2 Diabetes: Diet, lifestyle, biomarkers, and genetics. Am. J. Public Health *106*, 1624–1630.

Li, J., Zhang, Y., Liu, Y., Dai, X., Li, W., Cai, X., Yin, Y., Wang, Q., Xue, Y., Wang, C., et al. (2013). Microvesicle-mediated Transfer of MicroRNA-150 from Monocytes to Endothelial Cells Promotes Angiogenesis. J. Biol. Chem. *288*, 23586–23596.

Li, N., Ye, M., Li, Y., Yan, Z., Butcher, L.M., Sun, J., Han, X., Chen, Q., Zhang, X., and Wang, J. (2010). Whole genome DNA methylation analysis based on high throughput sequencing technology. Methods San Diego Calif *52*, 203–212.

Li, X., Du, N., Zhang, Q., Li, J., Chen, X., Liu, X., Hu, Y., Qin, W., Shen, N., Xu, C., et al. (2014). MicroRNA-30d regulates cardiomyocyte pyroptosis by directly targeting foxo3a in diabetic cardiomyopathy. Cell Death Dis. *5*, e1479.

Li, Y., Zhang, Y., Li, S., Lu, J., Chen, J., Wang, Y., Li, Y., Xu, J., and Li, X. (2015). Genome-wide DNA methylome analysis reveals epigenetically dysregulated non-coding RNAs in human breast cancer. Sci. Rep. *5*, 8790.

Lin, Y., Berg, A.H., Iyengar, P., Lam, T.K.T., Giacca, A., Combs, T.P., Rajala, M.W., Du, X., Rollman, B., Li, W., et al. (2005). The hyperglycemia-induced inflammatory response in adipocytes: The role of reactive oxygen species. J. Biol. Chem. *280*, 4617–4626.

Ling, C., and Groop, L. (2009). Epigenetics: a molecular link between environmental factors and type 2 diabetes. Diabetes *58*, 2718–2725.

Liu, B., Du, Q., Chen, L., Fu, G., Li, S., Fu, L., Zhang, X., Ma, C., and Bin, C. (2016). CpG methylation patterns of human mitochondrial DNA. Sci. Rep. *6*, 23421.

Lu, B., Ennis, D., Lai, R., Bogdanovic, E., Nikolov, R., Salamon, L., Fantus, C., Le-Tien, H., and Fantus, I.G. (2001). Enhanced sensitivity of insulin-resistant adipocytes to vanadate is associated with oxidative stress and decreased reduction of vanadate (+5) to vanadyl (+4). J. Biol. Chem. *276*, 35589–35598.

Maher, F., Davies-Hill, T.M., Lysko, P.G., Henneberry, R.C., and Simpson, I.A. (1991). Expression of two glucose transporters, GLUT1 and GLUT3, in cultured cerebellar neurons: Evidence for neuron-specific expression of GLUT3. Mol. Cell. Neurosci. *2*, 351–360.

Mao, Y., Mohan, R., Zhang, S., and Tang, X. (2013). MicroRNAs as pharmacological targets in Diabetes. Pharmacol. Res. Off. J. Ital. Pharmacol. Soc. *75*, 37–47.

Matough, F.A., Budin, S.B., Hamid, Z.A., Alwahaibi, N., and Mohamed, J. (2012). The Role of Oxidative Stress and Antioxidants in Diabetic Complications. Sultan Qaboos Univ. Med. J. *12*, 5–18.

Meijer, H.A., Smith, E.M., and Bushell, M. (2014). Regulation of miRNA strand selection: follow the leader? Biochem. Soc. Trans. *42*, 1135–1140.

Melmed, S., Polonsky, K.S., Larsen, P.R., and Kronenberg, H.M. (2015). Williams Textbook of Endocrinology (Elsevier Health Sciences).

Michael Agostino (2012). Book: Practical Bioinformatics.

Miranda, T.B., and Jones, P.A. (2007). DNA methylation: The nuts and bolts of repression. J. Cell. Physiol. *213*, 384–390.

Mittelman, S.D., Fu, Y.Y., Rebrin, K., Steil, G., and Bergman, R.N. (1997). Indirect effect of insulin to suppress endogenous glucose production is dominant, even with hyperglucagonemia. J. Clin. Invest. *100*, 3121–3130.

Mohn, F., Weber, M., Schübeler, D., and Roloff, T.-C. (2009). Methylated DNA immunoprecipitation (MeDIP). Methods Mol. Biol. Clifton NJ *507*, 55–64.

Morris, A.P. (2014). Fine mapping Type 2 Diabetes susceptibility loci (Karger Publishers).

National Institute of Diabetes and Digestive and Kidney Diseases (2015). Diagnosis of Diabetes and Prediabetes | NIDDK.

Ng, M., Fleming, T., Robinson, M., Thomson, B., Graetz, N., Margono, C., Mullany, E.C., Biryukov, S., Abbafati, C., Abera, S.F., et al. (2014). Global, regional, and national prevalence of overweight and obesity in children and adults during 1980–2013: a systematic analysis for the Global Burden of Disease Study 2013. The Lancet *384*, 766–781.

Novakofski, J. (2004). Adipogenesis: usefulness of in vitro and in vivo experimental models. J. Anim. Sci. *82*, 905–915.

O'Connell, T.M., and Markunas, C.A. (2016). DNA methylation and microRNA-based biomarkers for risk of Type 2 Diabetes. Curr. Diabetes Rev. *12*, 20–29.

Patterson, K., Molloy, L., Qu, W., and Clark, S. (2011). DNA methylation: Bisulphite modification and analysis. J. Vis. Exp. JoVE.

Peng, R., Liu, H., Peng, H., Zhou, J., Zha, H., Chen, X., Zhang, L., Sun, Y., Yin, P., Wen, L., et al. (2015). Promoter hypermethylation of let-7a-3 is relevant to its down-expression in diabetic nephropathy by targeting UHRF1. Gene *570*, 57–63.

Perret, P., Ghezzi, C., Ogier, L., Abbadi, M., Morin, C., Mathieu, J.-P., and Fagret, D. (2004). Biological studies of radiolabeled glucose analogues iodinated in positions 3, 4 or 6. Nucl. Med. Biol. *31*, 241–250.

Pheiffer, C., Dudhia, Z., Louw, J., Muller, C., and Joubert, E. (2013). Cyclopia maculata (honeybush tea) stimulates lipolysis in 3T3-L1 adipocytes. Phytomedicine Int. J. Phytother. Phytopharm. *20*, 1168–1171.

Pheiffer, C., Erasmus, R.T., Kengne, A.P., and Matsha, T.E. (2016). Differential DNA methylation of microRNAs within promoters, intergenic and intragenic regions of type 2 diabetic, pre-diabetic and non-diabetic individuals. Clin. Biochem. *49*, 433–438.

Piccolo, R.S., Subramanian, S.V., Pearce, N., Florez, J.C., and McKinlay, J.B. (2016). Relative contributions of socioeconomic, local environmental, psychosocial, lifestyle/behavioral, biophysiological, and ancestral factors to racial/ethnic disparities in Type 2 Diabetes. Diabetes Care *39*, 1208–1217.

Pradhan, S., Bacolla, A., Wells, R.D., and Roberts, R.J. (1999). Recombinant human DNA (Cytosine-5) methyltransferase I. Expression, purification and comparison of de novo and maintenance methylation. J. Biol. Chem. *274*, 33002–33010.

Prattichizzo, F., Giuliani, A., Ceka, A., Rippo, M.R., Bonfigli, A.R., Testa, R., Procopio, A.D., and Olivieri, F. (2015). Epigenetic mechanisms of endothelial dysfunction in type 2 diabetes. Clin. Epigenetics *7*, 56.

Ratner, R.E. (2007). Prevention of Type 2 Diabetes in Women With Previous Gestational Diabetes. Diabetes Care *30*, S242–S245.

Reik, W. (2007). Stability and flexibility of epigenetic gene regulation in mammalian development. Nature *447*, 425–432.

Rhee, I., Bachman, K.E., Park, B.H., Jair, K.-W., Yen, R.-W.C., Schuebel, K.E., Cui, H., Feinberg, A.P., Lengauer, C., Kinzler, K.W., et al. (2002). DNMT1 and DNMT3b cooperate to silence genes in human cancer cells. Nature *416*, 552–556.

Rhodes, C.J., Wharton, J., Boon, R.A., Roexe, T., Tsang, H., Wojciak-Stothard, B., Chakrabarti, A., Howard, L.S., Gibbs, J.S.R., Lawrie, A., et al. (2013). Reduced microRNA-150 is associated with poor survival in pulmonary arterial hypertension. Am. J. Respir. Crit. Care Med. *187*, 294–302.

Rivera, R.M., and Bennett, L.B. (2010). Epigenetics in humans: an overview. Curr. Opin. Endocrinol. Diabetes Obes. *17*, 493–499.

Robertson, K.D. (2005). DNA methylation and human disease. Nat. Rev. Genet. *6*, 597–610.

Roggli, E., Britan, A., Gattesco, S., Lin-Marq, N., Abderrahmani, A., Meda, P., and Regazzi, R. (2010). Involvement of microRNAs in the cytotoxic effects exerted by proinflammatory cytokines on pancreatic β-cells. Diabetes *59*, 978–986.

Rome, S. (2013). Are extracellular microRNAs involved in type 2 diabetes and related pathologies? Clin. Biochem. *46*, 937–945.

Rottiers, V., and Näär, A.M. (2012). MicroRNAs in metabolism and metabolic disorders. Nat. Rev. Mol. Cell Biol. *13*, 239–250.

Roush, S., and Slack, F.J. (2008). The let-7 family of microRNAs. Trends Cell Biol. *18*, 505–516.

Salmasi, A.-M., and Dancy, M. (2005). The glucose tolerance Test, but not HbA 1c, remains the gold standard in identifying unrecognized diabetes mellitus and impaired glucose tolerance in hypertensive subjects. Angiology *56*, 571–579.

Shai, I., Jiang, R., Manson, J.E., Stampfer, M.J., Willett, W.C., Colditz, G.A., and Hu, F.B. (2006). Ethnicity, obesity, and risk of Type 2 Diabetes in women. Diabetes Care *29*, 1585–1590.

Shantikumar, S., Caporali, A., and Emanueli, C. (2012). Role of microRNAs in diabetes and its cardiovascular complications. Cardiovasc. Res. *93*, 583–593.

Shen, J., Wang, S., Siegel, A.B., Remotti, H., Wang, Q., Sirosh, I., and Santella, R.M. (2015). Genome-wide expression of microRNAs is regulated by DNA methylation in hepatocarcinogenesis. Gastroenterol. Res. Pract. *2015*, e230642.

Shrayyef, M.Z., and Gerich, J.E. (2010). Normal glucose homeostasis. In Principles of Diabetes Mellitus, L. Poretsky, ed. (Springer US), pp. 19–35.

Simpson, I.A., Dwyer, D., Malide, D., Moley, K.H., Travis, A., and Vannucci, S.J. (2008). The facilitative glucose transporter GLUT3: 20 years of distinction. Am. J. Physiol. - Endocrinol. Metab. *295*, E242–E253.

Singh, P.K., and Campbell, M.J. (2013). The interactions of microRNA and epigenetic modifications in prostate cancer. Cancers *5*, 998–1019.

Singh, D.K., Bose, S., and Kumar, S. (2016). Regulation of expression of microRNAs by DNA methylation in lung cancer. Biomark. Biochem. Indic. Expo. Response Susceptibility Chem. *21*, 589–599.

Sols, A., and Crane, R.K. (1954). Substrate specificity of brain hexokinase. J. Biol. Chem. *210*, 581–595.

Stettler, C., Christ, E., and Diem, P. (2016). Novelties in Diabetes (S. Karger AG).

Strmsek, Z., and Kunej, T. (2015). MicroRNA silencing by DNA methylation in human cancer: a Literature analysis. Non-Coding RNA *1*, 44–52.

Stump, C.S., Short, K.R., Bigelow, M.L., Schimke, J.M., and Nair, K.S. (2003). Effect of insulin on human skeletal muscle mitochondrial ATP production, protein synthesis, and mRNA transcripts. Proc. Natl. Acad. Sci. *100*, 7996–8001.

Suetake, I., Miyazaki, J., Murakami, C., Takeshima, H., and Tajima, S. (2003). Distinct enzymatic properties of recombinant mouse DNA methyltransferases Dnmt3a and Dnmt3b. J. Biochem. (Tokyo) *133*, 737–744.

Sun, K., Chang, X., Yin, L., Li, J., Zhou, T., Zhang, C., and Chen, X. (2014). Expression and DNA methylation status of microRNA-375 in patients with type 2 diabetes mellitus. Mol. Med. Rep. *9*, 967–972.

Suzuki, H., Maruyama, R., Yamamoto, E., and Kai, M. (2012). DNA methylation and microRNA dysregulation in cancer. Mol. Oncol. *6*, 567–578.

Talior, I., Yarkoni, M., Bashan, N., and Eldar-Finkelman, H. (2003). Increased glucose uptake promotes oxidative stress and PKC-delta activation in adipocytes of obese, insulin-resistant mice. Am. J. Physiol. Endocrinol. Metab. *285*, E295-302.

Tang, S., Le-Tien, H., Goldstein, B.J., Shin, P., Lai, R., and Fantus, I.G. (2001). Decreased in situ insulin receptor dephosphorylation in hyperglycemia-induced insulin resistance in rat adipocytes. Diabetes *50*, 83–90.

Tang, X., Tang, G., and Özcan, S. (2008). Role of microRNAs in diabetes. Biochim. Biophys. Acta BBA - Gene Regul. Mech. *1779*, 697–701.

Tang, X., Muniappan, L., Tang, G., and Özcan, S. (2009). Identification of glucose-regulated miRNAs from pancreatic β cells reveals a role for miR-30d in insulin transcription. RNA.

The International Expert Committee (2009). International expert committee report on the role of the A1C assay in the diagnosis of Diabetes. Diabetes Care *32*, 1327–1334.

Thompson, R.F., Suzuki, M., Lau, K.W., and Greally, J.M. (2009). A pipeline for the quantitative analysis of CG dinucleotide methylation using mass spectrometry. Bioinforma. Oxf. Engl. *25*, 2164–2170.

Thu, K.L., Vucic, E.A., Kennett, J.Y., Heryet, C., Brown, C.J., Lam, W.L., and Wilson, I.M. (2009). Methylated DNA immunoprecipitation. J. Vis. Exp. JoVE.

Vannucci, S.J. (1994). Developmental expression of GLUT1 and GLUT3 glucose transporters in rat brain. J. Neurochem. *62*, 240–246.

Vinik, A., and Flemmer, M. (2002). Diabetes and macrovascular disease. J. Diabetes Complications *16*, 235–245.

Vinson, C., and Chatterjee, R. (2012). CG methylation. Epigenomics *4*, 655–663.

Voight, B.F., Scott, L.J., Steinthorsdottir, V., Morris, A.P., Dina, C., Welch, R.P., Zeggini, E., Huth, C., Aulchenko, Y.S., Thorleifsson, G., et al. (2010). Twelve type 2 diabetes susceptibility loci identified through large-scale association analysis. Nat. Genet. *42*, 579–589.

Wang, X., Chang, X., Li, J., Yin, L., and Sun, K. (2014). DNA methylation of microRNA-375 in impaired glucose tolerance. Exp. Ther. Med.

Wang, X.H., Qian, R.Z., Zhang, W., Chen, S.F., Jin, H.M., and Hu, R.M. (2009). MicroRNA-320 expression in myocardial microvascular endothelial cells and its relationship with insulin-like growth factor-1 in type 2 diabetic rats. Clin. Exp. Pharmacol. Physiol. *36*, 181–188.

Wang, Y., Goulart, R.A., and Pantanowitz, L. (2011). Oil red O staining in cytopathology. Diagn. Cytopathol. *39*, 272–273.

Weir, G.C., and Bonner-Weir, S. (2004). Five stages of evolving beta-cell dysfunction during progression to Diabetes. Diabetes *53*, S16–S21.

Wibom, R., and Hultman, E. (1990). ATP production rate in mitochondria isolated from microsamples of human muscle. Am. J. Physiol. - Endocrinol. Metab. *259*, E204–E209.

de Wit, E., Delport, W., Rugamika, C.E., Meintjes, A., Möller, M., van Helden, P.D., Seoighe, C., and Hoal, E.G. (2010). Genome-wide analysis of the structure of the South African Coloured Population in the Western Cape. Hum. Genet. *128*, 145–153.

World Health Organization (2006). WHO | Definition and diagnosis of diabetes mellitus and intermediate hyperglycaemia.

World Health Organization (2016). Diabetes: Fact sheet.

Wright, E., Scism-Bacon, J., and Glass, L. (2006). Oxidative stress in type 2 diabetes: the role of fasting and postprandial glycaemia. Int. J. Clin. Pract. *60*, 308–314.

Wu, X., Zhu, L., Zijlbering, A., Mahadev, K., Motshima, H., Yao, J., and Goldstein, B.J. (2005). Hyperglycemia potentiates H2O2 production in adipocytes and enhances insulin signal transduction: Potential role for oxidative inhibition of thiol-sensitive protein-tyrosine phosphatases. Antioxid. Redox Signal. *7*, 526–537.

Xiang, Y., Zhang, J., Li, Q., Zhou, X., Wang, T., Xu, M., Xia, S., Xing, Q., Wang, L., He, L., et al. (2014). DNA methylome profiling of maternal peripheral blood and placentas reveal potential fetal DNA markers for non-invasive prenatal testing. Mol. Hum. Reprod. *20*, 875–884.

Xiao, C., Calado, D.P., Galler, G., Thai, T.-H., Patterson, H.C., Wang, J., Rajewsky, N., Bender, T.P., and Rajewsky, K. (2007). MiR-150 controls B cell differentiation by targeting the transcription factor c-Myb. Cell *131*, 146–159.

Xie, S., Xie, N., Li, Y., Wang, P., Zhang, C., Li, Q., Liu, X., Deng, J., Zhang, C., and Lv, C. (2012). Upregulation of TRB2 induced by miR-98 in the early lesions of large artery of type-2 diabetic rat. Mol. Cell. Biochem. *361*, 305–314.

Ying, W., Tseng, A., Chang, R.C.-A., Wang, H., Lin, Y., Kanameni, S., Brehm, T., Morin, A., Jones, B., Splawn, T., et al. (2016). miR-150 regulates obesity-associated insulin resistance by controlling B cell functions. Sci. Rep. *6*, 20176.

Yokochi, T., and Robertson, K.D. (2002). Preferential methylation of unmethylated DNA by mammalian de novo DNA methyltransferase Dnmt3a. J. Biol. Chem. *277*, 11735–11745.

Yuan, Y., Kang, R., Yu, Y., Liu, J., Zhang, Y., Shen, C., Wang, J., Wu, P., Shen, C., and Wang, Z. (2016). Crosstalk between miRNAs and their regulated genes network in stroke. Sci. Rep. *6*.

Zezulak, K.M., and Green, H. (1985). Specificity of gene expression in adipocytes. Mol. Cell. Biol. *5*, 419–421.

Zhang, F., REN, Y., LIU, P., REN, Y., and WANG, D. (2016). Expression of TGF-β1 and miRNA-145 in patients with diabetic foot ulcers. Exp. Ther. Med. *11*, 2011–2014.

Zhao, H., Guan, J., Lee, H.-M., Sui, Y., He, L., Siu, J.J., Tse, P.P.P., Tong, P.C.Y., Lai, F.M.M., and Chan, J.C.N. (2010). Up-regulated pancreatic tissue microRNA-375 associates with human Type 2 Diabetes through β-cell deficit and islet amyloid deposition: Pancreas *39*, 843–846.

Zhong, J., Agha, G., and Baccarelli, A.A. (2016). The role of DNA methylation in cardiovascular risk and disease: Methodological aspects, study design, and data analysis for epidemiological studies. Circ. Res. *118*, 119–131.

Zhu, Y., and Zhang, C. (2016). Prevalence of gestational diabetes and risk of progression to Type 2 Diabetes: a Global perspective. Curr. Diab. Rep. *16*, 7.

Zimmet, P. (2000). Globalization, coca-colonization and the chronic disease epidemic: can the Doomsday scenario be averted? J. Intern. Med. *247*, 301–310.

Zoungas, S., Woodward, M., Li, Q., Cooper, M.E., Hamet, P., Harrap, S., Heller, S., Marre, M., Patel, A., Poulter, N., et al. (2014). Impact of age, age at diagnosis and duration of diabetes on the risk of macrovascular and microvascular complications and death in type 2 diabetes. Diabetologia *57*, 2465–2474.

6. Appendix

Reagents, buffers and solutions

1. List of reagents

Product name	Supplier
15 and 50 mL centrifuge tubes	Nest Scientific, Rahway, USA
2-Deoxy-[^{3}H]-D-glucose	ARC, St Louis, USA
3-isobutyl-1-methylxanthine (IBMX)	Sigma-Aldrich, St. Louis, USA
3T3-L1 pre-adipocytes	American Type Culture Collection (ATCC), Manassas, USA
Agena Biosciences PCR accessory kit with Hotstart Taq polymerase	Sequenom, San Diego, USA
Carbon dioxide	Air Products, SA
Cell counting chamber slides	Life Technologies, Carlsbad, USA
CELLBIND® 6-, 24- and 96-well plates	Corning Inc., Corning, USA
Cryotubes	Corning Inc., Corning, USA
Crystal violet (CV)	
Dexamethasone (Dex)	Sigma-Aldrich, St. Louis, USA
Dimethyl-sulfoxide (DMSO)	Sigma-Aldrich, St. Louis, USA
Dulbecco's modified eagle's medium (DMEM) (w/phenol red): 5.5 mM or 25 mM	Lonza, Basel, Switserland
Dulbecco's modified eagles medium (DMEM) powder	Sigma-Aldrich, St. Louis, USA
Dulbecco's phosphate buffered saline (DPBS)	Lonza, Basel, Switserland
EpiTYPER® complete reagent kit	Sequenom, San Diego, USA
Ethanol	Sigma-Aldrich, St. Louis, USA
EZ DNA methylation kit™	Zymo Research, Irvine, USA
Fetal bovine serum (FBS)	Biochrom Gmbh,Berlin, Germany
Filter pads	Sigma-Aldrich, St. Louis, USA
Formalin	
Glucose powder	Sigma-Aldrich, St. Louis, USA
Hanks buffered saline solution (HBSS)	Lonza, Basel, Switserland
Insulin (10 mg/mL)	Sigma-Aldrich, St. Louis, USA
Isopropanol	Sigma-Aldrich, St. Louis, USA
JC-1 solid kit	Sigma-Aldrich, St. Louis, USA
Microfuge tubes	Eppendorf, Hamburg, Germany
Newborn Calf serum (NSC)	Biochrom Gmbh,Berlin, Germany
Non-cellbinding 96-well plates	Corning Inc., Corning, USA
Oil Red O (ORO)	Ambion, Austian, USA
OxiSelect™ Intracellular ROS Assay Kit	Cell Biolabs, inc., San Diego, USA
Phenylmethane sulfonyl fluoride (PMSF)	Sigma-Aldrich, St. Louis, USA
QIAzol lysis reagent	Qiagen, Hilden, Germany
RiboGreen® RNA reagent kit	Thermo Fisher Scientific, Waltham, USA

RIPA buffer	Cell Signalling Technologies, Danvers, USA
Scintillation Vials and liquid	Perkin Elmer, Waltham, USA
Sodium Dodecyl Sulfate (SDS)	BioRAD, Hercules, USA
Sodium hydroxide (NaOH)	Merck, Whitehouse station, USA
Sterile TC water (USP-Wifi)	Lonza, Basel, Switserland
Trypan blue	Life technologies. Carlsbad, USA
Trypsin-versene	Lonza, Basel, Switserland
Vialight® plus Cell Proliferation and Cytotoxicity BioAssay Kit	Lonza, Basel, Switserland
Wizard® Genomic DNA isolation kit	Promega, Madison, USA
Zymo-Spin™ IC column	Zymo Research, Irvine, USA

2. Buffers and media used in this study

Preparation of complete growth medium (CGM):

Complete growth medium for 3T3-L1 pre-adipocytes was prepared by adding 50 mL of NCS to 450 mL of 5.5 mM or 25mM glucose DMEM.

Preparation of freezing medium:

The freezing media was prepared by adding 2 mL of NCS and 1.4 mL of DMSO to 16.6 mL 25 mM glucose DMEM. The media was sterile filtered into a sterile 50 mL tube and then placed on ice.

Preparation of adipocyte maintenance medium (AMM):

AMM was prepared by adding 50 mL of FBS to 450 mL of 5.5 mM or 25 mM glucose DMEM.

Preparation of adipocyte differentiation medium (ADM):

ADM was prepared freshly on each Day 0 of cell growth by adding the materials as described in the table below:

Reagent	Concentration	Volume
AMM	5.5 mM glucose 25 mM glucose	98.98 mL 98.98 mL
Dex	10 mM	10 µL
Insulin	10 mg/mL	10 µL
IBMX	50 mM	1 mL
Total:		100 mL

Preparation of the ORO and CV stains:

A) ORO:

A 1% ORO stock solution was prepared by dissolving 1 g of the ORO powder in 100 mL isopropanol. This solution was placed on a magnetic stirrer overnight to dissolve most of the ORO powder. A 70% working solution was prepared by adding 30 mL distilled H_2O to 70 mL ORO from the stock solution. The ORO working solution was mixed by inversion and then sterile filtered to remove all the precipitates. The ORO working solution was stored at RT, away from direct sunlight.

B) CV:

A 2% CV stock solution was prepared by dissolving 2 g CV powder in 100 mL USP-Wifi H_2O. The CV stock solution was placed on a magnetic stirrer overnight. A 0.5% working solution was prepared by adding 49.75 mL distilled H_2O to 250 µL of the CV stock solution and it was then mixed by inversion. A fresh CV working solution was prepared for every experiment on the day of the experiment.

Preparation of 0.1 M NaOH and 0.1% SDS lysis buffer:

To obtain a lysis reagent with a final concentration of 0.1 M NaOH and 0.1% SDS, 2 g of NaOH (Mw= 40.0 g/mol) and 5 g SDS was dissolved in 500 mL distilled H_2O.

Preparation of DMEM without phenol red: no glucose and 5.5 mM or 25 mM glucose.

Reagent	Final Concentration	Mw	Amount/L
DMEM	8.3 g/L	-	8.3 g
BSA (no fatty acids)	0.1%	-	1 g
$NaHCO_3$	3.7 g/L	84.01	3.7 g
D-glucose	4.5 g/L	180.16	4.5 g
	1 g/L		1 g
	0 g/L		0 g

Preparation of insulin media:

Reagent	Final Concentration	Volume
DMEM (w/o phenol red):	25 mM	4.997 mL
	5 mM	4.997 mL
Insulin	5.8 µg/mL	2.9 µL

Preparation of 2-DG radioactive media:

Reagent	Final Concentration	Volume
Basal media		
DMEM (w/o phenol red)	25 mM (basal)	9.995 mL
	5.5 mM (basal)	9.995 mL
2-DG	-	0.5 µL
	Total:	10 mL
Insulin media: Transferred 4.997 mL of 2-DG basal media to clean tubes		
DMEM (w/o phenol red) + 2-DG	25 mM	4.997 mL
	5.5 mM	4.997 mL
Insulin	5.8 µg/mL	2.9 µL

The 10 × RIPA buffer contains the following reagents:

Reagent	Concentration
Tris-HCl (pH 7.5)	20 mM
NaCl	150 mM
Na2 EDTA	1 mM
EGTA	1 mM
NP-40	1%
Sodium deoxycholate	1%
Sodium pyrophosphate	2.5 mM
B-glycerophosphate	1 mM
Na3 VO4	1 mM
Leupeptin	1 µg/ml

The 10 × RIPA buffer was diluted to a 1 × stock solution with ddH_2O and aliquots of 1 mL each was prepared. PMSF was added to this aliquot prior to use.

3. Ethical approval

South African Medical Research Council

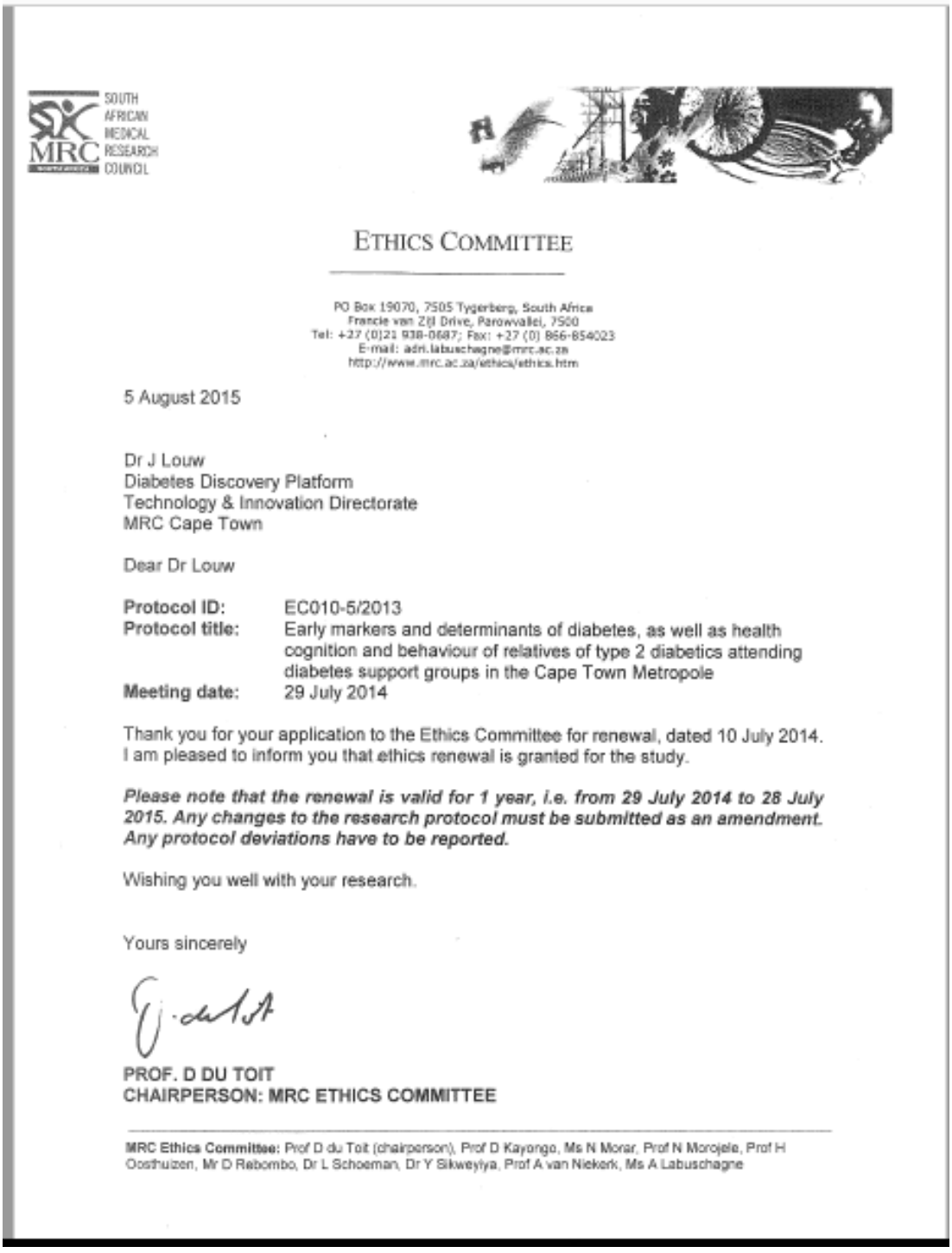

SOUTH AFRICAN MEDICAL RESEARCH COUNCIL

ETHICS COMMITTEE

PO Box 19070, 7505 Tygerberg, South Africa
Francie van Zijl Drive, Parowvallei, 7500
Tel: +27 (0)21 938-0687; Fax: +27 (0) 866-854023
E-mail: adri.labuschagne@mrc.ac.za
http://www.mrc.ac.za/ethics/ethics.htm

5 August 2015

Dr J Louw
Diabetes Discovery Platform
Technology & Innovation Directorate
MRC Cape Town

Dear Dr Louw

Protocol ID: EC010-5/2013
Protocol title: Early markers and determinants of diabetes, as well as health cognition and behaviour of relatives of type 2 diabetics attending diabetes support groups in the Cape Town Metropole
Meeting date: 29 July 2014

Thank you for your application to the Ethics Committee for renewal, dated 10 July 2014. I am pleased to inform you that ethics renewal is granted for the study.

Please note that the renewal is valid for 1 year, i.e. from 29 July 2014 to 28 July 2015. Any changes to the research protocol must be submitted as an amendment. Any protocol deviations have to be reported.

Wishing you well with your research.

Yours sincerely

PROF. D DU TOIT
CHAIRPERSON: MRC ETHICS COMMITTEE

MRC Ethics Committee: Prof D du Toit (chairperson), Prof D Kayongo, Ms N Monar, Prof N Morojele, Prof H Oosthuizen, Mr D Rebombo, Dr L Schoeman, Dr Y Sikweyiya, Prof A van Niekerk, Ms A Labuschagne

Stellenbosch University

UNIVERSITEIT•STELLENBOSCH•UNIVERSITY
jou kennisvennoot • your knowledge partner

Approval Notice

Response to Modifications- (New Application)

17-Aug-2015
Alley, Phifse-Jeanne P

Ethics Reference #: S15/04/096
Title: An Investigation of Differentially Methylated microRNAs in Type 2 Diabetes.

Dear Miss Phifse-Jeanne Alley,

The **Response to Modifications - *(New Application)*** received on **28-Jul-2015**, was reviewed by members of **Health Research Ethics Committee 1** via Expedited review procedures on **17-Aug-2015** and was approved.
Please note the following information about your approved research protocol:

Protocol Approval Period: **17-Aug-2015 -17-Aug-2016**

Please remember to use your **protocol number** (**S15/04/096**) on any documents or correspondence with the HREC concerning your research protocol.

Please note that the HREC has the prerogative and authority to ask further questions, seek additional information, require further modifications, or monitor the conduct of your research and the consent process.

After Ethical Review:
Please note a template of the progress report is obtainable on www.sun.ac.za/rds and should be submitted to the Committee before the year has expired. The Committee will then consider the continuation of the project for a further year (if necessary). Annually a number of projects may be selected randomly for an external audit.
Translation of the consent document to the language applicable to the study participants should be submitted.

Federal Wide Assurance Number: 00001372
Institutional Review Board (IRB) Number: IRB0005239

The Health Research Ethics Committee complies with the SA National Health Act No.61 2003 as it pertains to health research and the United States Code of Federal Regulations Title 45 Part 46. This committee abides by the ethical norms and principles for research, established by the Declaration of Helsinki, the South African Medical Research Council Guidelines as well as the Guidelines for Ethical Research: Principles Structures and Processes 2004 (Department of Health).

Provincial and City of Cape Town Approval

Please note that for research at a primary or secondary healthcare facility permission must still be obtained from the relevant authorities (Western Cape Department of Health and/or City Health) to conduct the research as stated in the protocol. Contact persons are Ms Claudette Abrahams at Western Cape Department of Health (healthres@pgwc.gov.za Tel: +27 21 483 9907) and Dr Helene Visser at City Health (Helene.Visser@capetown.gov.za Tel: +27 21 400 3981). Research that will be conducted at any tertiary academic institution requires approval from the relevant hospital manager. Ethics approval is required BEFORE approval can be obtained from these health authorities.

We wish you the best as you conduct your research.
For standard HREC forms and documents please visit: www.sun.ac.za/rds

If you have any questions or need further assistance, please contact the HREC office at 0219389657.

Included Documents:
CV P Alley
MOD_Protocol Synopsis
CV S Hemmings
Protocol